NASA Contractor Report 4474

Development and Application of a Time-Space Conversion Technique for Analysis of Weather Systems Passing Over the Kennedy Space Center

Gregory S. Forbes
Pennsylvania State University
University Park, Pennsylvania

Prepared for
George C. Marshall Space Flight Center
under Grant NAG8-754

National Aeronautics and
Space Administration

Office of Management

Scientific and Technical
Information Program

1992

ACKNOWLEDGMENTS

The research described in this report was sponsored by NASA Contract NAG8-754. The author is grateful to contract monitor Cathy Carlson Lapenta of Marshall Space Flight Center for her support. She also made available wind profiler data and rawinsonde and jimsphere data released in support of STS-27 from the Kennedy Space Center. Modifications to the time-space conversion scheme for this KSC application were supported by the above NASA contract. Development of the original time-space conversion scheme was performed by Gregory S. Forbes and Ming-Tzer Lee under Contract F19628-86-C-0092 from the Air Force Geophysics Laboratory, by Grant ATM-8601405 from the National Science Foundation, by Contracts N00014-86-K-0688 and N00014-84-C-0717 from the Office of Naval Research, and by Contract NAG8-754 from NASA. The author thanks Rose Auld Miller for her assistance in preparing the NGM-based pseudo-soundings.

TABLE OF CONTENTS

LIST OF ILLUSTRATIONS

LIST OF ILLUSTRATIONS (Continued)

LIST OF ILLUSTRATIONS (Continued)

LIST OF ILLUSTRATIONS (Concluded)

LIST OF TABLES

1. INTRODUCTION

Quantitative examination of the mesoscale structure of weather systems has always been a problem facing operational meteorologists. The conventional National Weather Service (NWS) network of rawinsondes yields horizontal resolution of 400-500 km; too coarse to resolve mesoscale features using synoptic (i.e., simultaneous) data. While high-resolution upper-air networks are often deployed for a few months in intensive research programs, a more feasible approach toward solving this problem on a long-term basis in an operational environment involves high-temporal-frequency sampling at one site (or a few sites). In this mode, weather systems are repeatedly sampled as they drift relatively slowly over a station. If sampling can be performed hourly, then an effective horizontal resolution of 50 km can generally be attained.

The Kennedy Space Center (KSC) has routinely launched serial ascents of rawinsondes and jimspheres before and immediately after launches of the Space Shuttle. More recently, a wind profiler has been deployed there, further enhancing the ability to examine the mesoscale variations within and substructures of weather systems passing over KSC. The formal transformation of this high-temporal-resolution data into high-horizontal-resolution analyses, however, requires a scheme to perform the time-to-space conversion.

Chapter 2 of this report describes the time-space conversion scheme developed at Penn State by Forbes and Lee (Forbes and Bankert, 1987; Lee, 1990), and its application to the KSC environment. The original development of the scheme was primarily supported by other research contracts (refer to the Acknowledgements for details). This contract has allowed for some modifications to the scheme needed to deal with the abrupt transition from the

comparatively data-"rich" continental United States to the essentially data void Gulf of Mexico and Atlantic Ocean regions.

Chapter 3 of this report is a case study of the weather system affecting KSC on 2 December 1988. In this study the time-space conversion technique (in its modified form) was used with NWS routine and special-launch rawinsonde data, serial ascent rawinsonde and jimsphere data from KSC, and wind profiler data from KSC. Horizontal analyses and cross-section analyses are presented for the time period during and immediately following a successful launch of the Space Shuttle (STS27) on this date, the second launch following the Challenger tragedy in 1986. Conclusions and a summary are presented in Chapter 4.

2. THE TIME-SPACE CONVERSION SCHEME

In this chapter the procedures involved in the time-space conversion scheme are outlined. Section 2.1 is extracted from Forbes et. al (1990), in which the time-space conversion scheme was first summarized. Sections 2.2 and 2.3 deal with modifications to the original scheme for the KSC application.

2.1 Concept of Time-Space Conversion

Time-space conversion techniques have been used for many years to determine the approximate structure of weather systems that are too small to be sampled by simultaneous measurements from the available weather station networks. The object of the time-space conversion is to take advantage of the ability to make frequent measurements at a few locations while the weather system passes overhead. Temporal changes of a parameter P are transformed to spatial gradients via

$$\frac{\Delta P}{\Delta t} = |\vec{C}| \frac{\Delta P}{\Delta s} \tag{1}$$

where $|\vec{C}|$ is the speed of movement of the weather system and s is a distance in the direction toward which the system is moving. The underlying assumption of the time-space conversion technique (1) is that the weather system is in a steady state during the period in which time-space conversion is applied. During such a period, a derived "simultaneous" spatial analysis is obtained by plotting the observation of parameter A at a location displaced from where it was measured, by distance

$$\Delta s = |\vec{C}| \Delta t \tag{2}$$

where Δt is the time difference between the observation and the reference (analysis) time, $\Delta t = t_{ref} - t_{obs}$. For a weather system moving eastward, observations taken earlier than the reference time are plotted as if they were taken at a location east of the actual point of observation (c.f., Fujita, 1963). Observations taken later than the reference time are plotted as if they were taken at locations west of the actual point of observation.

Actually, it is often necessary to perform the time-space conversion more carefully than suggested by the simple explanation above. A rigorous treatment must consider that the observed quantities may be the combined results of a mesoscale weather system travelling within a synoptic-scale environment, and moving with a velocity different from the larger-scale weather system in which it is embedded. In a typical case, the large-scale environmental fields are either moving slower than the mesoscale system or are quasi-stationary. A rigorous procedure, then, must separate the mesoscale perturbation quantities from the prevailing large-scale fields, and apply the time-space conversion only to the perturbation quantities.

Most studies involving time-space conversion have been performed on mesoscale convective systems, most notably by Fujita (1955, 1963). For these systems, which evolve rapidly, the period of time-space conversion is necessarily short. During these short periods, the weather systems move relatively small distances with respect to the large-scale environment in which they are embedded. In addition, the large-scale gradients are usually quite weak and the large-scale wind speeds rather weak. This allows the simple displacement of observations as a reasonable approximation to the more complicated displacement of perturbation quantities. However, when the time-space conversion technique is used with respect to larger weather systems

which can be considered steady state for longer periods, perturbation quantities must normally be used.

When time-space conversion periods are long, the moving weather system may travel through a sufficient distance that the background values of pressure, temperature, and humidity in the large-scale environment may change. Because of this, at first contemplation the perturbation concept may seem inconsistent with the steady-state assumption, and material advection of conserved quantities (as first indicated above) might seem to be correct. However, it must be remembered that even under adiabatic conditions the local change of temperature is controlled by a balance of horizontal advection, adiabatic warming or cooling, and mixing. The mixing ratio is, similarly, affected by horizontal and vertical advections and mixing. Thus, because most mesoscale systems are characterized by appreciable vertical velocities and, hence, adiabatic temperature changes and vertical fluxes, a steady-state mesoscale system (with a steady pattern of vertical velocities) must be treated as producing a perturbation on a large-scale background.

The concept of a moving perturbation (as opposed to advection of conserved values) also applies to air velocity, but with some subtleties owing to the vector character of this quantity. Figure 1 shows, by illustration, the manner in which perturbation velocity components must be computed and displaced. Because the large-scale flow pattern may contain curvature, mesoscale weather systems may change orientation perceptibly after a period of more than a few (~3-6) hours. Perturbation quantities u′ and v′ must, therefore, be computed in the natural system-oriented (or curved mean-flow) coordinate system, as opposed to a geographic (N-S-E-W) system. When the mesoscale system is characterized as inducing perturbations in the along-axis direction (n) and the axis-normal direction ($\hat{s}$), the perturbation quantities

in this frame of reference will tend to be conserved. If the system is steered by the mean flow, the s and n directions can be thought of as being along and normal to the system movement, respectively.

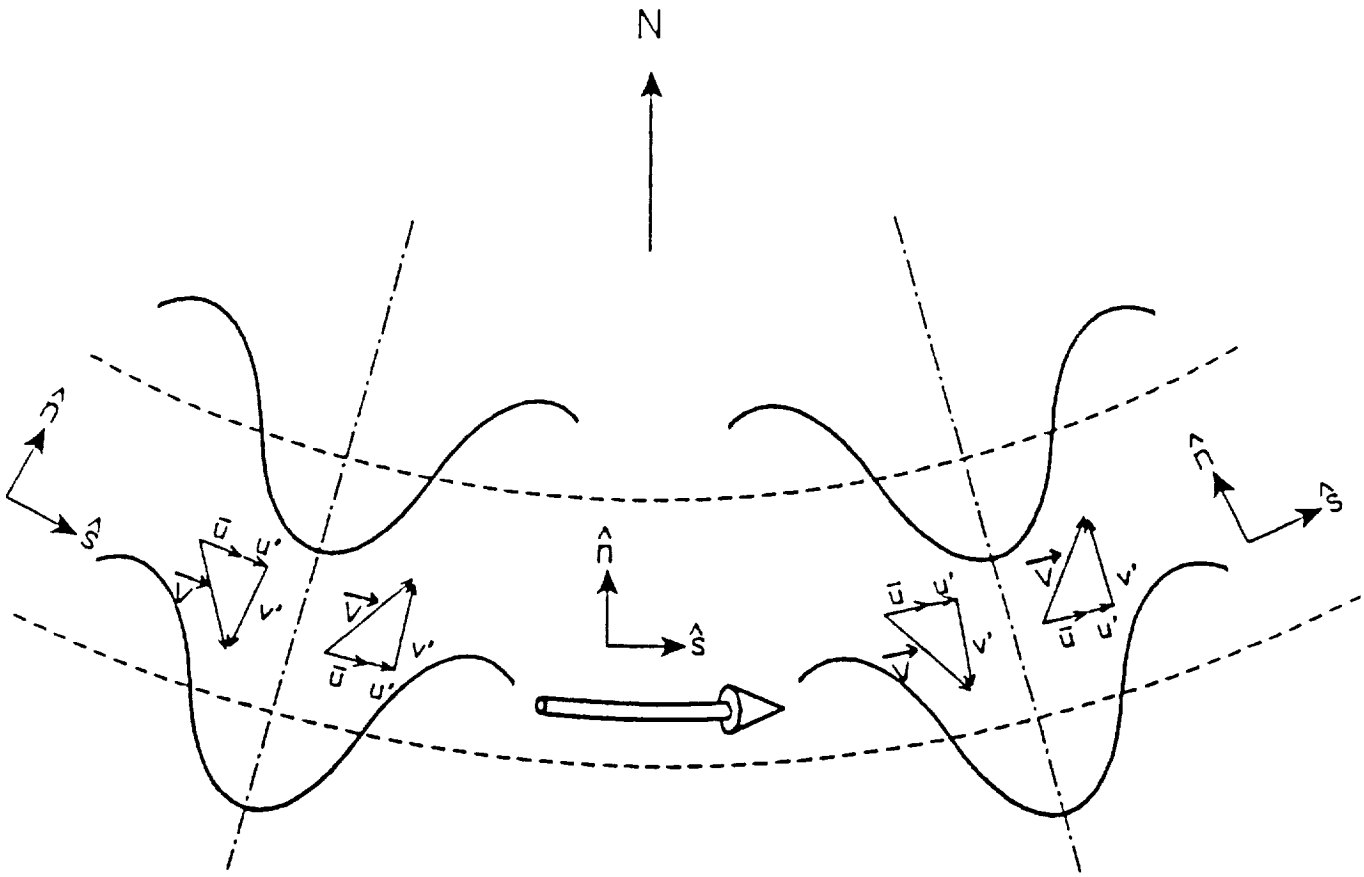

Figure 1. Schematic diagram depicting the movement of a sinusoidal disturbance through a curved prevailing mean flow (from Forbes and Bankert, 1987).

2.2 Procedures within the Time-Space Conversion Scheme

Large-scale mean fields of the u and v wind components and of air potential temperature) were obtained at 30 individual levels (from 0.5 km to 15.0 km MSL, at 0.5 km intervals) by temporal averaging of data for each of the conventional rawinsonde sites and for the KSC wind profiler site (winds only). The averaging interval was selected to be 36h, involving 4 successive rawinsonde releases from the operational network, at 0000 and 1200 UTC 2 December and at 0000 and 1200 UTC on 3 December 1988. Thirty-seven hourly wind profiles from the KSC wind profiler were averaged to yield the mean velocity components at that site. Conventional rawinsonde sites are shown by large dots on Figure 2. The KSC wind profiler site is denoted by letter "K". In addition to the sites shown on the figure, a few additional sites were used in the regions just beyond the borders of the map. The observations from Bermuda (WMO station 78016) were included in this group.

The sparsity of observation sites over the oceanic regions east and west of the Florida peninsula necessitated some adaptations to the time-space-conversion scheme--which had previously been used only for pure continental cases (Lee, 1990; Herzog, 1990). Analyzed fields used in the National Meteorological Center (NMC) Nested Grid Model (NGM) were used to construct "pseudo-soundings" over oceanic regions. The pseudo-soundings were constructed at each 5-degree latitude/longitude intersection (e.g., 30N, 65W), and at the point in the center of each of these 5-degree latitude/longitude "boxes" (e.g., 32.5N, 67.5W). Fig. 2 illustrates the locations of the pseudo-soundings used in the computation of the means.

The data used to construct the pseudo-soundings were part of the grid of data transmitted on the NMC Family of Services data line for use by operational meteorologists. Data were available for each of the mandatory

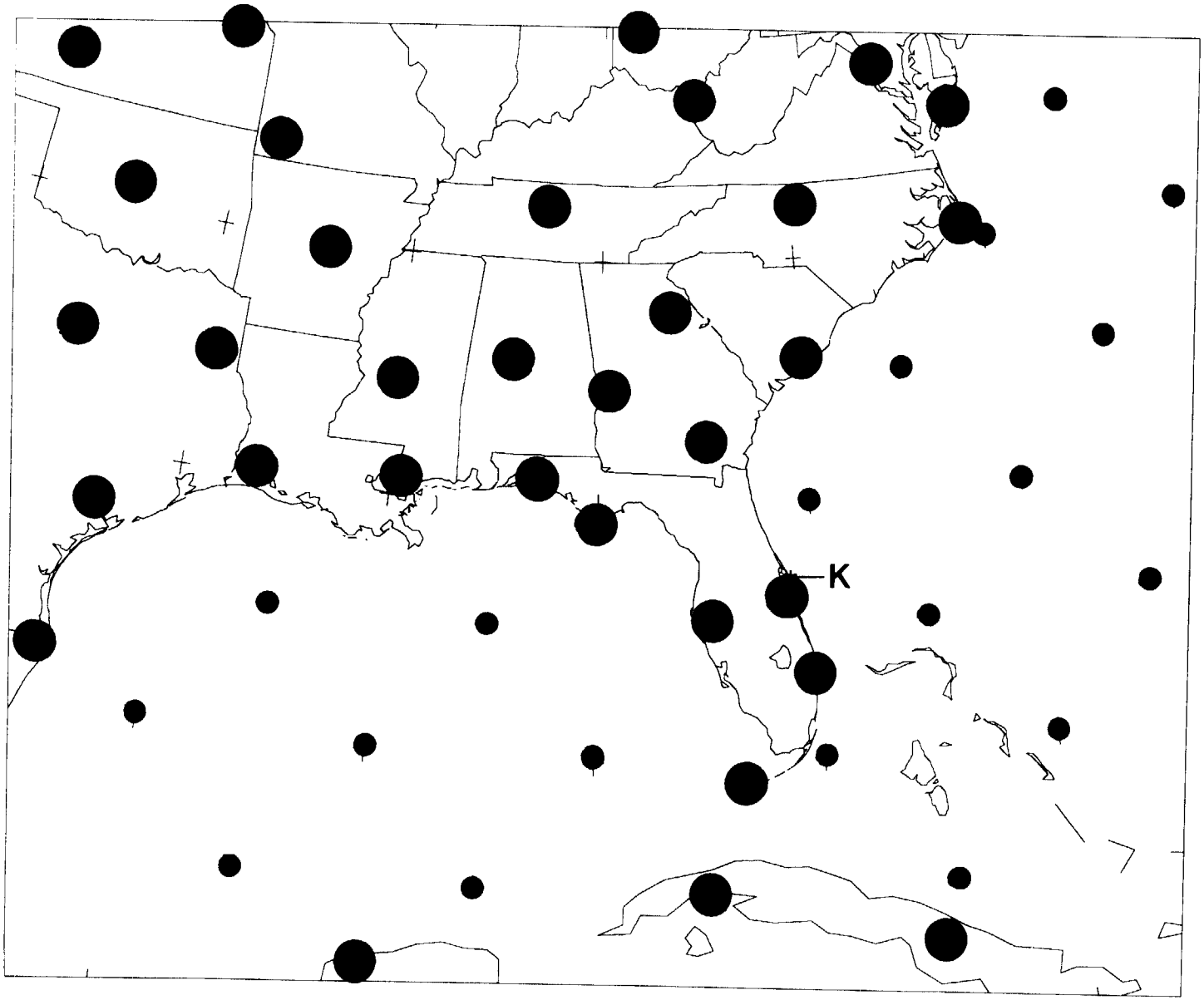

Figure 2. Locations of the rawinsonde sites from which data were used in the study of 2 December 1988 (large circles). Data from the Kennedy Space Center wind profiler (K) were also used, as were data from a few additional rawinsonde sites just beyond the borders of the map domain. Numerical model initial analysis data were used to compute approximate or "pseudo"-soundings (small circles) used in the computation of mean values.

pressure levels: 1000, 850, 700, 500, 400, 300, 250, 200, 150, and 100 mb. Interpolations were done between pressure levels to obtain values at the 30 constant-height levels. Parameter values were assumed to vary linearly with height (or with logarithm of pressure).

NGM-based "pseudo-soundings" were also generated for the location of any rawinsonde site that had missing data. A few soundings were missing entirely, while others had one or more parameters missing from certain levels, usually in the upper troposphere. The data gaps were then filled by values interpolated from the NGM-based pseudo-soundings.

Perturbation quantities were computed for individual observations with respect to the large-scale mean fields. In the case of velocity perturbations, they were computed as along-mean and cross-mean components with respect to the mean-wind (s, n) reference system explained in Section 2.1.

Weather system velocity had to be determined in a manner different from previous studies. In the previous applications, the velocity of the moving weather system, $\vec{C}$, was computed by tracking the movement of a satellite-observed cloud pattern characteristic of the travelling mesoscale weather system. Figure 3 reveals that in the 2 December 1988 case, however, the upper-level front and jet stream were largely free of clouds--except to the east of the axis of the jet stream--and even the clouds on the east side of the jet stream did not reveal much organized mesoscale structure. Accordingly, the movements of upper-tropospheric (200 mb and 300 mb) isotach maxima and minima and other velocity pattern features were tracked between the 1200 UTC 2 December and 0000 3 December 1988 NGM analyses, and used to compute the weather system velocity. Nine points were chosen, as shown in Figure 4, distributed over the domain in which the time-space conversion analyses were to be performed.

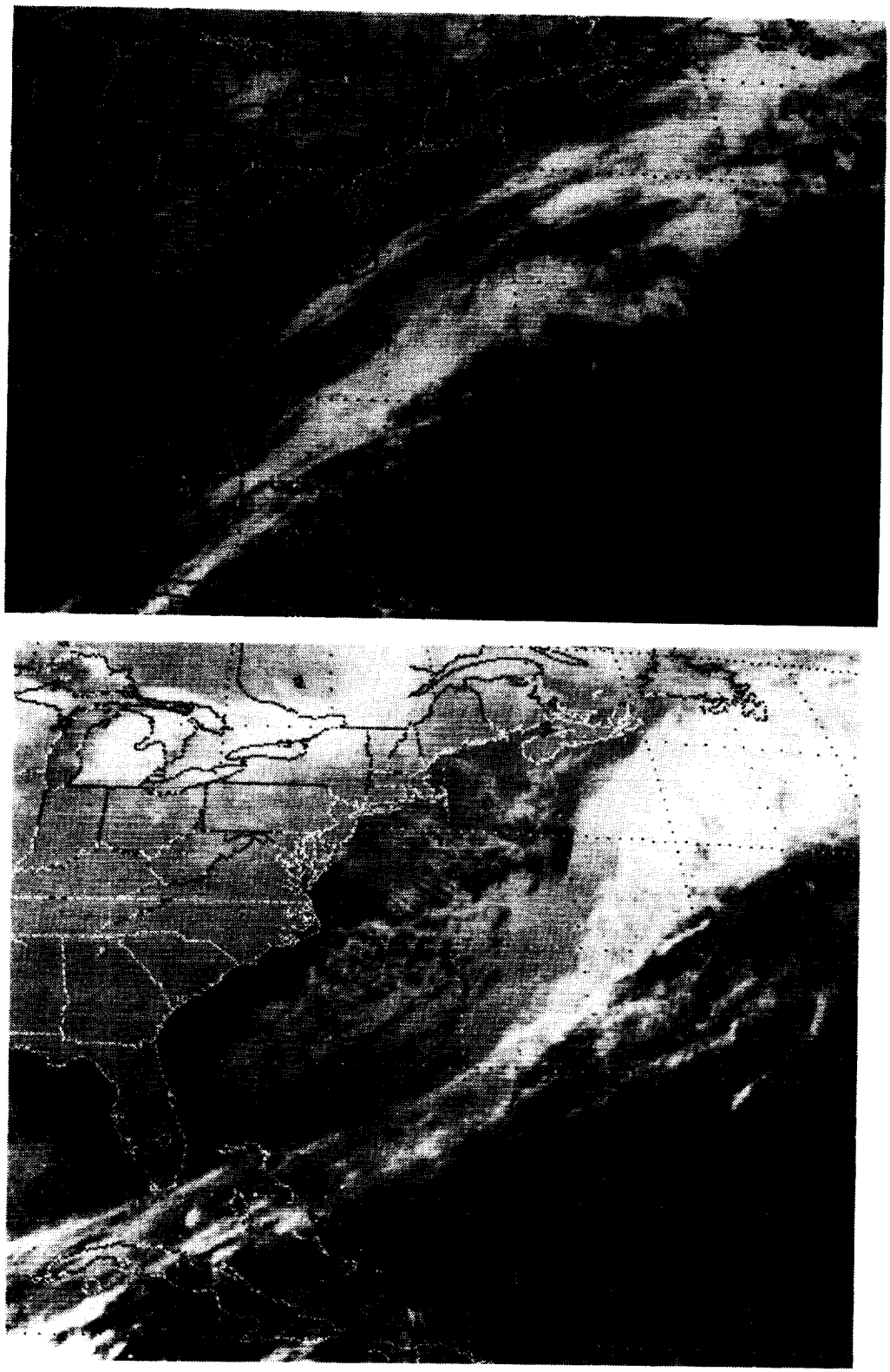

Figure 3. Sequence of satellite images from the 2 December 1988 case.
a. Infrared image from 1701 UTC 1 December 1988.
b. Infrared image from 1201 UTC 2 December 1988.
c. Water vapor image from 1601 UTC 2 December 1988.
d. Enhanced infrared image from 1901 UTC 2 December 1988.
e. Visible image from 1931 UTC 2 December 1988.

c

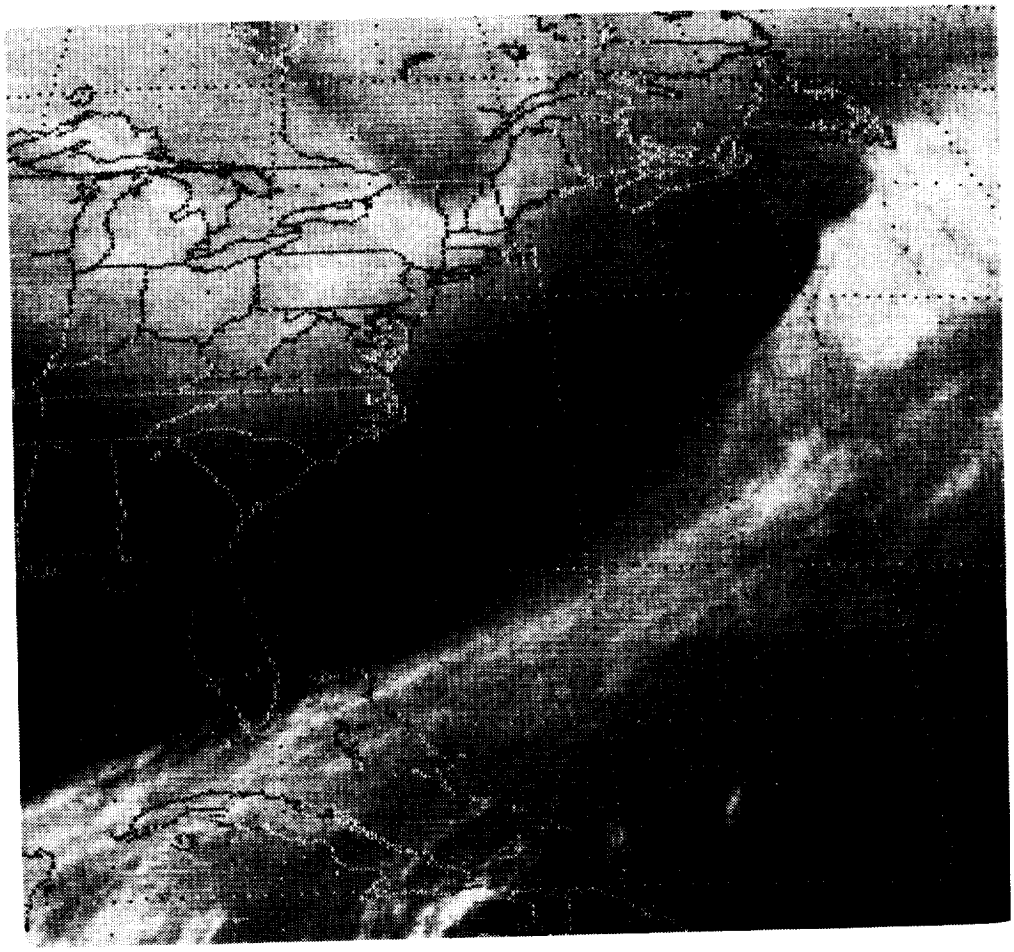

d

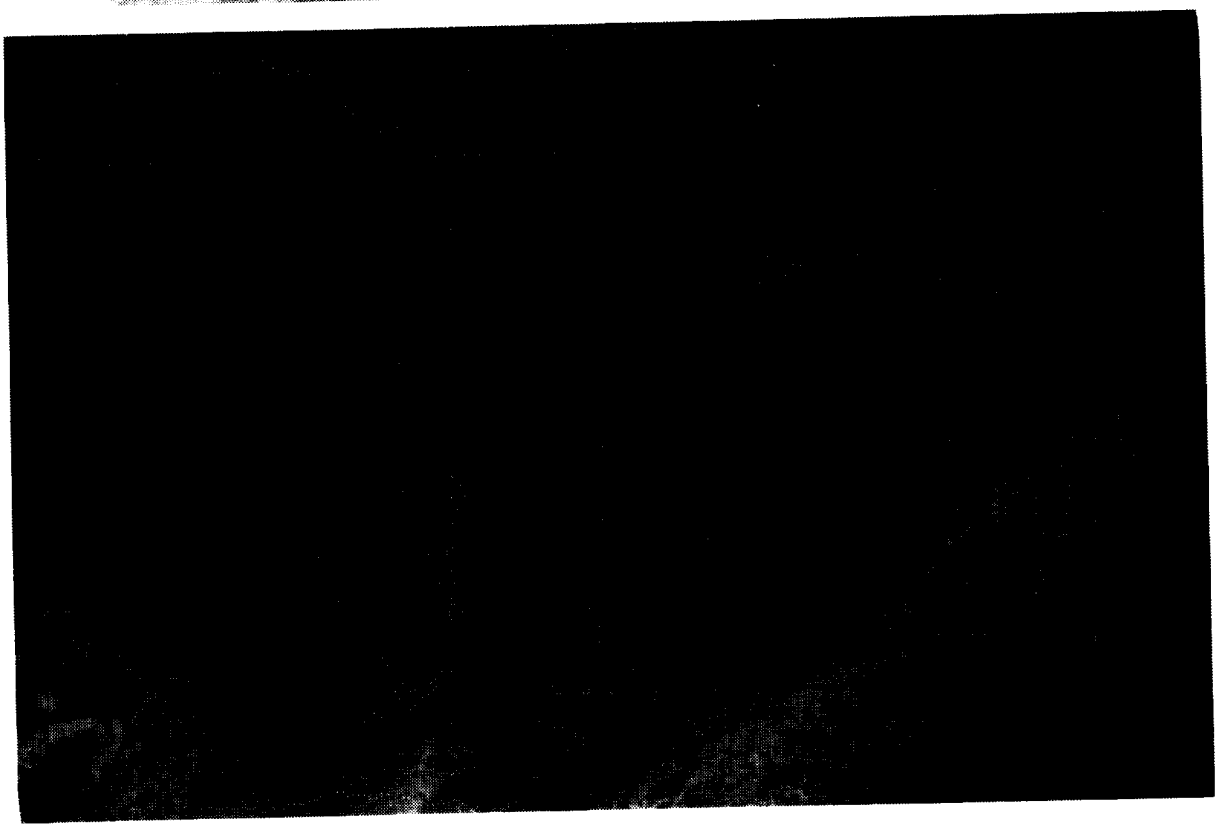

e

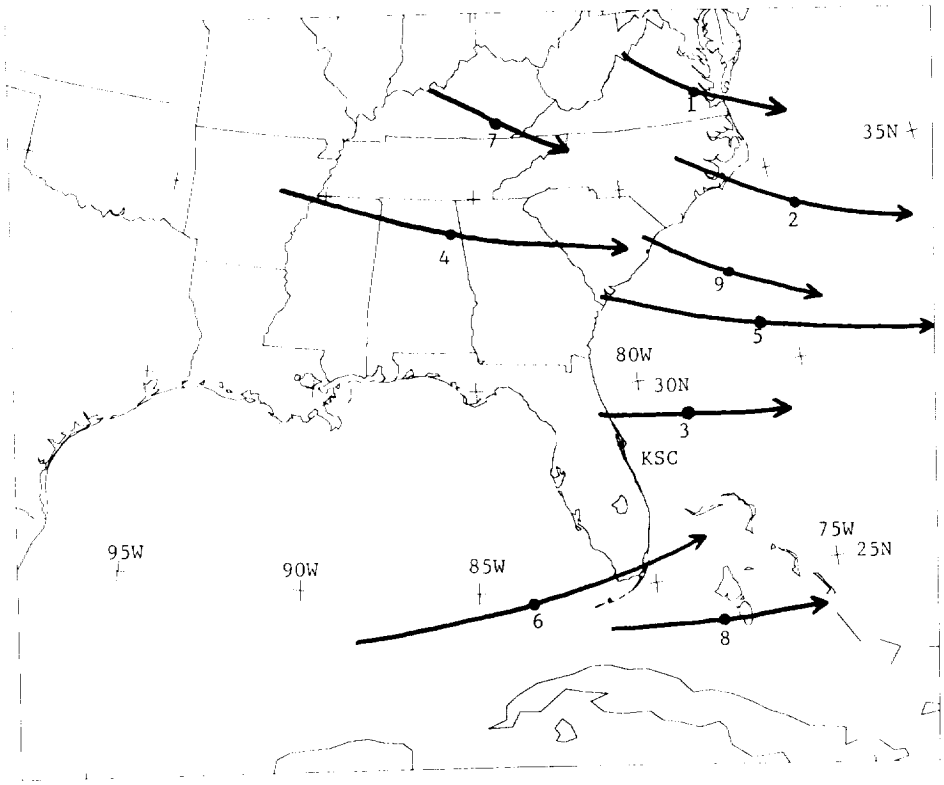

Figure 4. Movement of nine features in the Nested Grid Model (NGM) initial analyses in the upper troposphere between 1200 UTC 2 December and 0000 UTC 3 December.

The steering velocity field was determined based upon the displacement velocities. Rather than extrapolate from the 9 displacement velocities to obtain a steering velocity field, this group of velocities was compared to sets of trial "steering velocities" generated using winds at various levels. Trial steering velocity fields were computed at levels from 3.0 - 7.0 km as spatial means of the temporal-mean velocities described above. The spatial averaging was performed over a radius of 1000 km.

Table 1 documents the values of the trial steering velocities, and the 9 observed velocities of the upper-air features depicted in the NGM analysis fields. Individual errors were computed for each of the potential steering levels and observed data points, as documented in Table 2. The "best" steering level was then selected as the one whose temporal-spatial mean velocity field best matched, on average, the 9 observed velocities. In the 2 December 1988 case study, the steering field at 6.0 km MSL was used. This field is shown in Figure 5. In the days prior to the existence of numerical weather prediction models, steering velocities were often computed in this manner and used operationally in the course of making weather forecasts (Riehl, 1954; University of Chicago, 1956; Jarvis, 1965).

Time-space converted total wind velocities at the analysis time were obtained by displacing the perturbations to their appropriate locations using (2.2) and then performing the addition

$$\overline{V}_{total}=(u' + \overline{U})\,\hat{s} + V'\hat{n} \qquad (3)$$

where V_{total} is the vector velocity at the displaced location, u' and v' are the perturbation quantities, $\overline{U}$ is the large-scale mean velocity at the

TABLE 1

EVALUATION OF POTENTIAL STEERING LEVELS FOR 9 DATA POINTS

Level (km)	Data Points 1	2	3	4	5	6	7	8	9	
3.0	300	293	295	307	292	306	306	294	300	Direction
	13.6	12.1	8.5	10.2	9.8	6.2	12.0	8.5	13.6	Speed (m/s)
3.5	300	290	290	305	289	297	305	289	299	
	14.7	13.4	10.0	11.3	11.3	7.3	13.0	10.0	14.7	
4.0	298	287	286	304	286	292	305	286	298	
	15.7	14.6	11.4	12.3	12.7	8.4	13.9	11.5	15.7	
4.5	297	286	283	303	283	288	304	283	297	
	16.6	15.8	12.6	13.1	14.1	9.4	14.7	12.7	16.5	
5.0	295	283	280	301	279	285	303	280	295	
	17.3	16.9	13.6	13.9	15.3	10.2	15.2	13.7	17.3	
5.5	293	280	277	299	276	281	302	277	292	
	17.9	18.0	14.7	14.6	16.6	11.1	15.6	14.7	17.8	
6.0	290	278	274	297	273	277	300	274	290	
	18.5	19.1	16.0	15.5	18.0	12.4	16.1	16.1	18.4	
6.5	288	276	271	295	271	274	299	271	288	
	19.1	20.2	17.6	16.6	19.5	13.9	16.9	17.6	19.1	
7.0	287	274	270	292	269	271	297	269	287	
	19.9	21.3	19.2	17.8	21.0	15.6	17.8	19.3	19.9	
Data	299	297	275	280	284	257	293	274	298	Direction
Pts.	12.5	17.3	13.2	24.7	22.3	23.5	10.7	12.6	12.5	Speed (m/s)

TABLE 2

DIFFERENCE BETWEEN POTENTIAL STEERING VELOCITIES AND OBSERVED VALUES FOR 9 DATA POINTS (STEERING - OBSERVED)

Level (km)	Data Points 1	2	3	4	5	6	7	8	9	Mean
3.0	1	-4	20	27	8	49	13	20	2	15
	1.1	-5.3	-4.7	-14.5	-12.5	-17.3	1.3	-4.1	1.1	16.1
3.5	1	-7	15	25	5	40	12	15	1	12
	2.2	-3.9	-3.2	-13.4	-11.0	-16.2	2.3	-2.6	2.2	-4.8
4.0	-1	-10	11	24	2	35	12	12	0	9
	3.2	-2.7	-1.8	-12.4	-9.6	-15.1	3.2	-1.1	3.2	-3.7
4.5	-2	-11	8	23	-1	31	11	9	-1	7
	4.1	-1.5	-0.6	-11.6	-8.2	-14.1	4.0	0.1	4.0	-2.6
5.0	-4	-14	5	21	-5	28	10	6	-3	5
	4.8	-0.4	0.4	-10.8	-7.0	-13.3	4.5	1.1	4.8	-1.8
5.5	-6	-17	2	19	-8	24	9	3	-6	2
	5.4	0.7	1.5	-10.1	-5.7	-12.4	4.9	2.1	5.3	-0.9
6.0	-9	-19	-1	17	-11	20	7	0	-8	-0
	6.0	1.8	2.8	-9.2	-4.3	-11.1	5.4	3.4	5.9	0.1
6.5	-11	-21	-4	15	-13	17	6	-3	-10	-3
	6.6	2.9	4.4	-8.1	-2.8	-9.6	6.2	5.0	6.6	1.2
7.0	-12	-23	-5	12	-15	14	4	-5	-11	-5
	7.4	4.0	6.0	-6.9	-1.3	-7.9	7.1	6.7	7.4	2.5

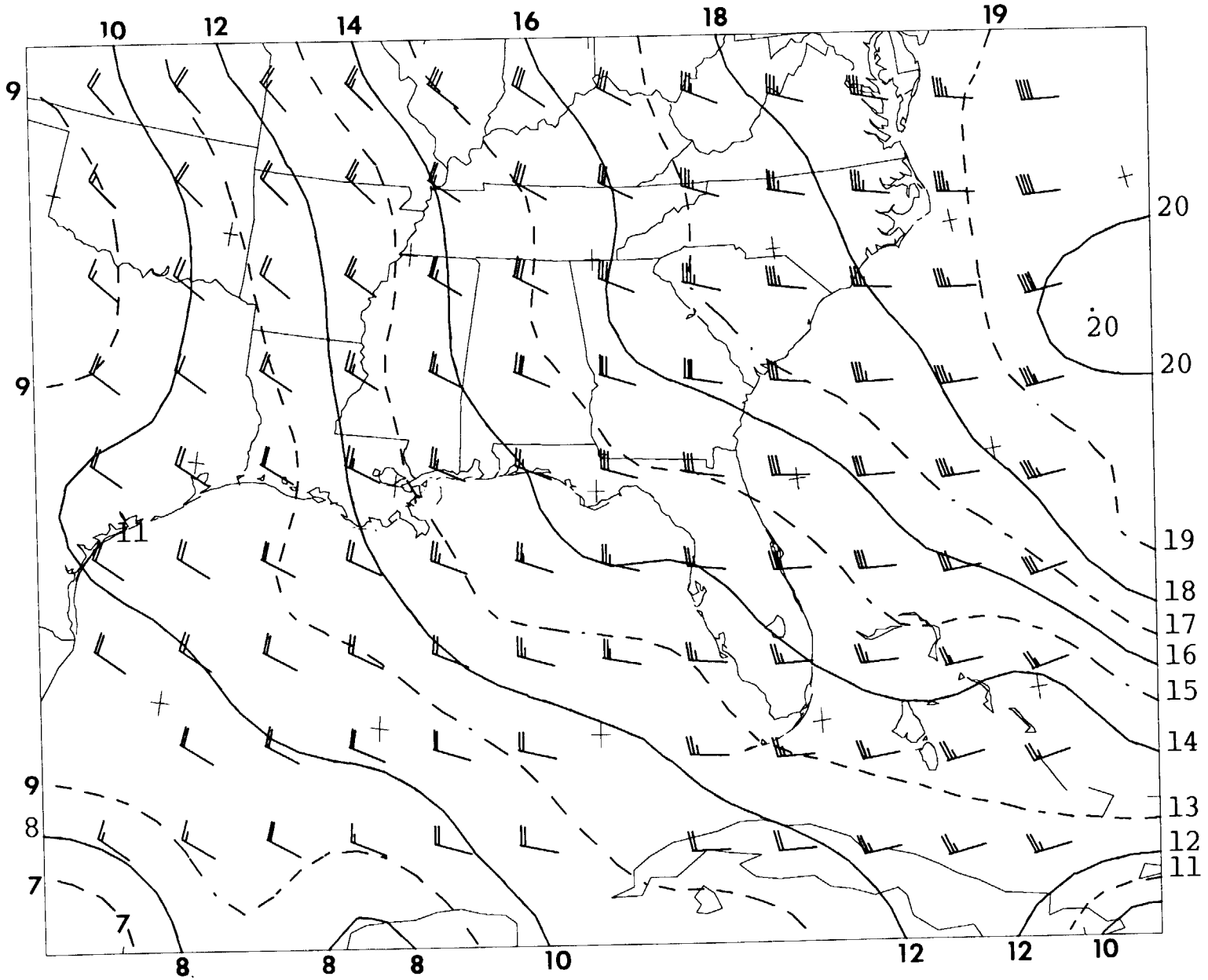

Figure 5. Steering velocity field used in the time-space conversion analyses of the case of 2 December 1988. Isopleths are isotachs in m/s. Wind vectors are in knots, displayed for every third grid point of the 30x40 grid of the analysis.

displaced location, and $\hat{s}$ and $\hat{n}$ are oriented along and normal to the mean flow at the displaced location.

Once the mean, perturbation, and total velocity data point locations and values were computed, gridded spatial fields were constructed in a three-step procedure. The geographical domain used was that of Fig. 5, covering the southeastern United States and a portion of the Caribbean. To this domain was assigned an array of grid points: 30 along the y axis (approximately S-N) and 40 along the x axis (approximately W-E). Grid points are spaced about 65 km apart.

In the first step of the analysis procedure, grid points were assigned the value of the nearest data point. The second step, applied once the 1200 grid points had been initially assigned values, was one pass of a 1:4:1 smoothing scheme. The net result is that the new value at a grid point became equal to 50% of its initial value plus 50% of the average value at the surrounding 4 grid points. The third step of the analysis procedure involved 3 passes of a Cressman (1959) fitting scheme. Each pass of this method, formally called the method of successive corrections, uses all data within a specified number of grid intervals in an inverse-distance-squared type weighting scheme, to adjust the grid point value. In the first pass, all data within 5 grid intervals was used; 3 and 1 grid intervals were used on the succeeding passes. The weighting function for an individual data point was

$$w = (R^2-D^2)/(R^2 + D^2), \qquad (4)$$

where R is the radius of influence (expressed as number of grid intervals) and D is the distance from the grid point to the data point (in grid intervals). Analysis-time and 36-hour-mean potential temperature grid fields were constructed in an identical procedure.

In the procedure above, some data from outside the map domain was used in the construction of the grid files of winds and potential temperatures. The outputted grid files included: directions, speeds, and u (W-E) and v (S-N) components for mean, total, and perturbation winds; 36-hour mean potential temperature and analysis-time potential temperature. In addition, the computerized time-space conversion algorithms also determined the vertical gradient of potential temperature in the layer from 0.5 km below the grid level to 0.5 km above the grid level, and outputted grid files of analysis-time and 36-hour-mean vertical gradients of potential temperature.

From the basic output grid files named above, additional meteorological fields were derived. These fields included:

(1) system-relative wind, $\vec{V}rel = \vec{V}total - \vec{C}$, (5)

where $\vec{C}$ is the steering velocity at the data point (Fig. 5);

(2) shear velocity, equal to the vector difference between the velocity 0.5 km above the analysis level and the velocity 0.5 km below the analysis level;

(3) Richardson number, $Ri = g\theta^{-1} \frac{\Delta\theta}{\Delta Z} \left(\left| \frac{\Delta \vec{V}}{\Delta Z} \right| \right)^{-2}$ (6)

where g is the acceleration due to gravity, θ is the potential temperature at the analysis level, $\frac{\Delta\theta}{\Delta z}$ is the vertical gradient of potential temperature, and is the shear velocity;

(4) vertical velocity, w.

Vertical velocity was not used directly from the wind profiler measurements because the errors of profiler-measured vertical velocity are likely to be nontrivial percentages of the true values and contaminated by the presence of smaller-scale features and turbulence. Instead, meso-alpha-scale

vertical velocities were computed through use of the thermodynamic (adiabatic) omega equation. In this method, the motion is assumed to be adiabatic, such that the observed temperature change is due to horizontal temperature advection, to adiabatic warming or cooling during descent or ascent, and to the translation of a steady state weather system over the observing location. With these assumptions, the vertical velocity becomes

$$w = -(\vec{v}-\vec{c}) \cdot \nabla\theta \left(\frac{\partial\theta}{\partial z}\right)^{-1} \qquad (7)$$

Thus, the vertical velocity computed by this method depends only upon the airflow relative to the moving pattern of adiabats and upon the ambient static stability $\frac{\Delta\theta}{\Delta z}$.

2.3 Refinements for the Kennedy Space Center Study

A wind profiler was installed at KSC during the fall of 1988, and some of its data was used in the case study of 2 December 1988. Computer programs were written to reformat the data from the KSC profiler format to a format used with the Penn State profiler data since 1985. This enabled the KSC data to be displayed and analyzed with existing Penn State wind profiler analysis software. The 50 MHz wind profiler operated at this time was a temporary deployment until a wind profiler specially designed for use at KSC could be constructed and installed.

The KSC data made available to Penn State contained gaps in the vertical coverage, apparently at altitudes where the original raw data was noisy and, accordingly, had been eliminated prior to distribution. The resulting irregularity of the vertical spacing of the profiler winds had no impact on

the time-height sections of the observed winds, Figures 6-12, but would have adversely affected other Penn State programs if left in that form. In particular, the time-space conversion programs which compute the temporal mean do so one gate number at a time, because no gates are skipped in the Penn State data files. In the Penn State data files, "bad" winds are denoted by -999.99, which is the signal for the program to ignore the value. Unfortunately, when levels were skipped in the KSC files at some, but not at all times, the result would be a mixing of levels by the Penn State program which computes the mean wind profile.

The above problems were avoided by first running a formatting program which reinserted the missing KSC gates, and inserted the code values (-999.99 or -999.9, depending on the field) at these altitudes. Because KSC data did not include consensus number, KSC data were arbitrarily assigned consensus numbers of 12 if values were reported and 0 if they were skipped.

Additional data were "flagged" as dubious by G. Forbes, most frequently at the 5.2, 5.8, and 6.4 km altitudes. In virtually every instance, the low-resolution speeds were at least 2 m/s less than the average of the four values at 150-meter gate spacings that would correspond to the low-resolution sample. Directions were approximately the same, suggesting that the low-resolution speeds were being contaminated by non-moving ground clutter or vertically propagating interference. Low-resolution data were flagged as questionable when the speed differed from the 4-level high-resolution average by more than 1 m/s. Most of the "flagged" data were then removed prior to use in the time-space conversion scheme.

Time-height sections showing sample analyses from the "cleaned-up" data set are shown in Figs. 6-7, from the period between 1200 UTC 1 December and 1200 UTC 2 December 1988, which lead up to the period of the time-space

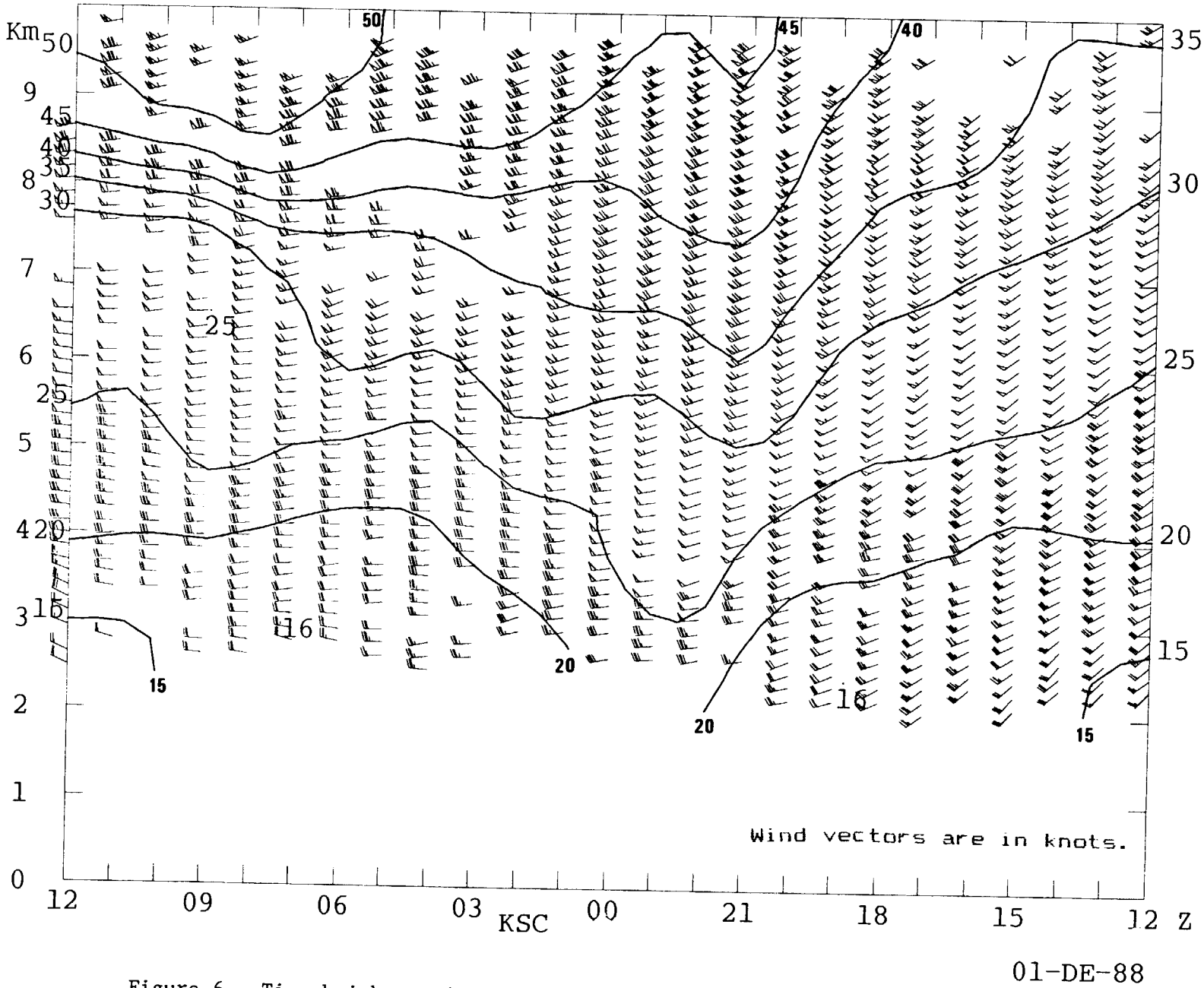

Figure 6. Time-height series of raw high-resolution winds, with flagged data eliminated, and with isotachs at 5 m/s intervals, 1200 UTC 1 December 1988 to 1200 UTC 2 December 1988. Wind vectors are in knots.

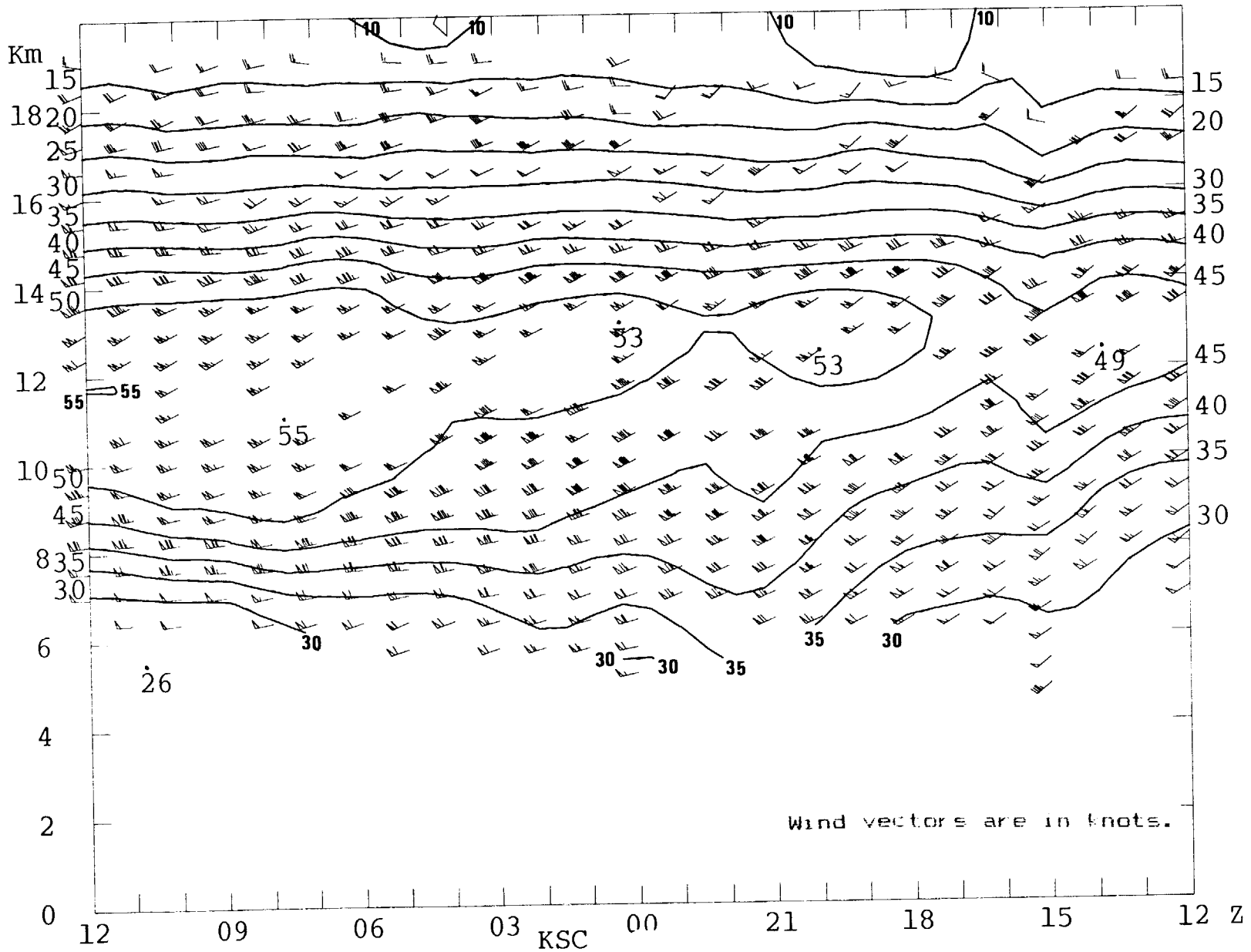

Figure 7. Time-height series of raw low-resolution winds, with flagged data eliminated, and with isotachs at 5 m/s intervals, 1200 UTC 1 December 1988 to 1200 UTC 2 December 1988. Wind vectors are in knots.

conversion. Blank spaces in the diagram indicate locations where data were removed. An interesting aspect of Figs. 6 and 7 is the sloping core of 30 m/s winds, from about 9 km (and above) at 1200 UTC 2 December to about 5.3 km (and above) at 2100 UTC 1 December.

Figure 8 shows a time-height section of perturbation velocities, defined in this instance as the departure from a 24-hour running mean, level by level. The "area" of winds exceeding 30 m/s in Fig. 7 is characterized in Fig. 8 as having northwesterly perturbation winds, whereas the perturbation winds were southerly or easterly prior to 2100 UTC 1 December and mainly westerly thereafter. Hence, the perturbation velocities suggest rather clearly the passage of a trough axis approximately coincident with the sloping zone of 30 m/s speeds. This was not so clear from the raw winds.

For use in the time-space conversion scheme, the high-resolution (0.15 km) and low-resolution (0.60 km) wind profiler data sets were merged into one single data set per hour, covering the altitudes from 1.60 to 16.0 km MSL. High-resolution data was used, when available (through 10.45 km), with low-resolution data used between 10.6 and 16.0 km. Missing data were replaced, according to the following strategy:

(1) Missing (or flagged) high-resolution winds below 10.45 were replaced by low-resolution winds when available and not flagged.

(2) The remaining missing or flagged winds at any level were replaced by winds through vertical interpolation, provided that straddling data could be found that were separated from the missing level vertically by no more than 3 profiler levels (0.45 km below 10.45 km; 1.80 km above 10.45 km).

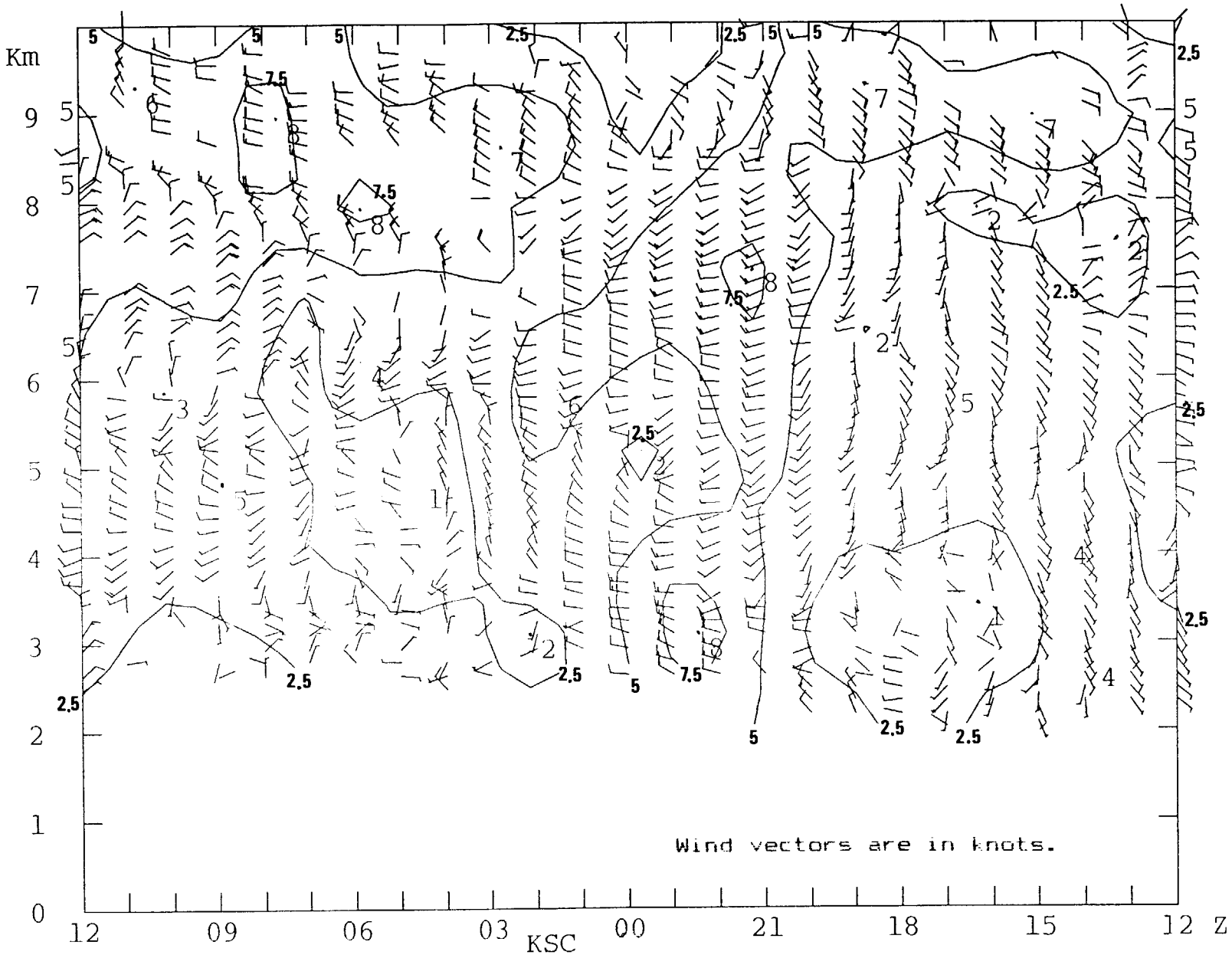

Figure 8. Time-height series of high-resolution perturbation velocities (vector departures from a 24-hour running mean, level by level), with flagged data eliminated, and with isotachs at 2.5 m/s intervals, 1200 UTC 1 December 1988 to 1200 UTC 2 December 1988. Wind vectors are in knots.

(3) Levels and times still showing missing or flagged winds were next filled via temporal interpolation, provided that straddling data could be found at that level which were separated temporally from the missing time by no more than 3h.

(4) Any remaining gaps that occurred at one of the four 12h operational rawinsonde launch times (0000 and 1200 UTC on 2 and 3 December) were filled through interpolation from NGM-based pseudo-sounding data.

(5) Any gaps still remaining were filled by an unrestricted temporal interpolation between the closest pair of straddling data points at the level.

Figures 9 and 10 show the resulting high-resolution time-height section after missing winds have been replaced following the above replacement heirarchy. Figures 11 and 12 show the resulting low-resolution time-height section. The blank upper-left portion of Figs. 11 and 12 results primarily because NMC analysis data was not available at these altitudes.

2.4 Comparison of KSC Wind Profiler Data with NMC-based Pseudo-Sounding Data

Since pseudo-soundings had to be prepared for the KSC site in order to fill some data gaps, it may be of interest to intercompare these two data sets for levels where unflagged KSC wind profiler data were available. Table 3 shows wind profiler and NGM-based pseudo-sounding velocities for each of the wind profiler measurement levels at 0000 UTC 2 December 1988 (except for 1.60 and 1.75 km, which were all flagged). Table 4 provides a comparison for 1200 UTC 2 December. Mean and root-mean-square (rms) differences of wind direction were 0.1 and 3.74 degrees at 0000 UTC, respectively, and 3.2 and 6.2 degrees at 1200 UTC. Mean and rms differences of wind speed were 1.0 m/s (1.9 kts) and

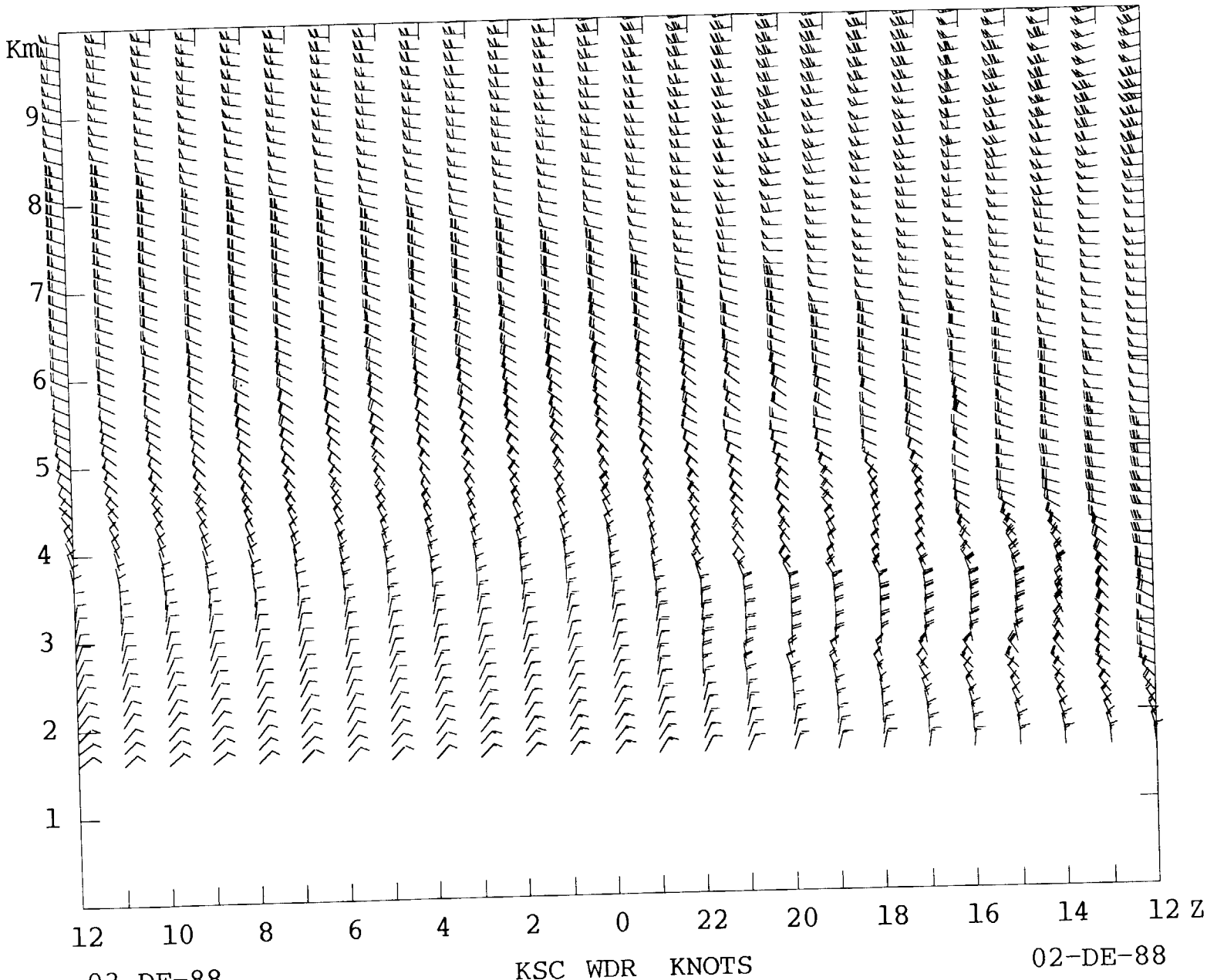

Figure 9. Time-height section of high-resolution winds, after missing or flagged data points have been filled through vertical or temporal interpolation, or through use of NMC-based pseudo-sounding data. Wind vectors are in knots.

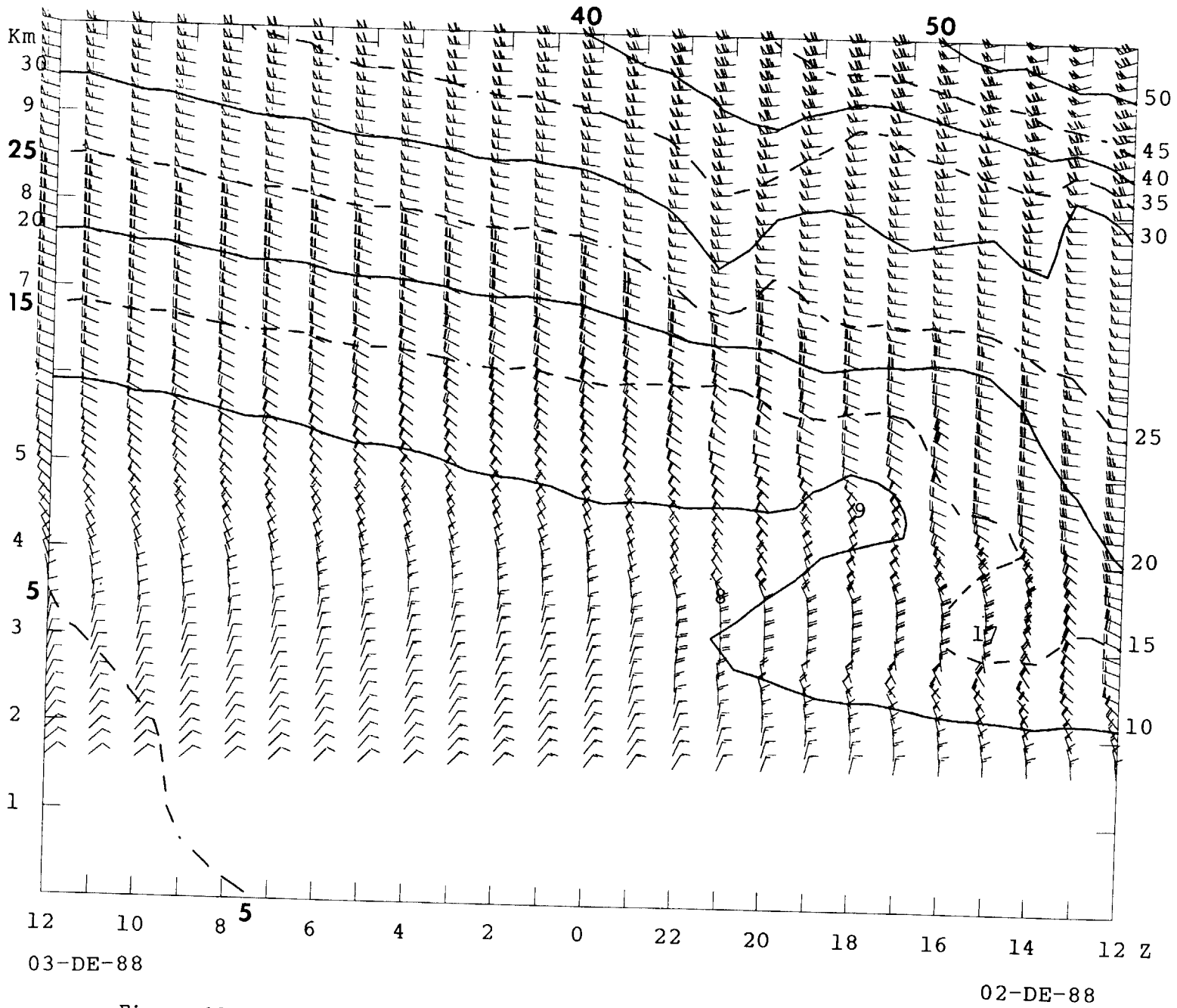

Figure 10. Time-height section of high-resolution wind speeds (m/s), after missing or flagged data points have been replaced.

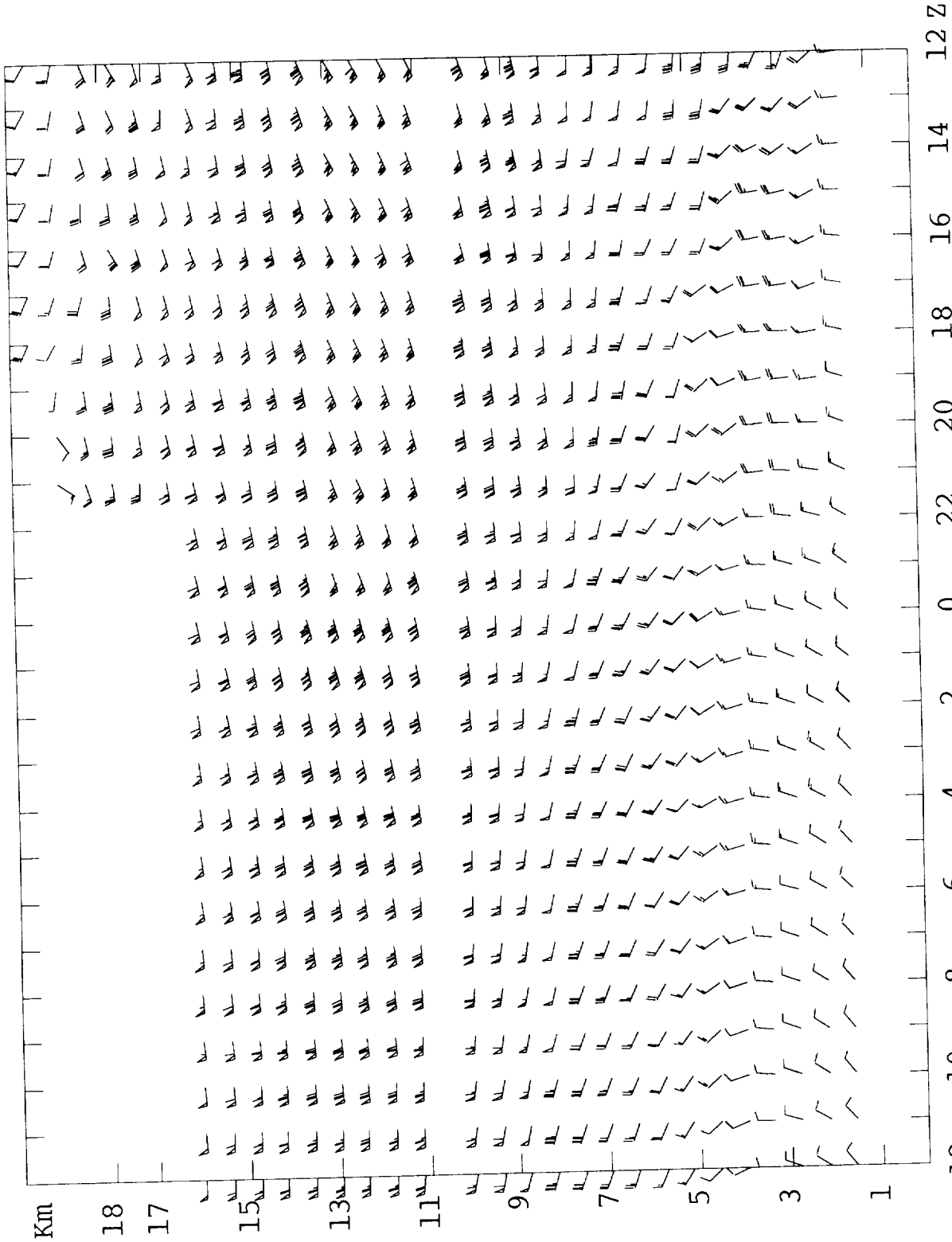

Figure 11. Time-height section of low-resolution winds, after missing or flagged data points have been replaced. Wind vectors are in knots.

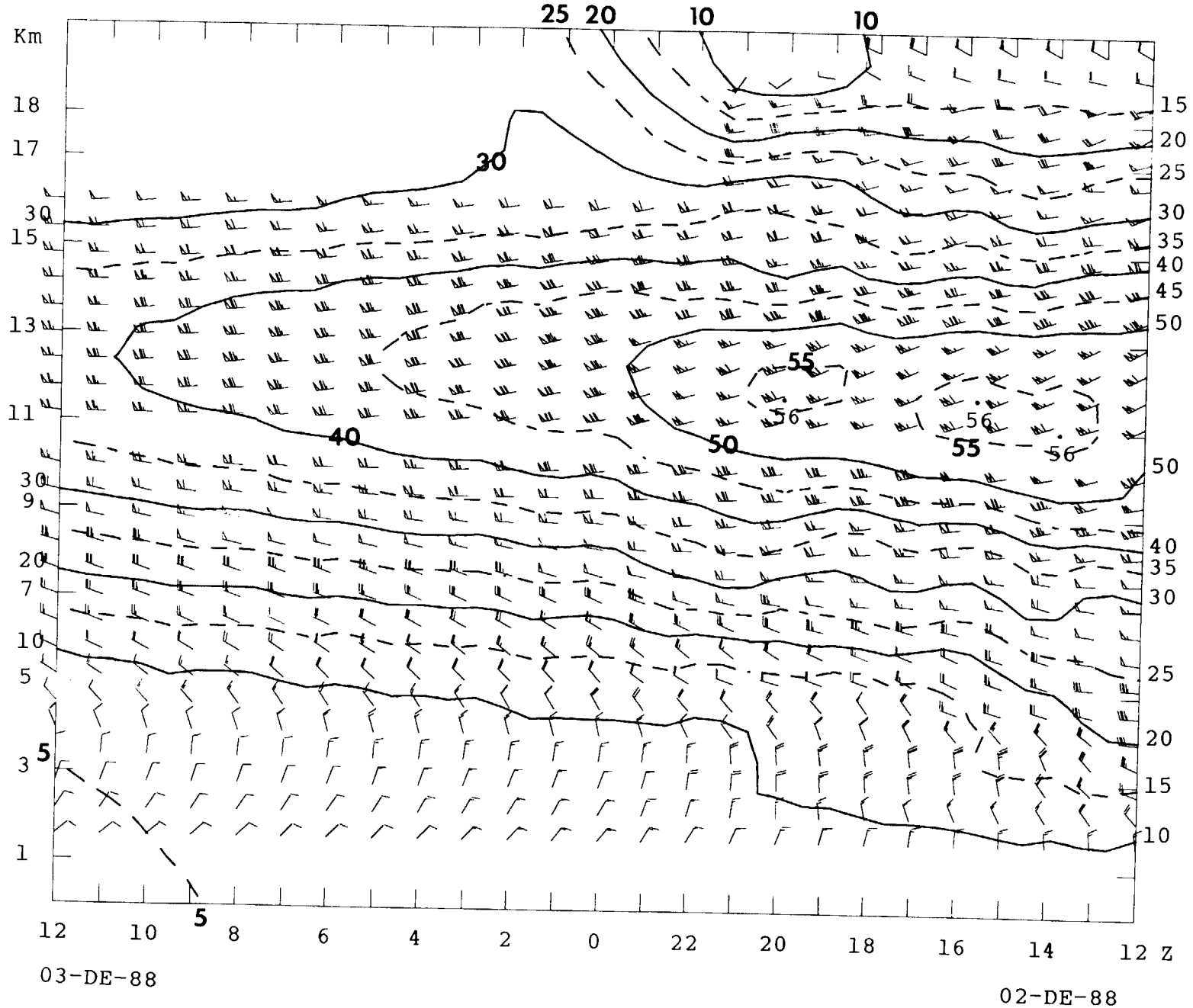

Figure 12. Time-height section of low-resolution wind speeds (m/s), after missing or flagged data points have been replaced.

TABLE 3.

KSC WIND PROFILER DATA, INTERPOLATED "PSEUDO-SOUNDING" DATA BASED UPON NGM INITIAL ANALYSES AT 0000 UTC 2 DECEMBER 1988, AND THE DIFFERENCE BETWEEN THEIR VALUES AT THE WIND PROFILER LEVELS.

00021288 PROFILER			NGM "SOUNDING"			DIFFERENCE	
HGT	WDR	WSP	HGT	WDR	WSP	DDIR	DSPD
1.89	-999.9	-999.99	1.89	287.7	23.57	-999.9	-999.99
2.05	-999.9	-999.99	2.05	282.9	25.48	-999.9	-999.99
2.19	-999.9	-999.99	2.19	279.3	27.28	-999.9	-999.99
2.35	-999.9	-999.99	2.35	275.7	29.44	-999.9	-999.99
2.49	-999.9	-999.99	2.49	273.0	31.42	-999.9	-999.99
2.64	259.3	38.63	2.64	270.5	33.61	-11.2	5.02
2.80	-999.9	-999.99	2.80	268.1	36.00	-999.9	-999.99
2.94	263.4	41.18	2.94	266.3	38.14	-2.9	3.04
3.10	266.8	44.36	3.10	264.5	40.63	2.3	3.74
3.24	265.8	46.10	3.24	263.9	41.95	1.9	4.15
3.39	265.1	47.85	3.39	263.6	43.06	1.5	4.80
3.55	265.6	49.26	3.55	263.3	44.24	2.3	5.02
3.69	265.4	49.80	3.69	263.0	45.28	2.4	4.52
3.85	264.5	50.10	3.85	262.8	46.47	1.7	3.63
3.99	263.6	50.49	3.99	262.5	47.50	1.1	2.98
4.14	262.6	50.37	4.14	262.3	48.62	0.3	1.75
4.30	264.4	50.02	4.30	262.1	49.81	2.3	0.21
4.45	264.3	48.59	4.45	261.8	50.92	2.5	-2.33
4.59	263.0	47.78	4.59	261.6	51.96	1.4	-4.19
4.74	260.3	46.90	4.74	261.4	53.08	-1.1	-6.18
4.89	258.7	47.19	4.89	261.3	54.20	-2.6	-7.01
5.05	256.9	49.78	5.05	261.1	55.39	-4.2	-5.61
5.20	257.8	49.35	5.20	260.9	56.51	-3.1	-7.16
5.34	256.4	53.00	5.34	260.7	57.55	-4.3	-4.55
5.49	253.3	57.12	5.49	260.6	58.67	-7.3	-1.56
5.64	253.5	61.09	5.64	260.4	59.79	-6.9	1.30
5.80	254.1	63.61	5.80	260.2	60.98	-6.1	2.63
5.95	256.3	64.31	5.95	259.5	61.92	-3.2	2.39
6.09	257.7	66.18	6.09	258.9	62.82	-1.2	3.37
6.24	257.2	66.75	6.24	258.3	63.78	-1.1	2.97
6.40	257.1	66.81	6.40	257.6	64.82	-0.5	1.99
6.55	257.4	68.31	6.55	257.0	65.80	0.4	2.51
6.70	257.4	69.32	6.70	256.4	66.79	1.0	2.54
6.85	254.4	70.10	6.85	255.8	67.78	-1.4	2.32
7.00	252.4	71.64	7.00	255.2	68.78	-2.8	2.86
7.15	251.1	72.91	7.15	254.7	69.79	-3.6	3.12
7.30	250.0	73.48	7.30	254.2	70.81	-4.2	2.67
7.45	250.1	74.70	7.45	253.6	71.83	-3.5	2.88
7.60	249.7	76.26	7.60	252.9	72.90	-3.2	3.37
7.75	249.0	75.93	7.75	252.1	73.98	-3.1	1.95
7.90	249.9	76.19	7.90	251.3	75.08	-1.4	1.10
8.05	250.7	77.30	8.05	250.6	76.20	0.1	1.10
8.20	251.7	78.62	8.20	249.9	77.32	1.8	1.30
8.35	251.6	80.94	8.35	249.2	78.46	2.4	2.48
8.50	252.7	82.64	8.50	248.5	79.61	4.2	3.03
8.65	251.9	82.93	8.65	247.9	80.77	4.0	2.17
8.80	250.9	85.16	8.80	247.2	81.94	3.7	3.22
8.95	249.6	86.19	8.95	246.6	83.12	3.0	3.07
9.10	248.3	86.95	9.10	246.0	84.31	2.3	2.64
9.25	247.1	88.00	9.25	245.4	85.50	1.7	2.50

TABLE 3, Cont'd.

9.40	245.9	88.71	9.40	244.9	86.71	1.0	2.00
9.55	246.9	87.26	9.55	244.3	87.83	2.6	-0.57
9.70	246.7	91.07	9.70	243.7	88.48	3.0	2.58
9.85	-999.9	-999.99	9.85	243.2	89.15	-999.9	-999.99
10.00	243.8	89.76	10.00	242.6	89.82	1.2	-0.06
10.15	-999.9	-999.99	10.15	242.0	90.50	-999.9	-999.99
10.30	-999.9	-999.99	10.30	241.5	91.19	-999.9	-999.99
10.45	-999.9	-999.99	10.45	241.0	91.89	-999.9	-999.99
10.60	245.4	94.54	10.60	240.4	92.59	5.0	1.95
11.20	-999.9	-999.99	11.20	239.2	94.11	-999.9	-999.99
11.80	245.2	94.69	11.80	238.2	95.14	7.0	-0.44
12.40	239.3	104.99	12.40	237.8	95.43	1.5	9.56
13.00	240.9	106.47	13.00	238.6	94.08	2.3	12.39
13.60	241.5	104.31	13.60	239.5	92.74	2.0	11.56
14.20	244.9	93.70	14.20	240.3	88.10	4.6	5.60
14.80	252.7	73.83	14.80	241.3	77.67	11.4	-3.84
15.40	243.7	68.58	15.40	242.7	67.26	1.0	1.32
16.00	-999.9	-999.99	16.00	244.5	56.91	-999.9	-999.99

Mean 0.1 degrees, 1.9 kts (1.0 m/s)
RMS 3.7 degrees, 3.8 kts (1.9 m/s)

Values of -999.99 and -999.9 indicate missing or flagged wind profiler data. NGM data were available at mandatory levels at 2.5 x 2.5 degree latitude-longitude intervals.

TABLE 4.

KSC WIND PROFILER DATA, INTERPOLATED "PSEUDO-SOUNDING" DATA BASED UPON NGM INITIAL ANALYSES AT 1200 UTC 2 DECEMBER 1988, AND THE DIFFERENCE BETWEEN THEIR VALUES AT THE WIND PROFILER LEVELS.

12021288 PROFILER			NGM "SOUNDING"			DIFFERENCE	
HGT	WDR	WSP	HGT	WDR	WSP	DDIR	DSPD
1.89	-999.9	-999.99	1.89	336.7	16.79	-999.9	-999.99
2.05	-999.9	-999.99	2.05	327.8	17.34	-999.9	-999.99
2.19	-999.9	-999.99	2.19	320.7	18.14	-999.9	-999.99
2.35	-999.9	-999.99	2.35	313.3	19.36	-999.9	-999.99
2.49	297.2	26.95	2.49	307.7	20.66	-10.5	6.29
2.64	294.9	24.71	2.64	302.5	22.25	-7.6	2.46
2.80	-999.9	-999.99	2.80	297.7	24.12	-999.9	-999.99
2.94	292.1	26.29	2.94	294.1	25.87	-2.0	0.42
3.10	295.3	29.11	3.10	290.5	27.98	4.8	1.13
3.24	299.0	31.82	3.24	288.8	29.11	10.2	2.72
3.39	297.2	33.42	3.39	287.3	30.14	9.9	3.29
3.55	291.3	36.41	3.55	285.8	31.25	5.5	5.15
3.69	285.1	37.50	3.69	284.6	32.25	0.5	5.25
3.85	278.1	38.55	3.85	283.3	33.40	-5.2	5.15
3.99	274.5	40.29	3.99	282.2	34.43	-7.7	5.86
4.14	273.8	43.33	4.14	281.1	35.54	-7.3	7.79
4.30	275.2	46.59	4.30	280.0	36.73	-4.8	9.85
4.45	275.3	45.57	4.45	279.1	37.87	-3.8	7.70
4.59	275.2	43.84	4.59	278.2	38.93	-3.0	4.90
4.74	276.6	42.94	4.74	277.4	40.08	-0.8	2.85
4.89	276.1	42.69	4.89	276.6	41.24	-0.5	1.44
5.05	275.6	43.49	5.05	275.8	42.49	-0.2	1.00
5.20	276.6	46.68	5.20	275.1	43.66	1.5	3.02
5.34	277.2	49.98	5.34	274.4	44.76	2.8	5.21
5.49	278.9	51.81	5.49	273.8	45.95	5.1	5.86
5.64	279.3	52.51	5.64	273.2	47.14	6.1	5.37
5.80	279.4	50.35	5.80	272.5	48.42	6.9	1.93
5.95	279.8	51.66	5.95	271.6	49.63	8.2	2.02
6.09	280.5	52.24	6.09	270.9	50.78	9.6	1.46
6.24	277.4	52.79	6.24	270.1	52.01	7.3	0.77
6.40	275.1	54.07	6.40	269.2	53.34	5.9	0.73
6.55	272.9	52.83	6.55	268.5	54.59	4.4	-1.77
6.70	-999.9	-999.99	6.70	267.8	55.86	-999.	-999.99
6.85	275.8	54.80	6.85	267.2	57.13	8.6	-2.33
7.00	-999.9	-999.99	7.00	266.5	58.41	-999.9	-999.99
7.15	-999.9	-999.99	7.15	265.9	59.69	-999.9	-999.99
7.30	-999.9	-999.99	7.30	265.3	60.98	-999.9	-999.99
7.45	-999.9	-999.99	7.45	264.7	62.33	-999.9	-999.99
7.60	270.7	53.06	7.60	263.7	64.27	7.0	-11.21
7.75	270.2	53.64	7.75	262.8	66.24	7.4	-12.59
7.90	266.7	57.60	7.90	261.9	68.22	4.8	-10.61
8.05	269.2	63.38	8.05	261.1	70.21	8.1	-6.84
8.20	266.3	70.96	8.20	260.3	72.22	6.0	-1.26
8.35	264.0	79.07	8.35	259.5	74.25	4.5	4.83
8.50	261.4	85.51	8.50	258.8	76.28	2.6	9.23
8.65	260.1	95.22	8.65	258.2	78.33	1.9	16.89
8.80	258.2	92.31	8.80	257.5	80.38	0.7	11.93
8.95	-999.9	-999.99	8.95	256.9	82.45	-999.9	-999.99
9.10	-999.9	-999.99	9.10	256.3	84.53	-999.9	-999.99
9.25	-999.9	-999.99	9.25	255.8	86.61	-999.9	-999.99

TABLE 4, Cont'd.

9.40	260.0	97.31	9.40	255.3	88.70	4.7	8.61
9.55	-999.9	-999.99	9.55	254.6	90.33	-999.9	-999.99
9.70	-999.9	-999.99	9.70	253.5	91.27	-999.9	-999.99
9.85	-999.9	-999.99	9.85	252.5	92.24	-999.9	-999.99
10.00	260.8	101.60	10.00	251.6	93.23	9.2	8.36
10.15	-999.9	-999.99	10.15	250.6	94.25	-999.9	-999.99
10.30	-999.9	-999.99	10.30	249.7	95.30	-999.9	-999.99
10.45	-999.9	-999.99	10.45	248.7	96.37	-999.9	-999.99
10.60	-999.9	-999.99	10.60	247.9	97.47	-999.9	-999.99
11.20	-999.9	-999.99	11.20	245.6	99.14	-999.9	-999.99
11.80	-999.9	-999.99	11.80	243.8	100.12	-999.9	-999.99
12.40	242.4	110.60	12.40	243.3	99.50	-0.9	11.10
13.00	241.5	106.04	13.00	245.2	96.10	-3.7	9.95
13.60	250.4	95.18	13.60	247.2	92.80	3.2	2.38
14.20	258.7	91.77	14.20	248.5	86.53	10.2	5.24
14.80	268.3	84.59	14.80	248.8	76.04	19.5	8.55
15.40	265.6	64.82	15.40	249.2	65.56	16.4	-0.74
16.00	249.8	55.22	16.00	249.7	55.08	0.1	0.14

Mean 3.2 degrees, 3.3 kts (1.7 m/s)
RMS 6.2 degrees, 5.8 kts (3.0 m/s)

Values of -999.99 and -999.9 indicate missing or flagged wind profiler data. NGM data were available at mandatory levels at 2.5 x 2.5 degree latitude-longitude intervals.

1.9 m/s (3.8 kts) at 0000 UTC, respectively, and 3.0 m/s (5.8 kts) and 3.0 m/s (5.8 kts) at 1200 UTC. These values are quite small--especially at 0000 UTC--and are comparable to differences between wind profilers and co-located rawinsonde releases tabulated by Thomson and Williams (1990).

It must be pointed out that the differences of Tables 3 and 4 should not be interpreted as wind profiler errors. Instead, it should be recognized that differences of this magnitude easily fall within the expected rawinsonde measurement errors at these wind speeds. Furthermore, the differences easily fall within the known errors of the first-guess fields (12h forecasts used as a starting point for the initial analysis) used as part of the data analysis procedure at NMC. In view of the small magnitudes of the differences, and since KSC wind profiler data were not used as a part of the NGM initial analyses, the high degree of agreement between the data sets lends confidence to both the wind profiler measurements and to the use of NGM-based pseudo-soundings when and where actual data was missing.

Table 5 gives statistics on how often profiler data had to be vertically or temporally interpolated or replaced by pseudo-sounding data, for a sample of the 37h period used in computation of the mean velocities over KSC. While there are quite a few data dropouts, it should be pointed out that this wind profiler was only in place temporarily at KSC, until a specially designed system could be built and installed.

TABLE 5

KSC WIND PROFILER DATA STATISTICS, AFTER SUBJECTIVE EDITING FOR QUALITY CONTROL, 0000 - 2100 UTC 2 DECEMBER 1988

Level	Height	% Good	Level	Height	% Good
1	1.89	0	35	7.00	77
2	2.05	0	36	7.15	45
3	2.19	0	37	7.30	32
4	2.35	0	38	7.45	45
5	2.49	14	39	7.60	82
6	2.64	41	40	7.75	59
7	2.80	45	41	7.90	50
8	2.94	36	42	8.05	50
9	3.10	36	43	8.20	95
10	3.24	64	44	8.35	41
11	3.39	64	45	8.50	41
12	3.55	77	46	8.65	59
13	3.69	95	47	8.80	86
14	3.85	95	48	8.95	64
15	3.99	100	49	9.10	59
16	4.14	82	50	9.25	50
17	4.30	82	51	9.40	55
18	4.45	82	52	9.55	36
19	4.59	91	53	9.70	18
20	4.74	86	54	9.85	5
21	4.89	91	55	10.00	59
22	5.05	82	56	10.15	5
23	5.20	86	57	10.30	5
24	5.34	91	58	10.45	0
25	5.49	95	59	10.60	73
26	5.64	95	60	11.20	64
27	5.80	95	61	11.80	27
28	5.95	91	62	12.40	77
29	6.09	82	63	13.00	95
30	6.24	86	64	13.60	100
31	6.40	73	65	14.20	100
32	6.55	73	66	14.80	77
33	6.70	59	67	15.40	86
34	6.85	55	68	16.00	41

3. ANALYSIS OF THE CASE OF 2 DECEMBER 1988--SPACE SHUTTLE LAUNCH STS27

3.1 An Overview

As has been stated previously, the main features of interest on 2 December across the southeastern United States were a strong jet stream and associated upper-level front. These features were drifting eastward (from about 285 degrees) at a speed of about 17 m/s (see Fig. 5 for variations with location). At low levels, high pressure and cold advection dominated the Southeast, and the area was devoid of precipitation. The surface cold front ushering in the cold air had pushed as far southeast as eastern Cuba.

Figure 13 illustrates the translation of the 40 m/s isotach of the jet stream at 300 mb (about 9 km) across Florida between 1200 UTC 2 December and 0000 UTC 3 December 1988, based upon NGM analyses. The dashed isotach for 1800 UTC was obtained by interpolation between the 1200 and 0000 UTC positions. It can be seen that the axis of the jet stream was near KSC during most of the 12-hour period, and crossed KSC at or shortly before 1800 UTC.

The other lobe of 40 m/s velocities which travelled across West Virginia and Virginia in Fig. 13, was in a current of air that originated much farther to the north in a "northern branch" jet stream which headed southeastward. This airstream approached the jet stream confluence zone along the Atlantic Coast and slowed as it turned cyclonically, first eastward, and finally northeastward, before accelerating northeastward as a part of the "southern branch" jet stream whose "tail" extended southwestward over Florida.

It can easily be visualized that KSC was in the confluent entrance region of the jet stream, whose velocity maximum was centered farther to the east-northeast, over the Atlantic. This helps explain why wind speeds in Figs. 9-12 were decreasing, or at best constant, during this period: the speed increases which would have occurred as the axis of the jet approached

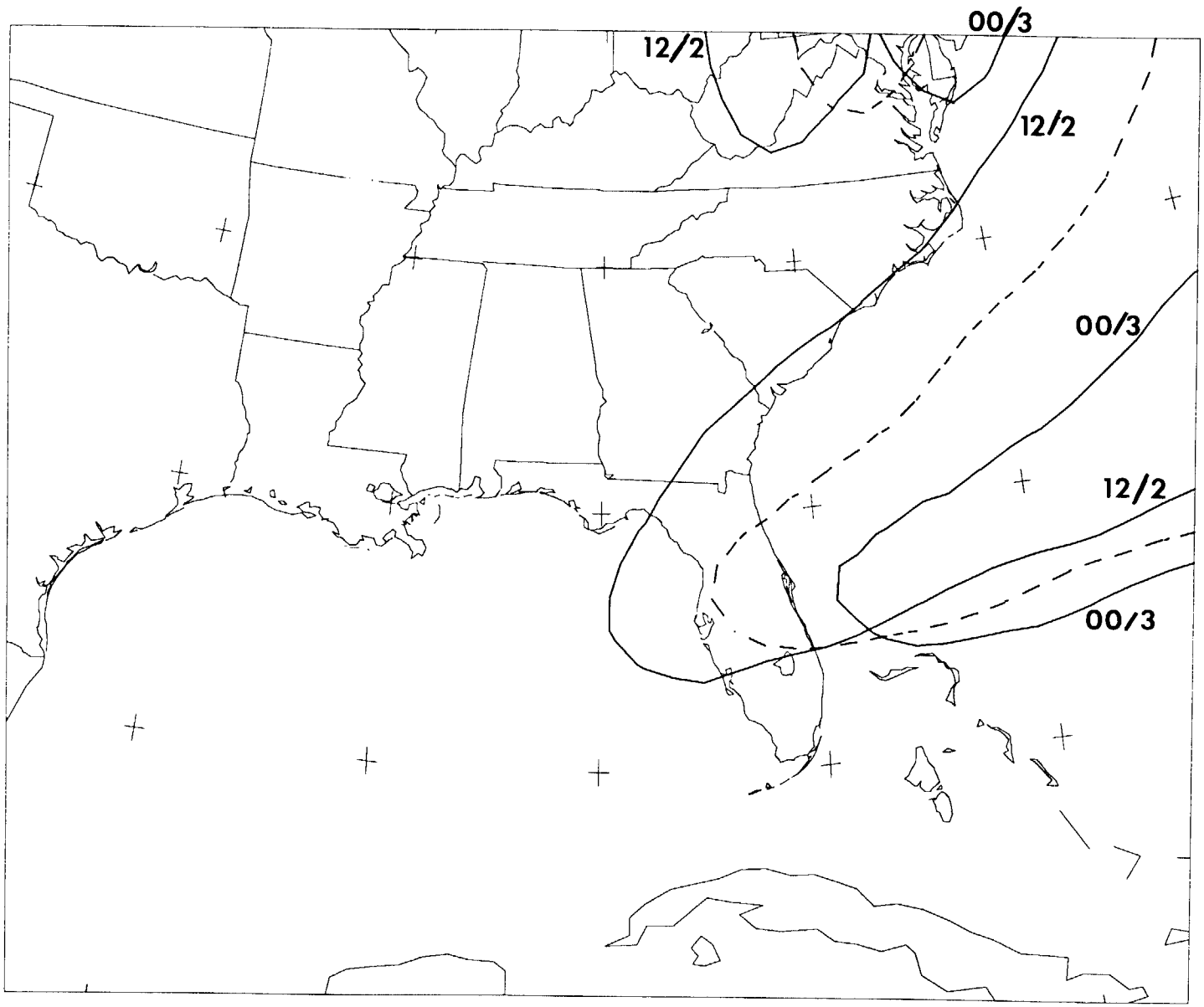

Figure 13. Movement of the 40 m/s isotach across KSC at 300 mb between 1200 UTC 2 December and 0000 UTC 3 December 1988. Based upon NGM analysis data.

were being offset by the drifting away of the wind speed maximum well to the east-northeast. Thus, KSC was becoming farther away from the jet core, and more and further into the lower-wind-speed "tail" portion of the jet stream. This type of situation is difficult to interpret from wind profiler time-height sections alone, and can only be fully deciphered by use of companion horizontal analyses.

Figure 14 shows the sounding from Apalachicola, FL at 1200 UTC 2 December 1988. This station was upstream of KSC at this time, and is characteristic of what a sounding ~100 km north of KSC would have been expected to look like at 1800-1900 UTC. Strong vertical wind shears are present at a number of levels, especially near 10.5 and 13.5 km (about 35 kft, 250 mb; 44 kft, 160 mb, respectively). The lowest static stability within a layer of strong vertical wind shear occurs near 350 mb (potential temperature increase of 2.62 K/km; near 8.5 km), but static stabilities are only moderate through about 177 mb (12.85 km). Table 6 shows values of Richardson number (Ri) that accompany Fig. 14. Lowest values of Ri are found near 10.5 km (about 34.5 kft; 255 mb). While none of the layers of Table 6 reach the theoretical critical value of 0.25, layers having values below 1.0 are likely to have episodes of turbulence.

Figure 15 shows the sounding from Tampa, FL at 1200 UTC 2 December. This station was upstream of KSC at this time, and is characteristic of what a sounding ~50 km south of KSC would have been expected to look like at 1500-1600 UTC. Strong winds and shears are evident, with strongest vertical wind shear near 8 km. Static stabilities are low at several levels: near 750, 500, 300, and 250 mb. Table 7 gives the Richardson number values corresponding to Fig. 15. The lowest value, 0.21, is found near 8.08 km (about 27.5 kft; 365 mb), and values below 1.0 are present at two other widely

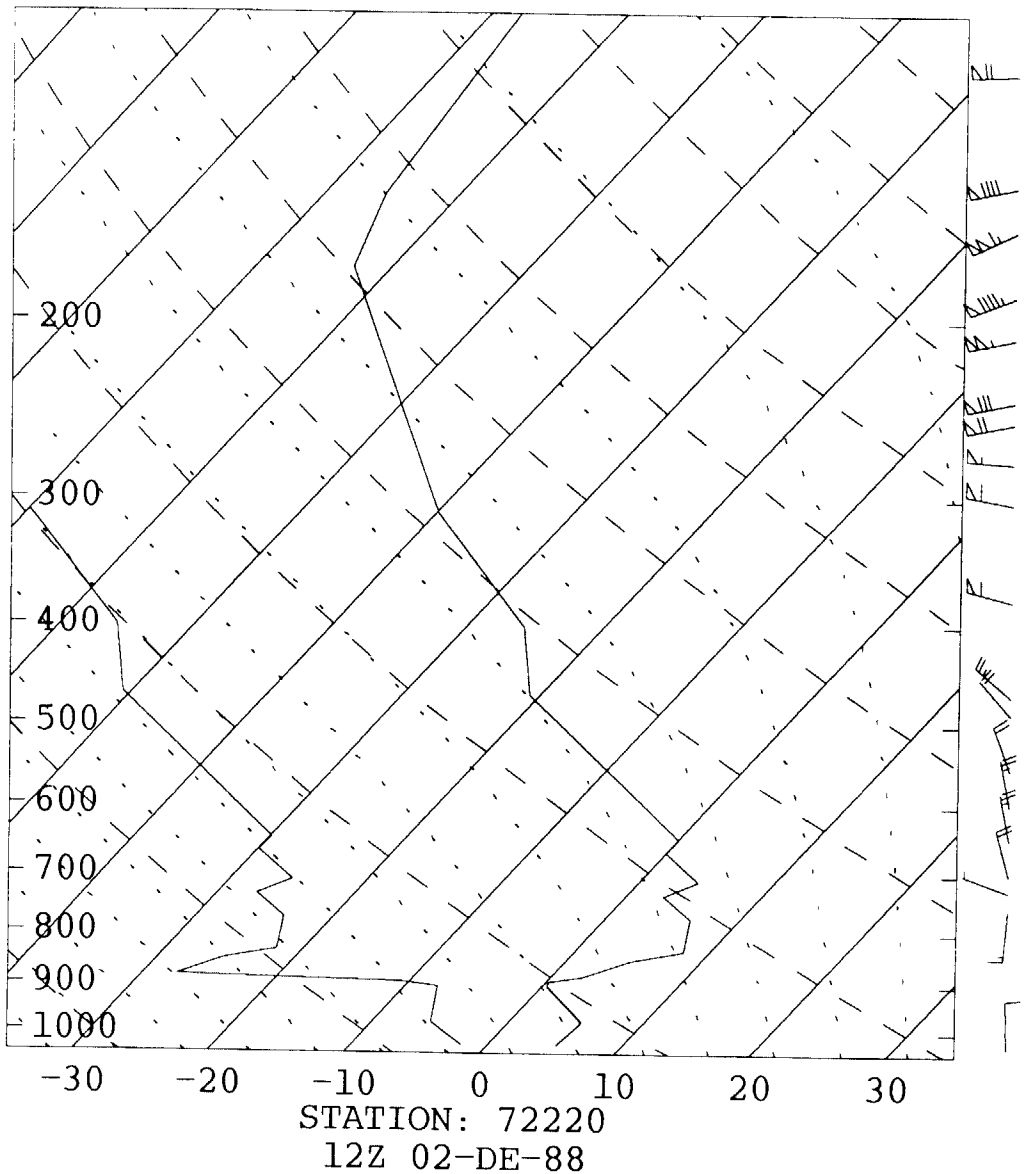

P	T	TD	RH	HT	WS	WD
100	-67			980	45	270
150	-65			920	25	255
177	-62			900	23	275
309	-39	-69	2	860	19	305
400	-25	-55	3	810	17	280
467	-20	-50	4	700	9	290
645	0	-30	8	660	14	285
664	0	-30	8	650	10	245
710	4	-25	8	610	19	280
733	2	-27	8	520	56	260
774	6	-23	9	500	69	270
830	8	-22	9	450	90	260
850	4	-25	8	420	114	245
881	2	-27	8	400	96	250
890	0	-10	43	370	106	260
902	0	-7	54	350	80	260
979	5	-5	44	330	69	260
1029	5	-2	60	310	56	275
				300	60	280
				250	62	285
				200	23	310
				180	20	320
				150	18	340
				130	23	350
				110	23	350
				100	18	345
				80	4	290
				70	15	185
				00	8	360

Figure 14. Sounding from Apalachicola, FL (72220) at 1200 UTC 2 December 1988.

TABLE 6

WIND SHEARS AND RICHARDSON NUMBERS AT MIDDLE AND UPPER-TROPOSPHERIC SIGNIFICANT LEVELS FROM THE 1200 UTC 2 DECEMBER 1988 RAWINSONDE AT APALACHICOLA, FL (72220)

Level (km)	Shear (m/s per km)	Richardson No.
6.86	13.12	1.21
10.06	10.94	1.27
10.52	18.51	0.44 *
11.13	14.58	0.70 *
11.89	8.41	2.09
12.65	10.09	1.46
13.41	20.19	0.82 *
14.48	7.07	3.66
15.70	7.29	7.58

* signifies that turbulence is likely

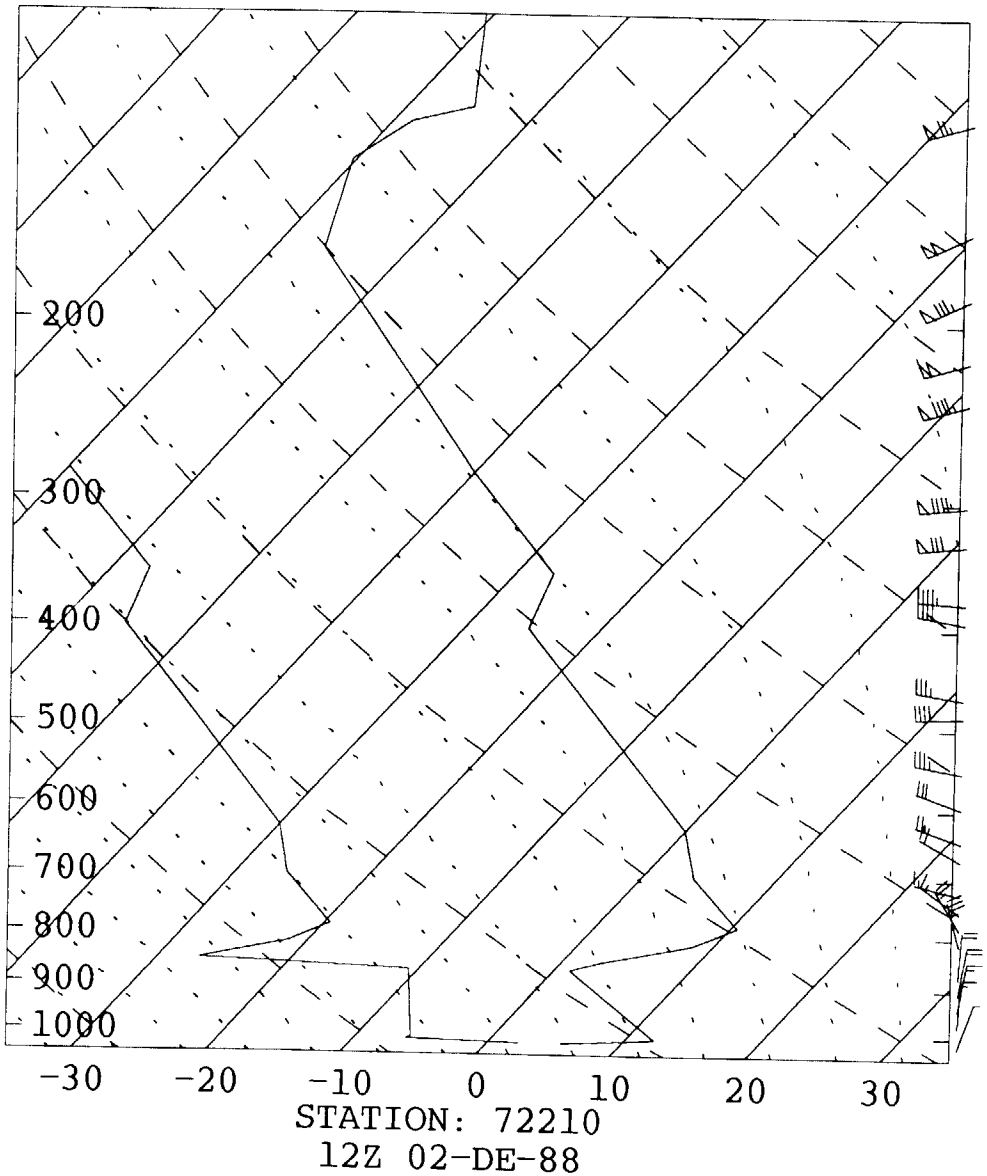

P	T	TD	RH	HT	WS	WD
100	-70			960	39	255
123	-65			950	45	255
127	-68			910	26	245
139	-70			900	36	255
170	-66			900	22	255
282	-39	-69	2	860	38	270
353	-27	-57	3	850	16	290
400	-25	-55	3	820	15	305
630	0	-30	8	800	23	285
700	3	-26	8	780	12	300
783	10	-19	10	770	11	285
816	8	-21	9	700	12	325
850	3	-27	8	650	10	245
867	1	-10	40	620	12	135
1009	12	-6	27	470	75	255
1015	10	-6	29	420	102	245
1025	5	2	79	400	87	245
				360	100	255
				350	95	255
				300	89	265
				270	81	265
				250	46	275
				230	38	280
				200	37	280
				180	38	270
				150	34	280
				130	30	290
				110	25	290
				100	19	300
				80	15	285
				70	16	305
				60	25	330
				50	34	345
				30	21	5
				20	19	10

Figure 15. Sounding from Tampa, FL (72210) at 1200 UTC 2 December 1988.

TABLE 7

WIND SHEARS AND RICHARDSON NUMBERS AT MIDDLE AND UPPER-TROPOSPHERIC SIGNIFICANT LEVELS FROM THE 1200 UTC 2 DECEMBER 1988 RAWINSONDE AT TAMPA, FL (72210)

Level (km)	Shear (m/s per km)	Richardson No.
1.52	10.94	6.35
2.29	15.14	0.40 *
7.47	13.46	1.70
8.08	38.28	0.21 **
8.84	6.73	1.58
11.73	7.29	1.30
12.65	8.41	0.98 *
13.87	9.09	3.44

* signifies that turbulence is likely
** indicates that turbulence is present, based upon theoretical critical Ri = 0.25

spaced levels: 2.29 and 12.65 km (about 7.5 and 41.5 kft; 780 and 190 mb, respectively).

It can be seen from the sounding diagrams (Figs. 14 and 15) that most of the layers of lowest Ri occurred just above inversions or stable layers, where a layer of strong vertical wind shear extended upward into a layer of reduced static stability. The rest occurred near the base of or just below a stable layer where a layer of strong vertical wind shear extended downward into a layer of reduced static stability.

Cross sections of potential temperature can assist in the interpretation of soundings; particularly with regard to the nature of stable layers. Figure 16 shows the orientation of two cross sections (constructed only from rawinsonde data at the sites shown by asterisks) at 1200 UTC 2 December 1988. The first, Figure 17, runs almost due N-S through Tampa, FL. This reveals that the strong inversion on Fig. 15 was affiliated with a lower-tropospheric frontal zone. The low Ri layer near 780 mb above Tampa was at the top (advancing/warm side) of the frontal zone. The stable layer near 400 mb represents the upper-level frontal zone, and the lowest Ri of the sounding occurred near the top (advancing/warm side) of this frontal zone.

The uppermost layer of low Ri (near 190 mb) above Tampa is more readily evaluated with respect to Figure 18, which is a cross section orientated basically NW-SE. The Apalachicola sounding is also a part of this cross section. The tropopause above these stations can readily be distinguished from the upper-level frontal zone on the cross section, and reveals that the tropopause above Tampa was at 170 mb, rather than one of the higher levels of Fig. 15. The low Ri values occurred just below, and at, the tropopause. As can be seen from Fig. 18, the lower portion of the stratosphere above Tampa was not particularly stable at altitudes below the 139 mb level.

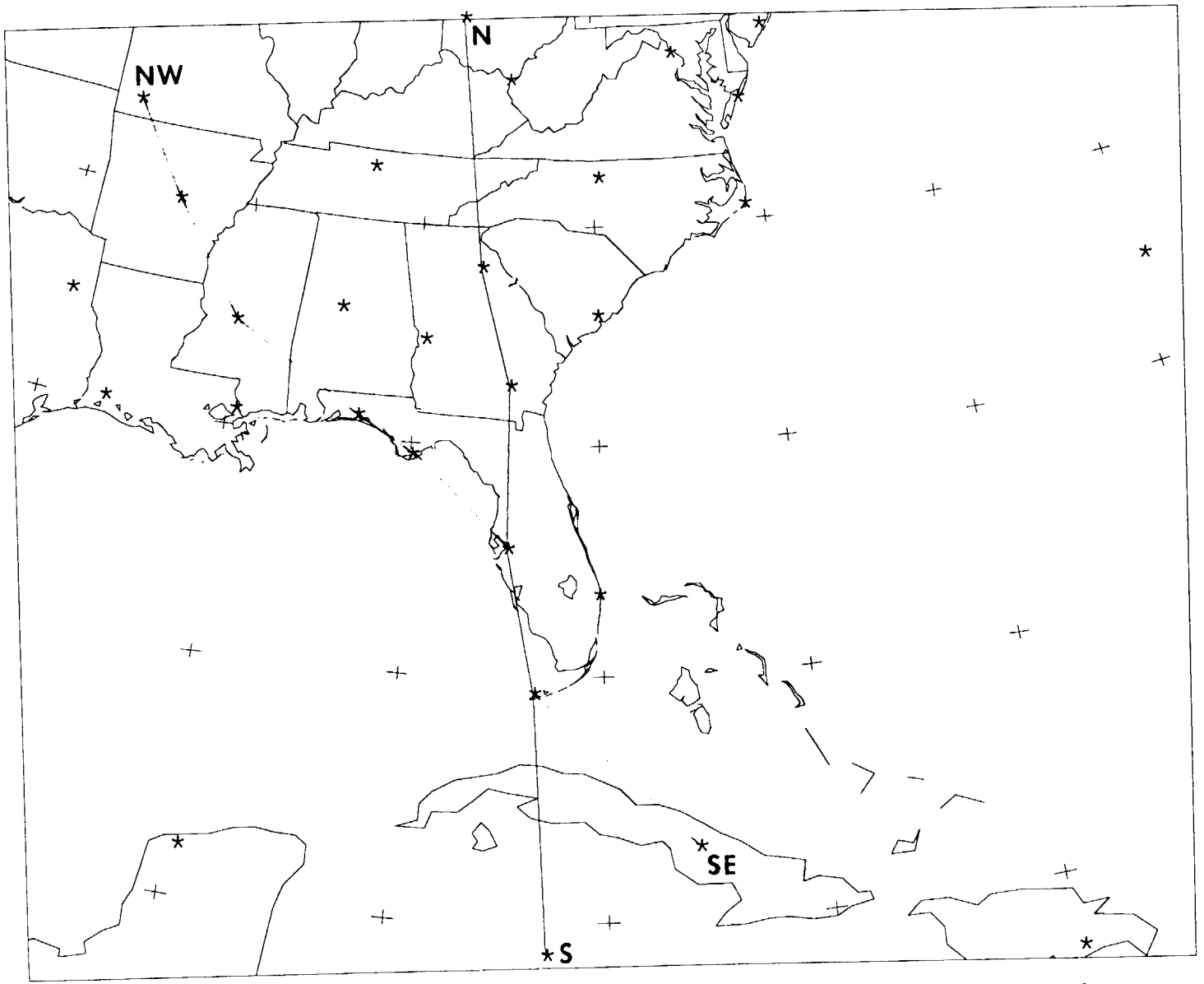

Figure 16. Mapping of the orientations of two cross sections, constructed from rawinsonde data at the sites shown by asterisks, at 1200 UTC 2 December 1988.

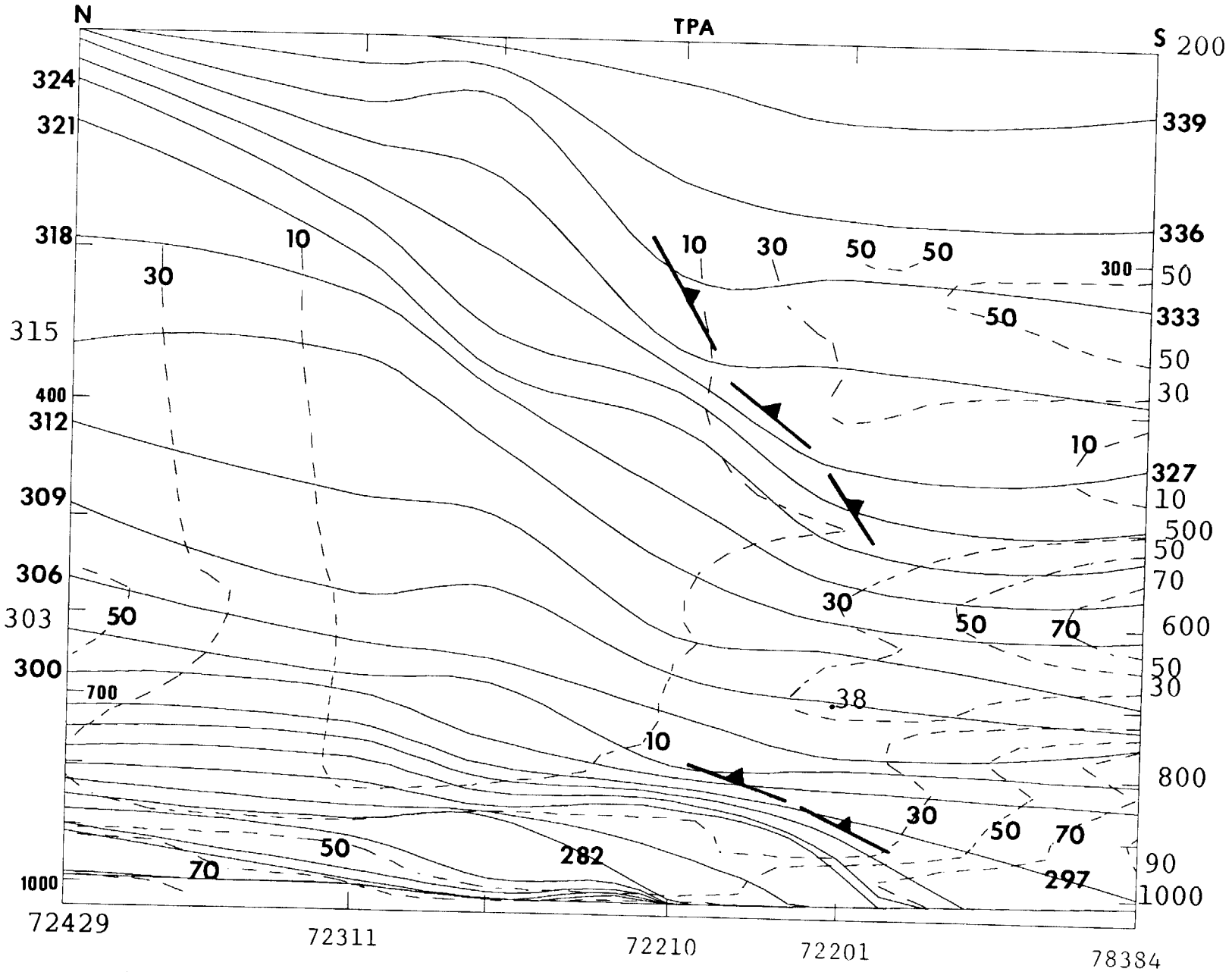

Figure 17. North-south cross section of Fig. 16. Solid lines are isopleths of potential temperature (K) and dashed lines are of relative humidity (%).

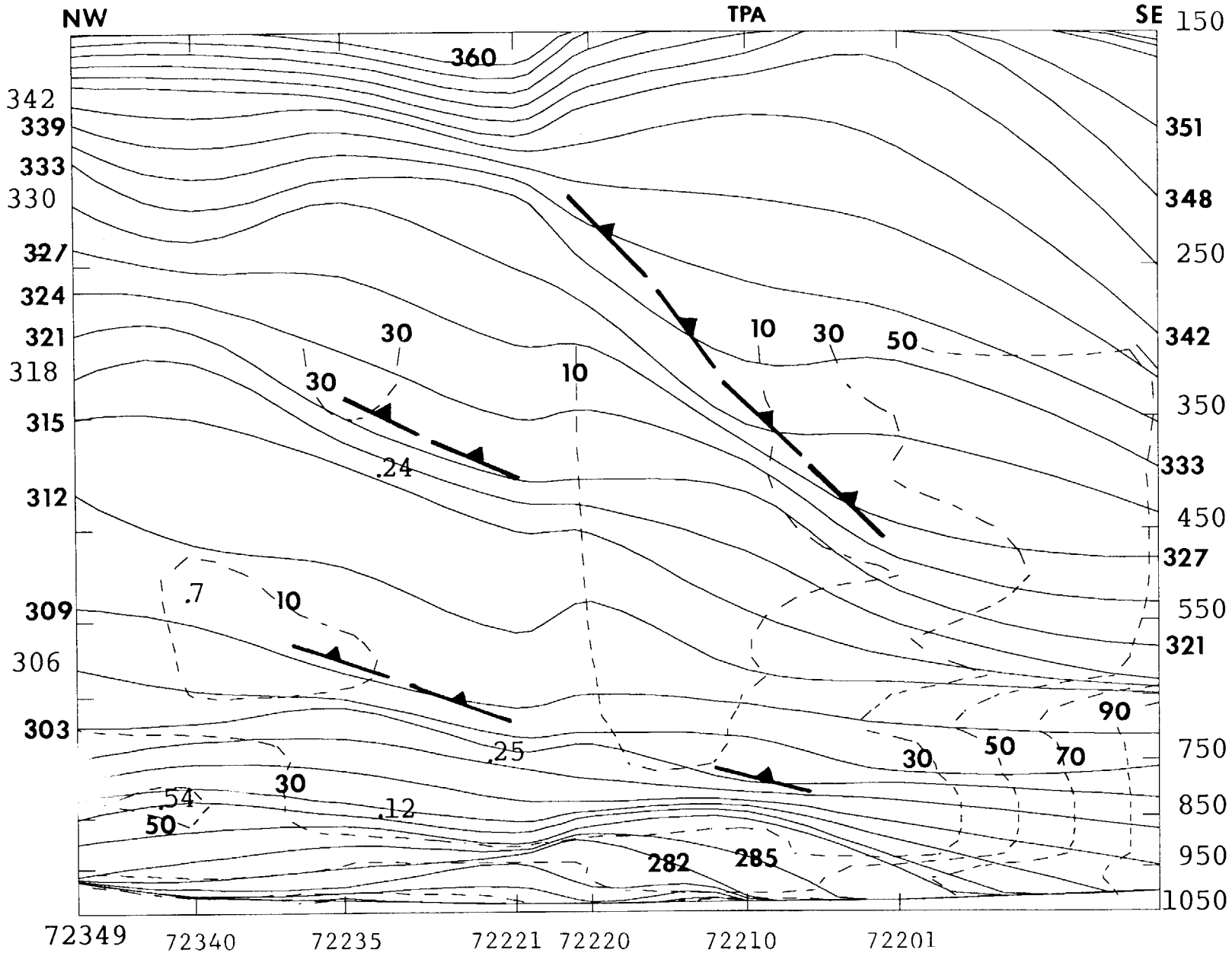

Figure 18. Northwest-southeast cross section of Fig. 16. Solid lines are isopleths of potential temperature (K) and dashed lines are of relative humidity (%).

The layer of lowest Ri above Apalachicola was found near the base (and trailing/cold side) of the upper-level frontal zone. The two other layers of nearly equal low Ri were centered near 230 and 160 mb. The first of these was at the top (and advancing/warm side) of the upper-level frontal zone, and the second was just above the tropopause.

An intercomparison of Figs. 14 and 18 is interesting, in that the stable layer near 450 mb above Apalachicola does not appear to be the main portion of the upper-level front. The leading edge of the main upper-level front is clearly located at about 240 mb. Instead, the stable layer at 450 mb appears to have formed within the lower portion of the upper-level frontal zone, and may represent a secondary frontogenesis that has occurred or is occurring there. Frontolysis may be occurring in the region near 350 mb, while the main front remains intact farther aloft. In any event, the low values of Ri are affiliated with the under-side of the top part of the frontal zone. This zone was not revealed by any notably stable layer in Fig. 14.

Given that the Space Shuttle was about to be launched from KSC, the presence of large vertical wind shears and possible clear-air turbulence are of obvious potential hazards. It is beyond the scope of this report to determine critical values of vertical wind shear and Richardson number that are of most relevance to the Shuttle. That assessment would require running sensitivity studies using NASA's "wind loads" program, which takes into consideration the size and characteristics of the Shuttle vehicle. In the case study which follows, the report focuses on layers having strong vertical wind shear, layers having Richardson numbers of about 3 or less, and on the atmospheric structure accompanying and adjacent to these layers.

Because there is an implicit steady-state assumption embedded within the time-space conversion procedure, an analysis time at 0600 or 1800 UTC turns

out to be preferable if 12-hour operational rawinsonde network data are to be used from both before and after the analysis time. Hence, most of the time-space conversion analyses of this report have been prepared for 1800 UTC 2 December 1988. This time was a bit more than 3 hours after the launch of STS27 at 1438 UTC. A few analyses are presented for 1400 and 1500 UTC 2 December.

As an aside, the steady-state assumption did not turn out to be a major limitation, as it often turned out that there were several data points within the radius of influence of a grid point. When one of these was from 1200 UTC and one was from the subsequent 0000 UTC, any non-steady nature of the travelling perturbation would show up in the form of a difference between the data values over a short distance. The weighting scheme (4) would then "average out" the discrepancy.

In one further aside, most of the analyses which follow present "raw" grid field values output from the time-space conversion scheme. The only smoothing which has been done is twofold. Horizontal fields of raw potential temperature often possessed minor, very-small-scale patterns linked to individual, adjacent data points. A filter was run over the potential temperature fields which would eliminate wavy patterns having wavelength less than 2.6 grid intervals. The other type of smoothing was even more minor, and involved cross-sections. When isopleths were oriented at angles of about 45 degrees on the cross sections, the lines tended to become a bit step-like as a consequence of the contouring scheme and the finite number of grid points. In such cases--for presentation only--one pass of a 1:4:1 smoothing function was run over the field to suppress the "step" tendency.

3.2 Time-Space Conversion Analyses at Selected Levels

The KSC wind profiler measured velocities of 54-56 m/s in the layer from 11 km to 13 km. Time-space conversion analyses yielded winds of 52-54 m/s at these altitudes, with the 2 m/s reduction apparently due to a small smoothing influence of some distant data points during the analysis. In the next few figures we shall examine the mechanics of the time-space-converted wind fields at the 13.0 km level.

Figure 19 shows the 36h mean velocity field at 13.0 km, with data points superimposed. By intercomparison with the rawinsonde sites of Fig. 2, it can be seen that wind vectors have not been plotted at a few of the sites, such as over Cuba and the northern Yucatan Peninsula. This indicates that data were missing at this level from one or more of the four 12-hour launch times. As discussed previously, the missing data was replaced with NGM-analysis-based data. At the regular latitude-longitude intersections over water, however, the means which are solely NGM-based have been plotted. While there are a few undulations in the isotachs that may be unreal artifacts of the analysis procedure, overall the pattern looks quite realistic. The persistence of the jet stream over the western Atlantic is evident.

Along-mean and cross-mean departures of the 1200 UTC 2 December and 0000 UTC 3 December observed velocities from this mean velocity (likewise, hourly velocities from the KSC wind profiler) were computed and displaced to their appropriate positions for an 1800 UTC analysis, using the steering velocity field of Fig. 5. There the departure components were added to the mean wind vector to obtain the total wind field, shown in Figure 20. The string of hourly KSC profiler winds are displaced slightly south so that the map position of KSC would not be obliterated. The gap in the 50 m/s isotach near 30N, 75W is most likely not real, and instead reveals the lack of data points

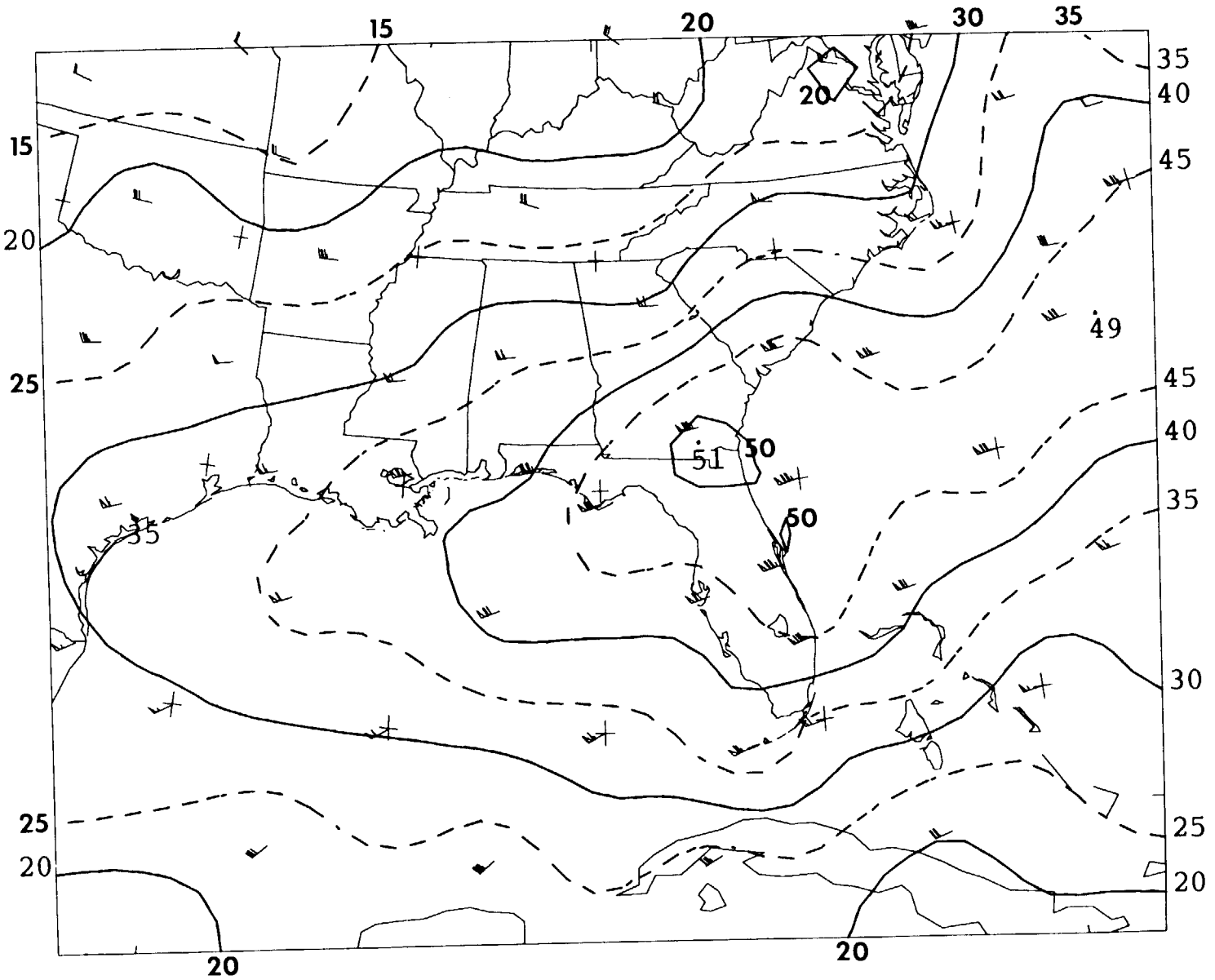

Figure 19. Mean winds at 13.0 km, 0000 UTC 2 December 1988 to 1200 UTC 3 December 1988. Isotachs are in m/s. Wind vectors represent contributing rawinsonde, profiler, and NGM data point locations and are in knots. A few data points are omitted where a mixture of rawinsonde and NGM-based data had to be used due to missing rawinsonde data.

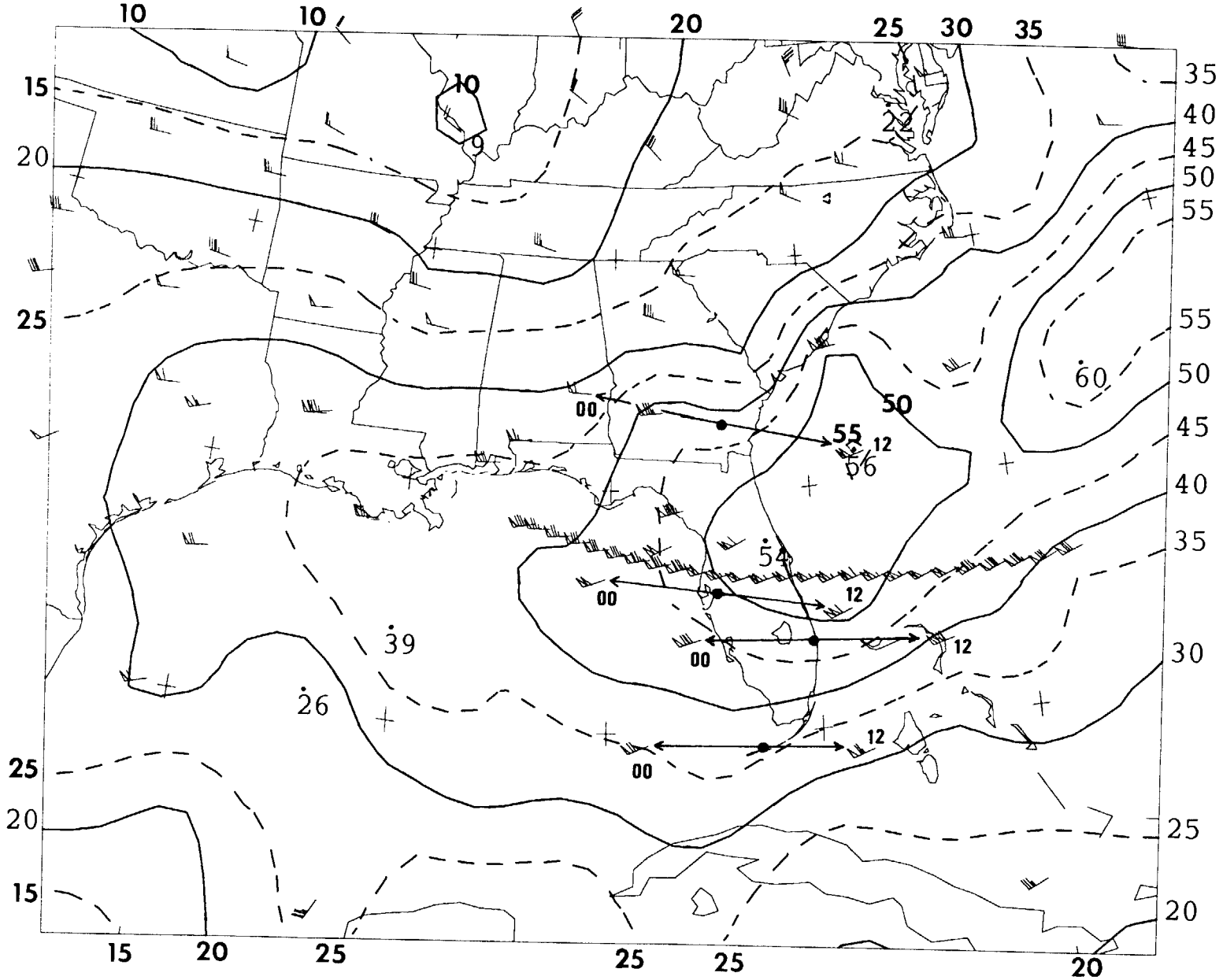

Figure 20. Total winds at 13.0 km, 1800 UTC 2 December 1988, based upon the time-space-conversion analysis. Isotachs are in m/s. Vectors represent contributing data points at their time-space-converted locations, and have speeds in knots.

near that position which would have added strongly to the mean winds there (which were probably wrongly analyzed as less than 50 m/s). A few sample displacement vectors are shown, such as the displaced positions of the Tampa, FL (72210) rawinsonde data. The two data points over FL to the west-northwest of KSC are from special 1400 and 1900 UTC rawinsonde releases at Valparaiso, FL (72221). A protrusion of the 50 m/s isotach toward coastal South Carolina may reveal that the actual isotach pattern was a bit broad there, at the location where was strong confluence between the northern-branch northwesterly flow and the southern-branch jet stream.

Figure 21 shows the perturbation wind field at 13.0 km. Here there are some apparent contradictions between the individual perturbation data points near 29N, 83W (northwest of Tampa, FL), which may reveal a bit of non-steady translation of the perturbation field. However, the overall perturbation velocity field is quite coherent, with primarily northeasterly perturbation velocities over the southeastern United States and southerlies or southwesterlies over the Caribbean.

Figure 22 reveals the perturbation velocity pattern better, in the form of streamlines. The apparent cyclonic wind shift across northern FL and near the coasts of GA, SC and NC is partly due to the presence of a trough there and partly due to the temporal changes of speeds that are occurring as the jet stream slides eastward. The latter factor appears to be particularly dominant in the section of profiler winds. West of FL--where the jet stream is moving away--speeds are now becoming slower than the mean; hence, in the direction opposite the mean winds (from the northeast). Over and just east of FL--where the jet stream axis is approaching--winds have become faster than the mean; hence, having components in the same direction as the jet stream.

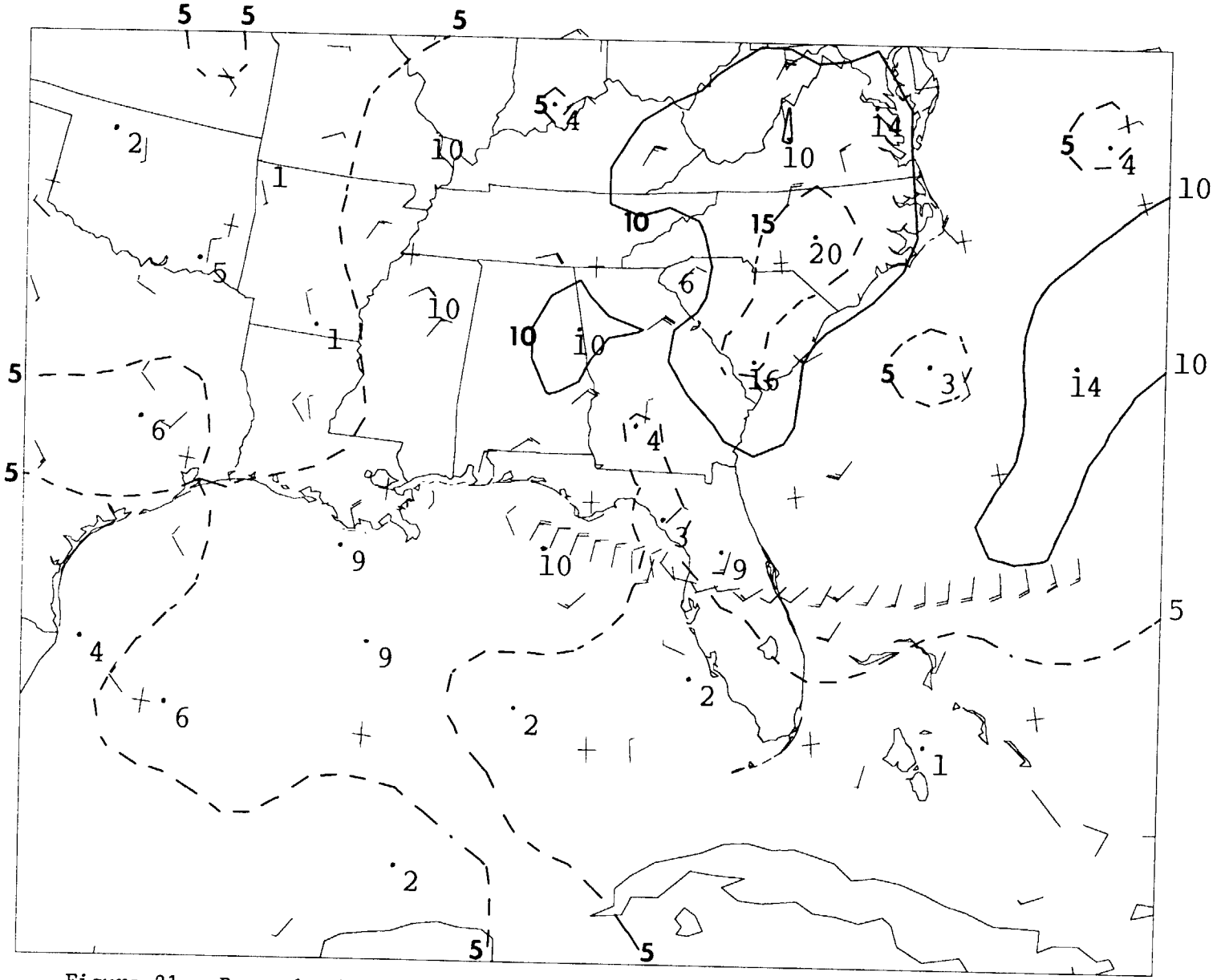

Figure 21. Perturbation velocities at 13.0 km, 1800 UTC 2 December 1988, based upon the time-space-conversion analysis. Isotachs are in m/s. Vectors represent contributing data points at their time-space-converted locations, and have speeds in knots.

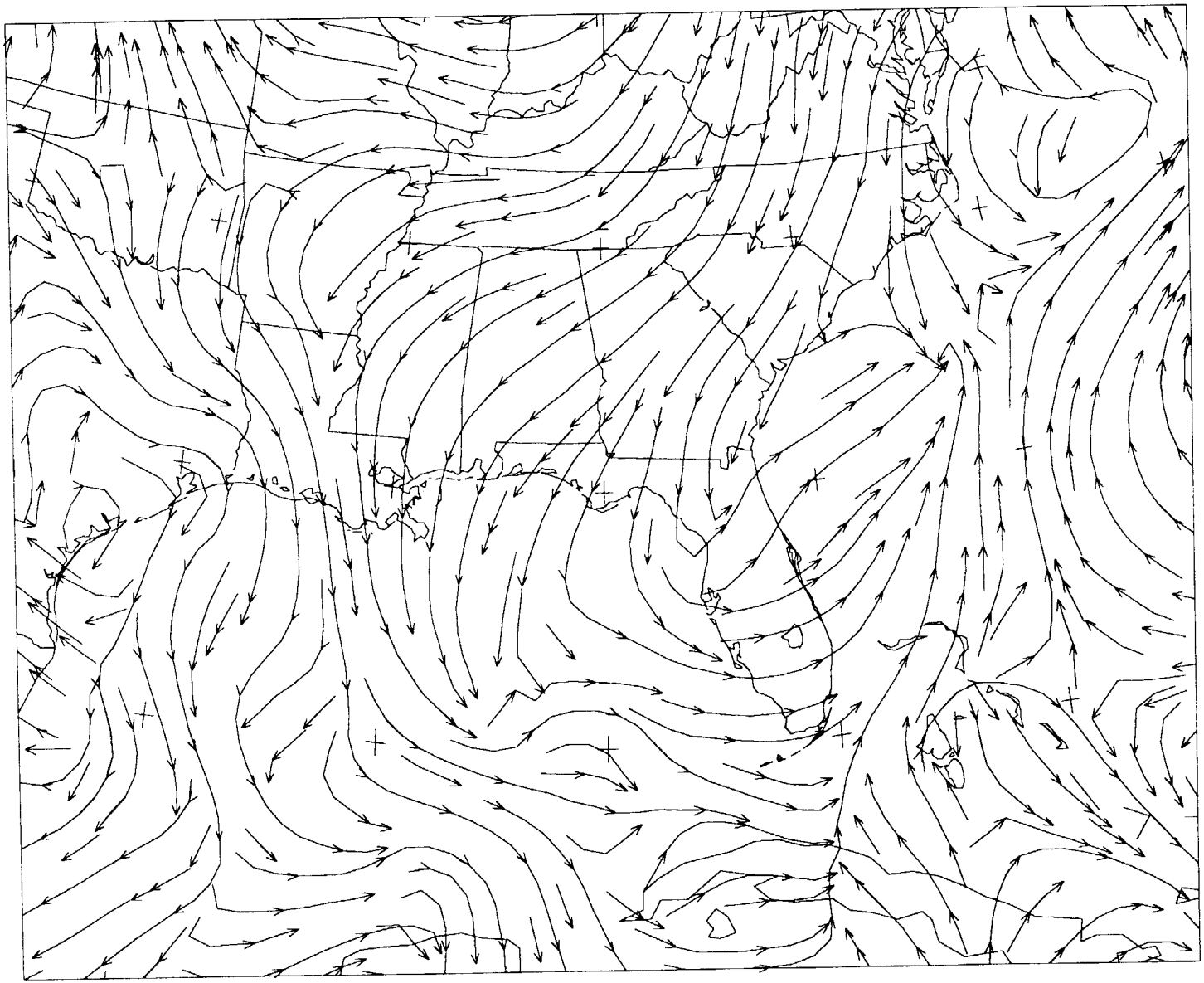

Figure 22. Streamlines of the perturbation velocity at 13.0 km, 1800 UTC 2 December 1988. A perturbation velocity trough line occurs on the northwest side of the axis of the jet stream of Fig. 20. Confluence toward the faster portions of the jet stream can also be noted.

Figure 23 shows the mean potential temperature pattern at 13.0 km. Western FL shows up as a cool pocket, with temperatures becoming progressively warmer toward the northeast. This pattern is as expected, since this altitude is near the level of maximum winds in the jet stream. At this altitude, the jet stream axis typically separates warm stratospheric temperatures (to the north) from cooler tropospheric temperatures (to the south). in view of the fact that the axis of the southern branch of the jet stream flows eastward from central FL toward the northeast (Fig. 21), the warm temperatures off the East Coast and cool temperatures south of latitude 30N are indicative of the higher tropopause south of the jet stream axis.

Using the rationale of the preceding paragraph, a possible discrepancy between rawinsonde-based means and NGM-based means emerges over the Gulf of Mexico. While the southern branch jet stream axis flows eastward along the Gulf Coast, the warm pocket near coastal AL unexpectedly extends across the jet stream axis into the central Gulf of Mexico. Values over this region are influenced solely by NGM-based data. Cooler temperatures once again appear where rawinsonde data is present over the Yucatan Peninsula. This is not meant to indicate that the NGM model is initialized improperly or makes poor predictions of the tropopause level. Instead, the most likely cause of the problem is that the set of NGM data used in this study was available only at mandatory levels (e.g., 200, 250, 300,... mb), which allowed considerable errors to be introduced via vertical interpolation between mandatory levels, especially in regions straddling the sloping tropopause. This problem could be avoided by obtaining higher-resolution NGM data, or by manual correction (bogusing) of the unrealistic portions of the analysis. These options were beyond the scope of this project.

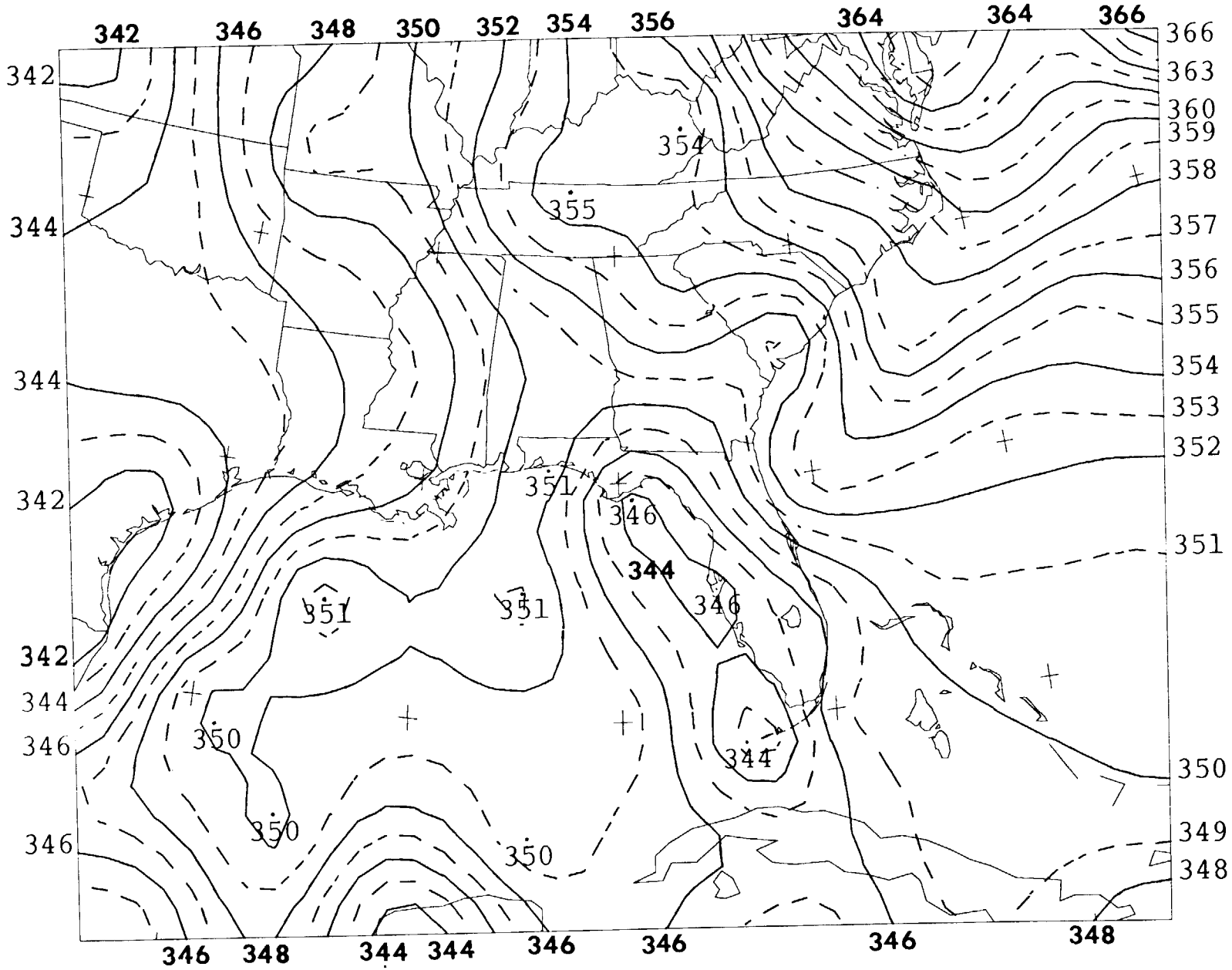

Figure 23. Isopleths of 36-hour mean potential temperature at 13.0 km, in degrees Kelvin.

Figure 24 shows the time-space-conversion analysis of potential temperature at 13.0 km for 1800 UTC 2 December 1988. It can be seen that the problem noted with the mean values (Fig. 23) over the Gulf of Mexico have been carried into the analysis at this level. In addition, a warm pocket near 27N, 77W may be another manifestation of the problems in the analysis over oceanic regions. However, it can generally be seen that the axis of the jet stream separates warmer stratospheric temperatures on the north side of the jet stream axis with cooler tropospheric temperatures to its south. This is especially true from SC north-eastward. This region is not only north of the southern branch of the jet stream, but is also on the stratospheric side (north-east) of the northern branch of the jet stream (referred to in Fig. 13, and subsequently in this section).

Also plotted on Fig. 24 are relative winds. It is the advection of potential temperature by these winds, in conjunction with (7), that are used in the computation of vertical velocity. Since the potential pattern is faulty at this level, the vertical velocity field will also be flawed.

Figure 25 illustrates the vertical gradient of potential temperature at 13.0 km for 1800 UTC 2 December 1988. This analysis much more clearly reveals the relationship between the jet stream axis and the tropopause. Large values north of the jet stream axis reveal large stratospheric static stabilities. Much lower, and quite similar, values occur in the less-stable tropospheric air south of the jet stream axis. Only a modest bulge of stable air toward the Gulf of Mexico reflects the problems with use of NGM-based mean values which polluted Figs. 23 and 24.

Figure 26 shows the pattern of vertical velocity at 13.0 km based upon the input fields of Figs. 24 and 25, using (6). It can be seen that the values are nearly zero, as would be expected, except in the gradient regions

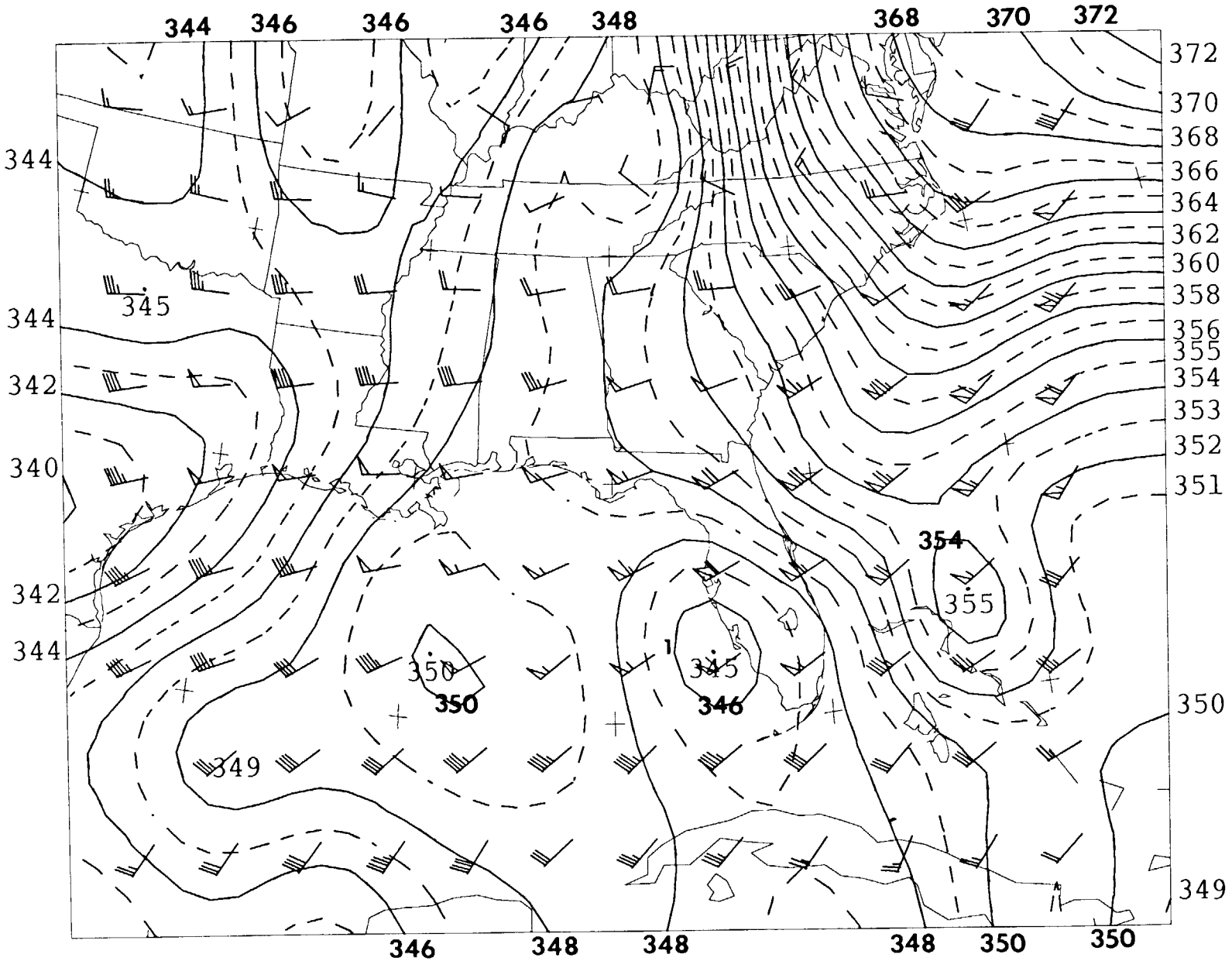

Figure 24. Isopleths of time-space-converted potential temperature at 13.0 km for 1800 UTC 2 December 1988, in degrees Kelvin. Velocity vectors are of the relative winds, with speeds in knots.

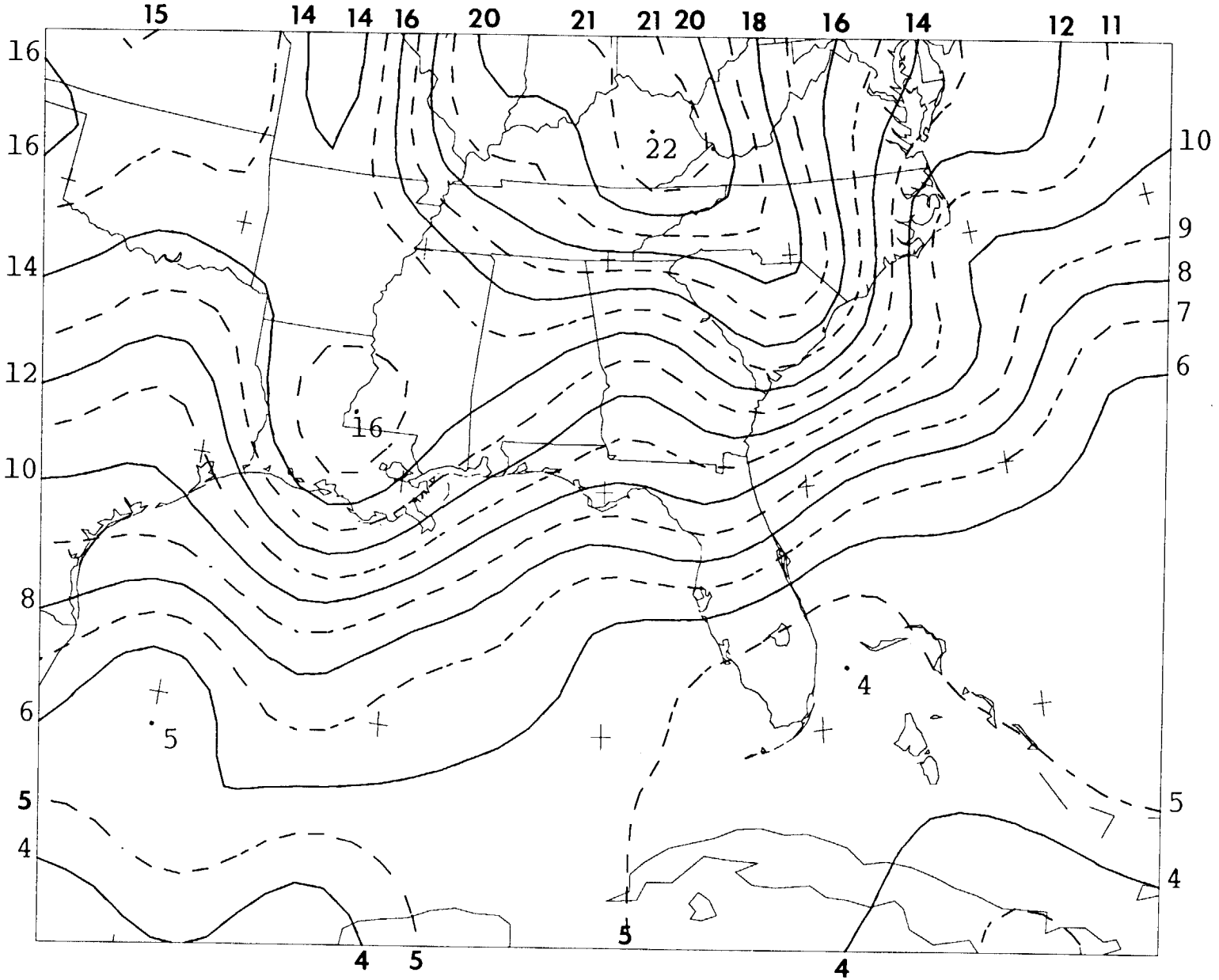

Figure 25. Vertical gradient of potential temperature in the layer from 12.5 to 13.5 km at 1800 UTC 2 December 1988, in degrees K per km.

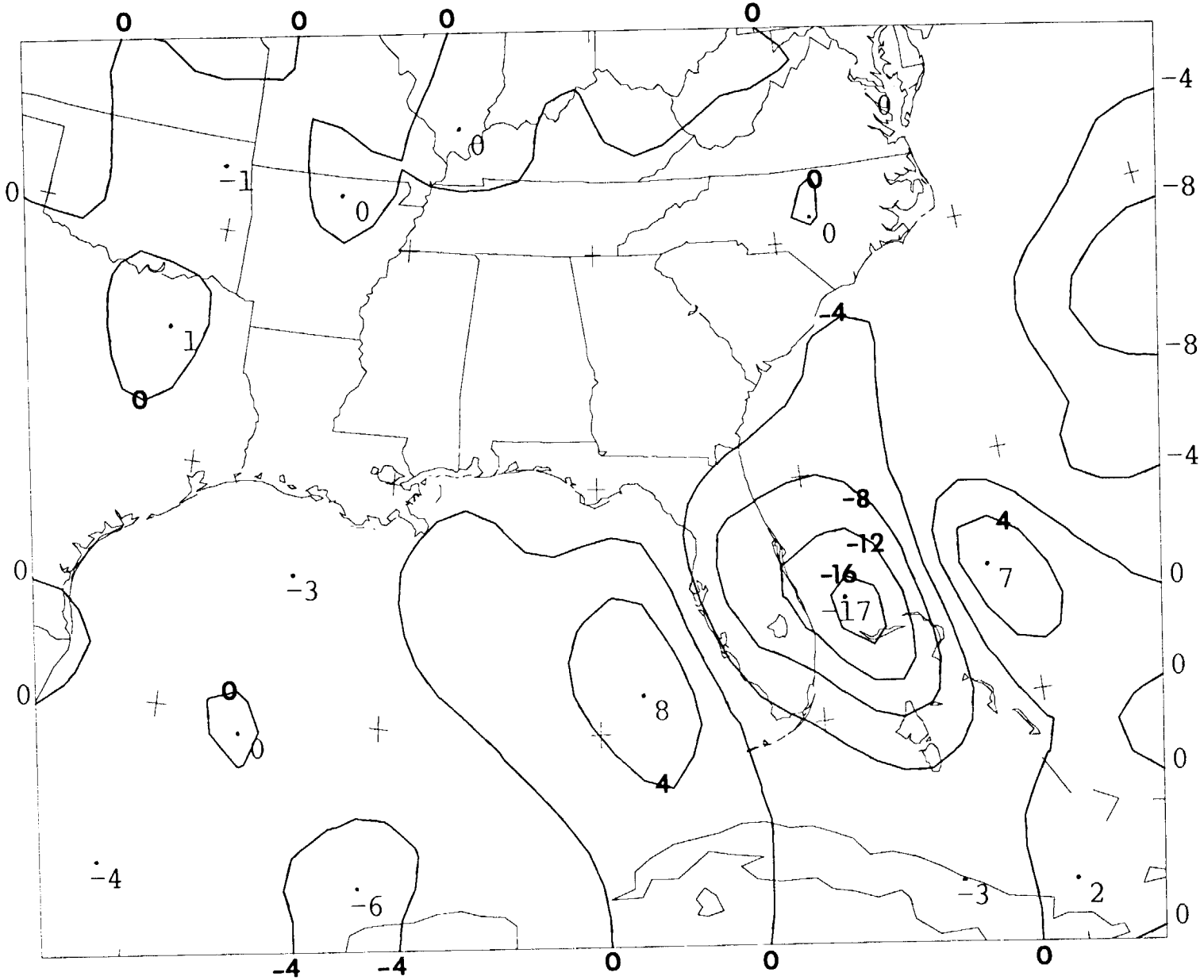

Figure 26. Adiabatic vertical velocity at 13.0 km for 1800 UTC 2 December 1988, in cm/s. Positive values indicate upward motion.

of Fig. 23 and 24, which do not likely exist in reality--yielding unrealistic vertical velocities.

Figure 27 shows the magnitude and direction of the vertical wind shear in the layer from 12.5-13.5 km, based upon the total time-space-converted wind fields at the 12.5 and 13.5 km levels. Beneath the core of the jet stream from central FL northeastward the wind shear is "negative"; i.e., opposite to the wind directions at 13.0 km. Hence, winds here are beginning to decrease with height, where higher altitudes are within the stratosphere.

Figure 28 shows the Richardson number pattern in the layer between 12.5 and 13.5 km, using the fields of Figs. 24, 25, and 27, based upon (7). The axis of lowest Ri extends along the jet stream and directly over KSC. The approximate value at KSC is 4.

Potential temperature discrepancies between rawinsonde-based and NGM-based analysis regions were not as large at altitudes higher in the stratosphere. Figure 29 shows the potential temperature and total velocity analysis for 14.5 km. Isotherms run more nearly parallel to the axis of the jet stream along the Gulf Coast. Within the jet stream cooler potential temperatures are found to the south, indicating a thermal wind directed from the east or east-northeast. Only the patterns at the south edge of the chart suggest that some problems remain.

Figure 30 shows the shear velocities between 14.0 and 15.0 km. Within the core of the jet stream, there is a negative shear at all locations, consistent with the thermal wind dictated in Fig. 29.

Consistent with the more realistic potential temperature field, the pattern and magnitude of vertical velocities has been suppressed, as shown in Figure 31. Vertical velocities are generally less than 2 cm/s, except near the Yucatan Peninsula, where the potential temperature analysis was

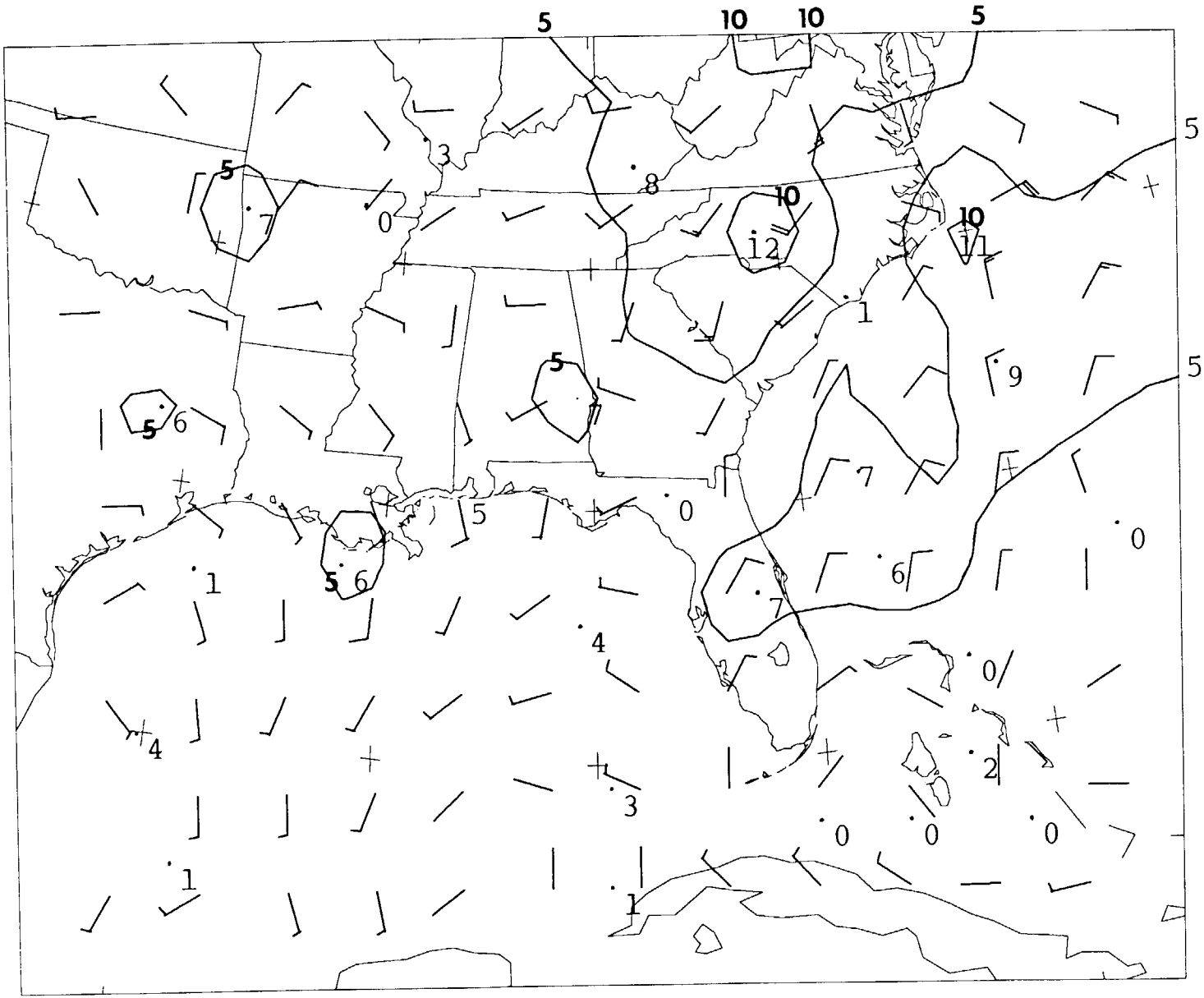

Figure 27. Magnitude and direction of the vertical wind shear vector, obtained by subtracting the 12.5 km velocity from that at 13.5 km. Isotachs are in m/s; vectors are in knots.

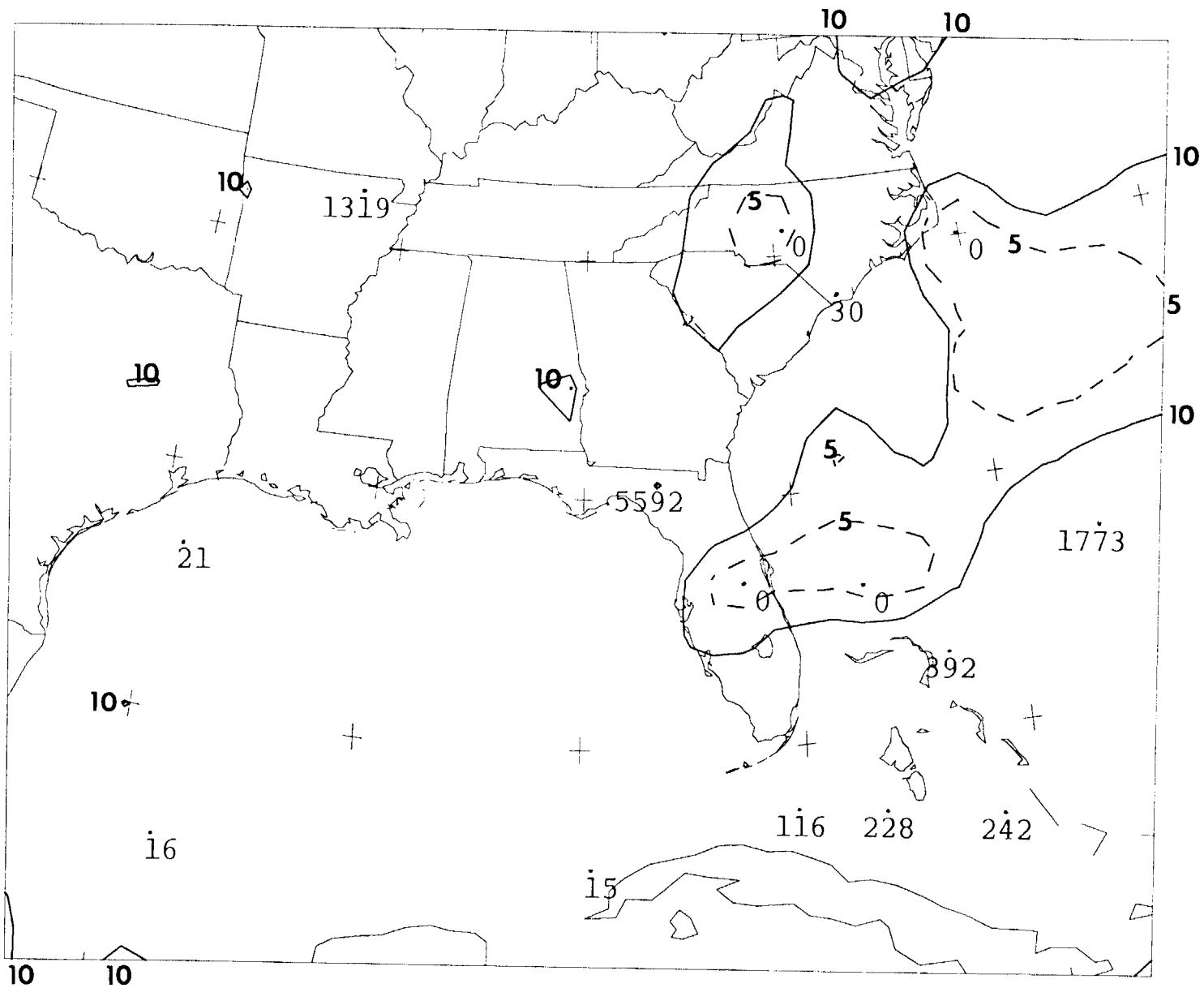

Figure 28. Time-space-conversion analysis of Richardson number. Solid isopleth has Ri = 10; dashed isopleth, 5.

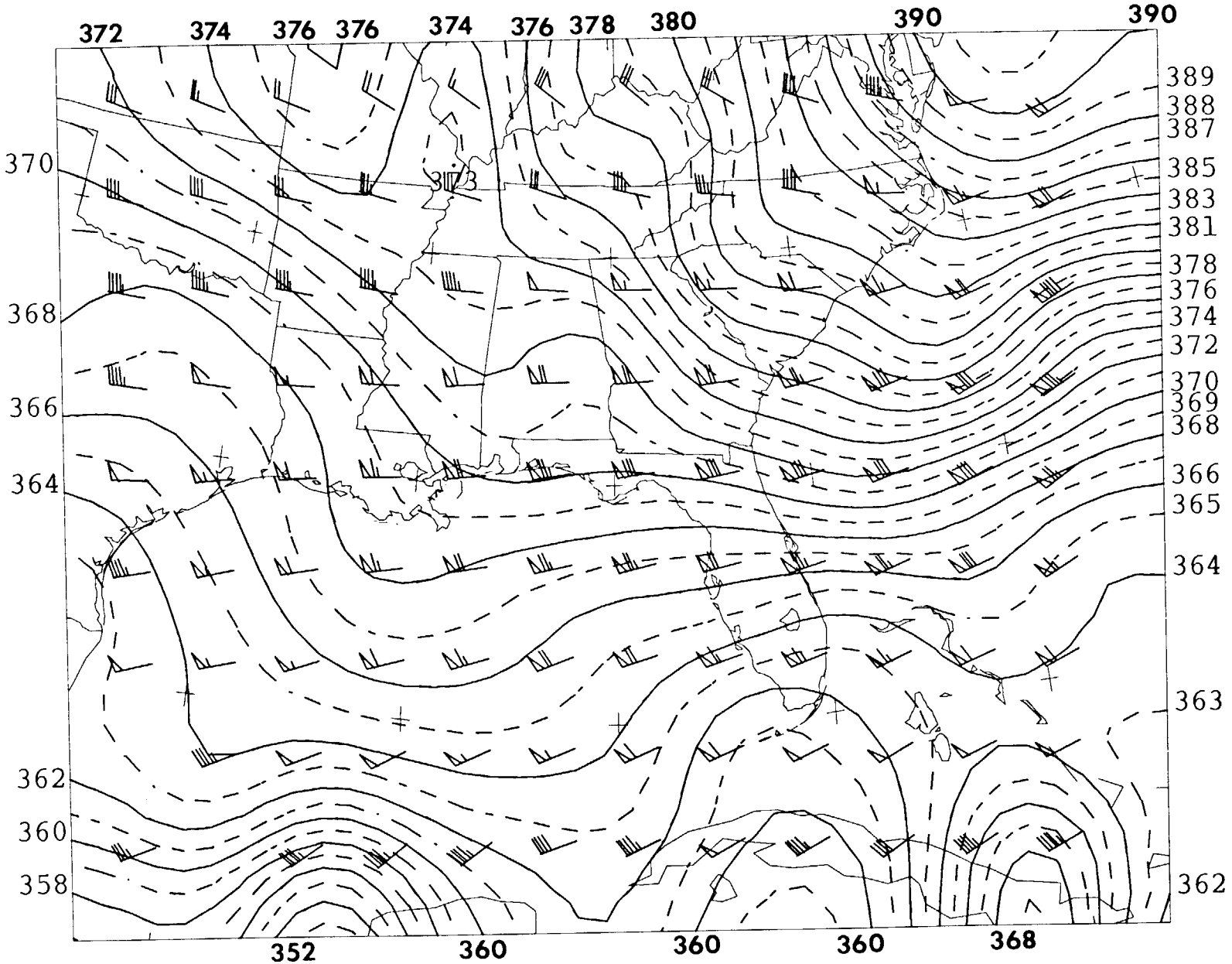

Figure 29. Time-space-conversion analysis of potential temperature (K) and total winds at 14.5 km at 1800 UTC 2 December 1988. Wind vectors are in knots.

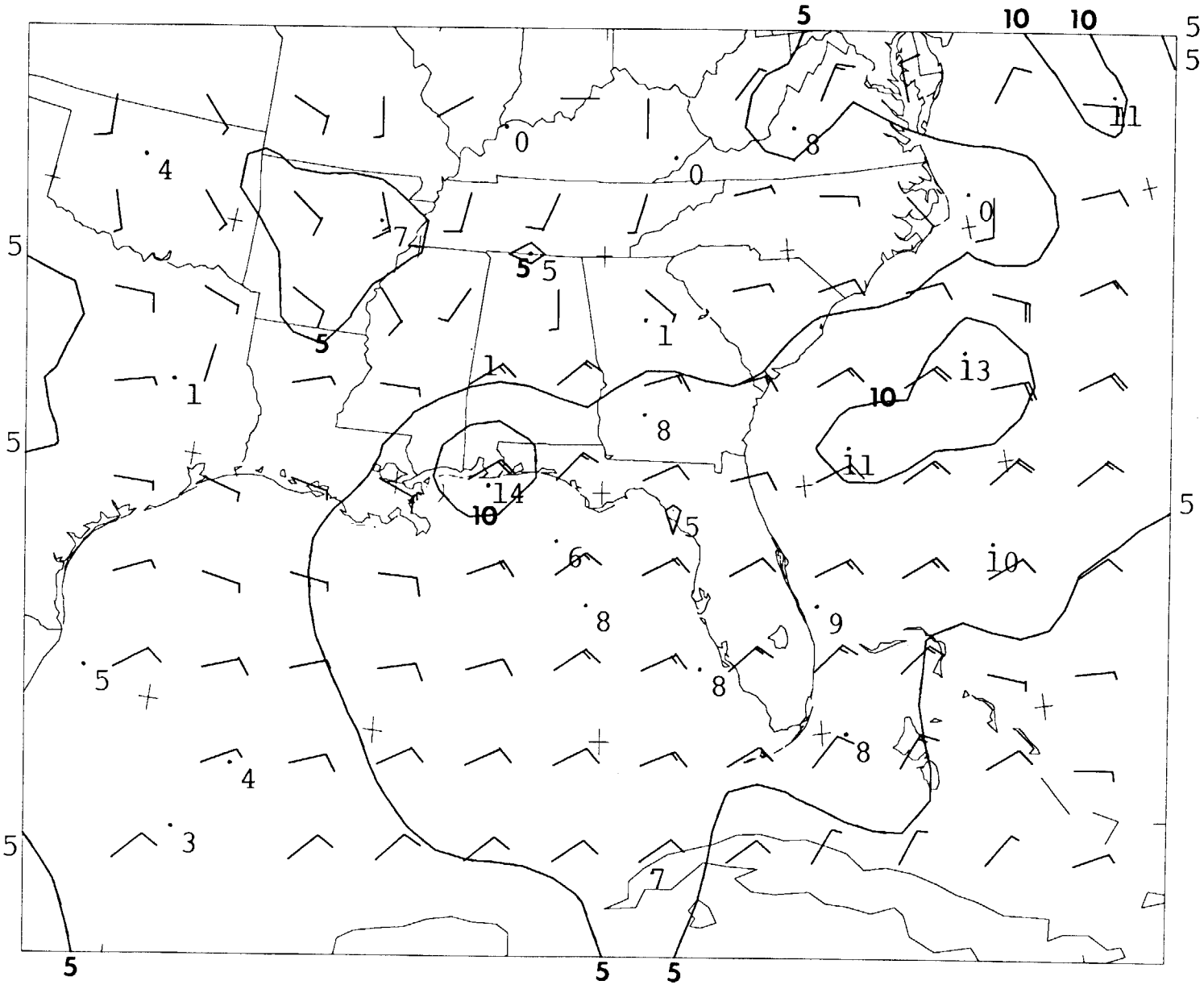

Figure 30. Time-space-conversion analysis of shear velocity between 14.0 and 15.0 km, upper minus lower, in m/s. Shear vectors are in knots.

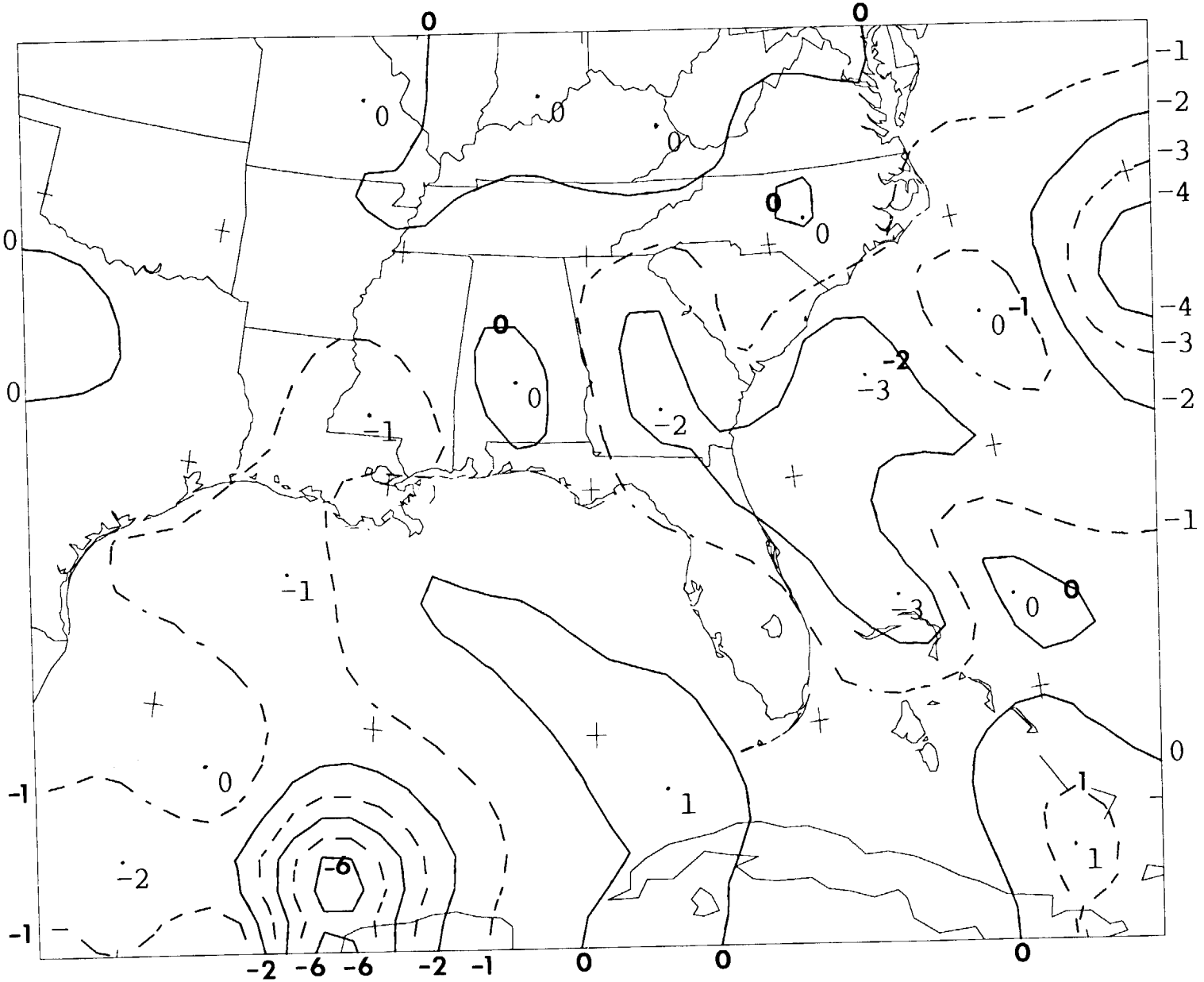

Figure 31. Time-space-conversion analysis of adiabatic vertical velocity at 14.5 km, in cm/s.

questionable, and near the right edge of the chart. Hence, the adiabatic vertical velocities have converged toward zero in the lower stratosphere without the analysis having had to resort to any artificial devices, such as the O'Brien (1970) scheme often used with kinematic vertical velocities.

Figure 32 shows the total wind field at 11.5 km. The axis of the jet stream at this level is almost exactly over KSC. The northern branch jet stream begins to appear over northwestern VA, in this and the successively lower analyses that follow.

Figure 33 shows the potential temperatures at this level, with the wind vectors of Fig. 32 superimposed. This level is clearly within the troposphere at virtually all locations, as temperatures decrease toward the north. Only in the upper-right corner of the diagram, where temperatures are increasing toward the northeast, does the stratosphere appear to descend to this level. This warm pocket is linked to the northern branch jet heading southeast across VA. Problems over the oceanic regions near the tropopause (Fig. 23) have all but disappeared, as the gradient is quite weak--as expected--south of the axis of the jet stream.

At 10.0 km, KSC is located slightly north of the axis of the jet stream, Figure 34, which slopes gradually toward the north at higher levels (Figs. 29, 32). KSC is also clearly in the entrance region of the jet stream, as wind speeds along the jet axis increase from about 30 to 66 m/s in a distance of about 1300 km. There is a hint at another branch of the southern jet stream across southern GA. The northern branch jet stream is easily distinguished over western VA and northern NC, then turning eastward to merge with the stronger southern branch jet. Streamlines of the total winds, Figure 35, clearly reveal the confluence into the jet stream across the Gulf of Mexico and along and offshore of the Southeast Coast. Also shown in Fig. 35 is the

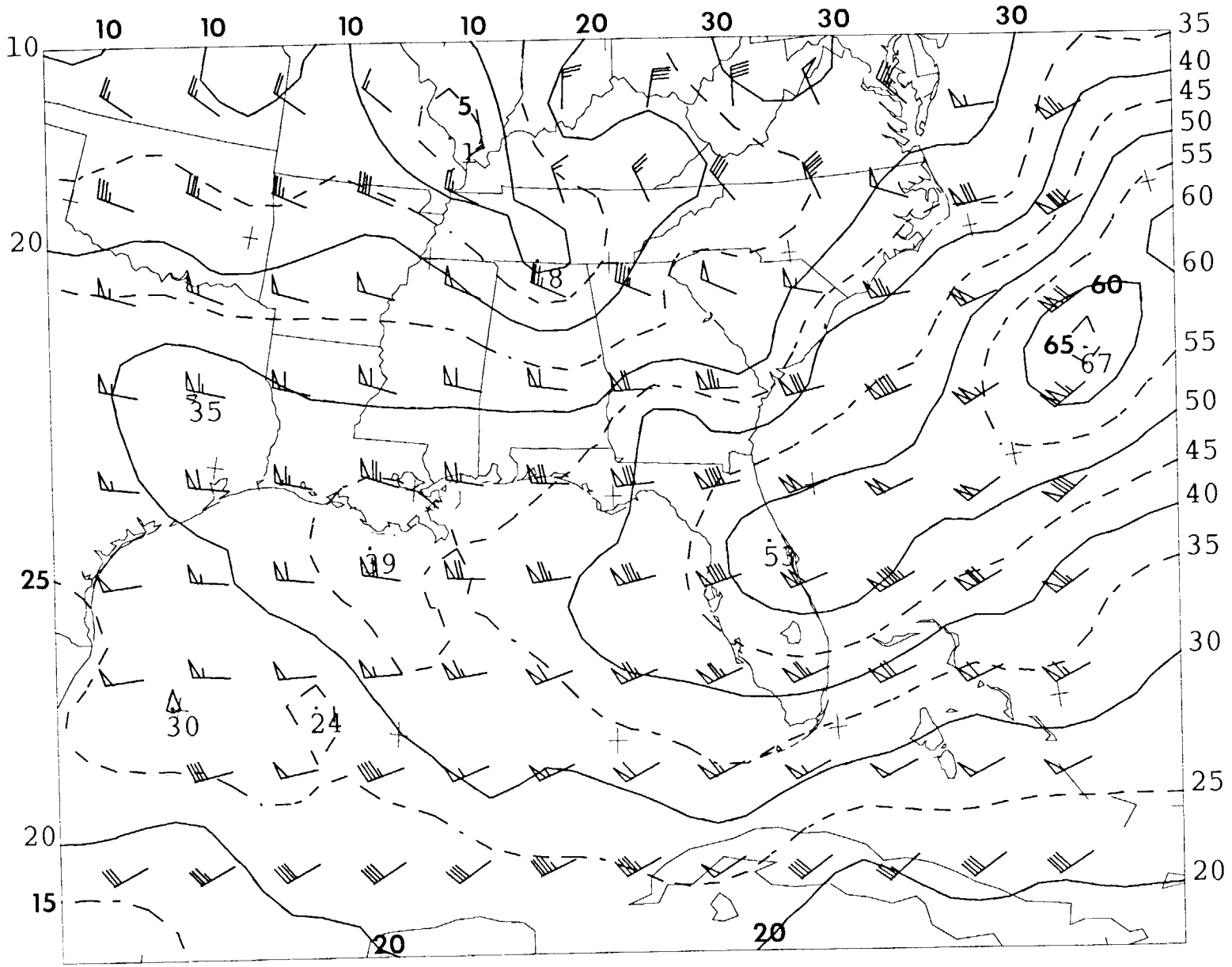

Figure 32. Time-space-conversion analysis of winds at 11.5 km, 1800 UTC 2 December 1988. Isotachs are in m/s; vectors are in knots.

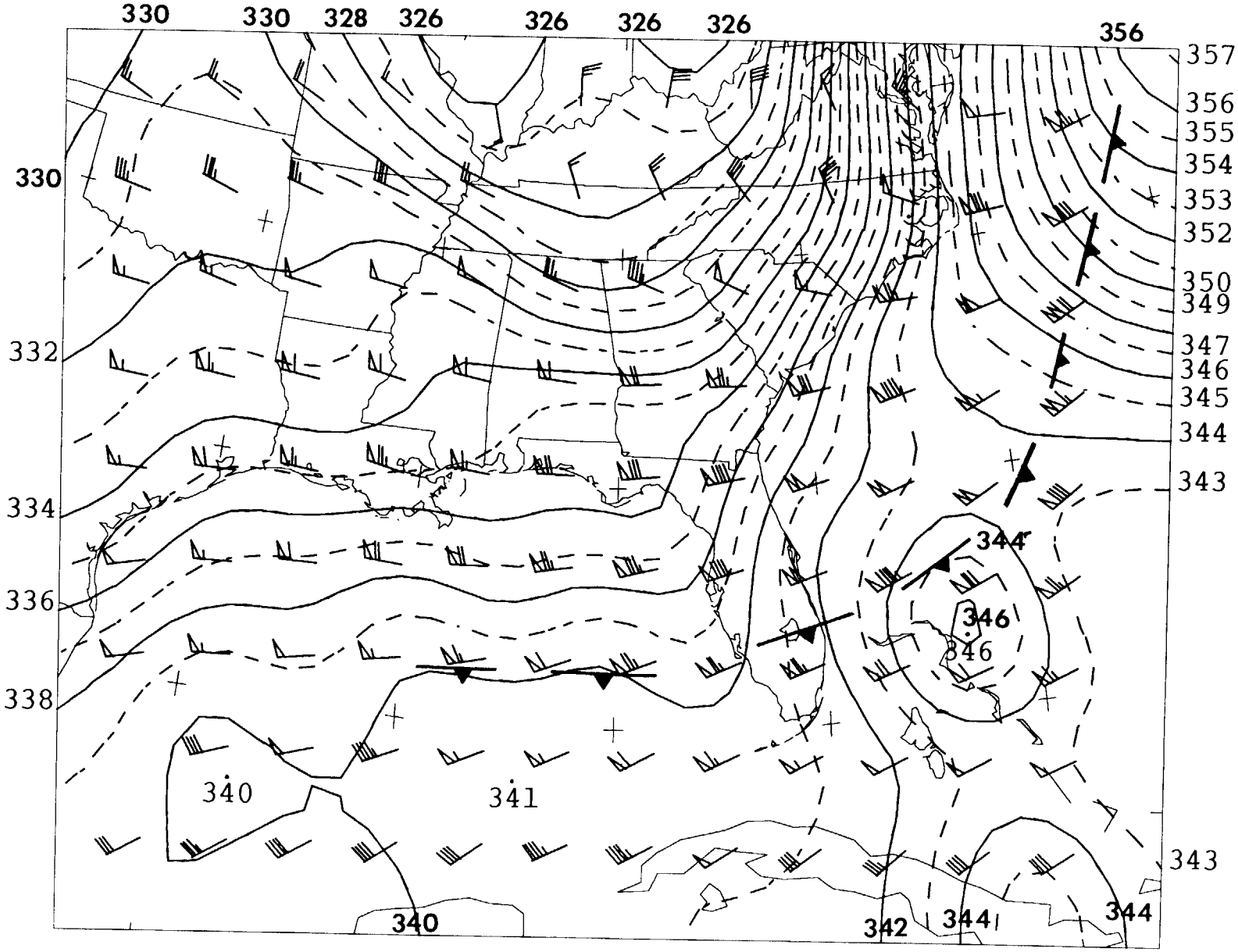

Figure 33. Time-space-conversion analysis of potential temperatures (K) and winds at 11.5 km, 1800 UTC 2 December 1988. Vectors are in knots.

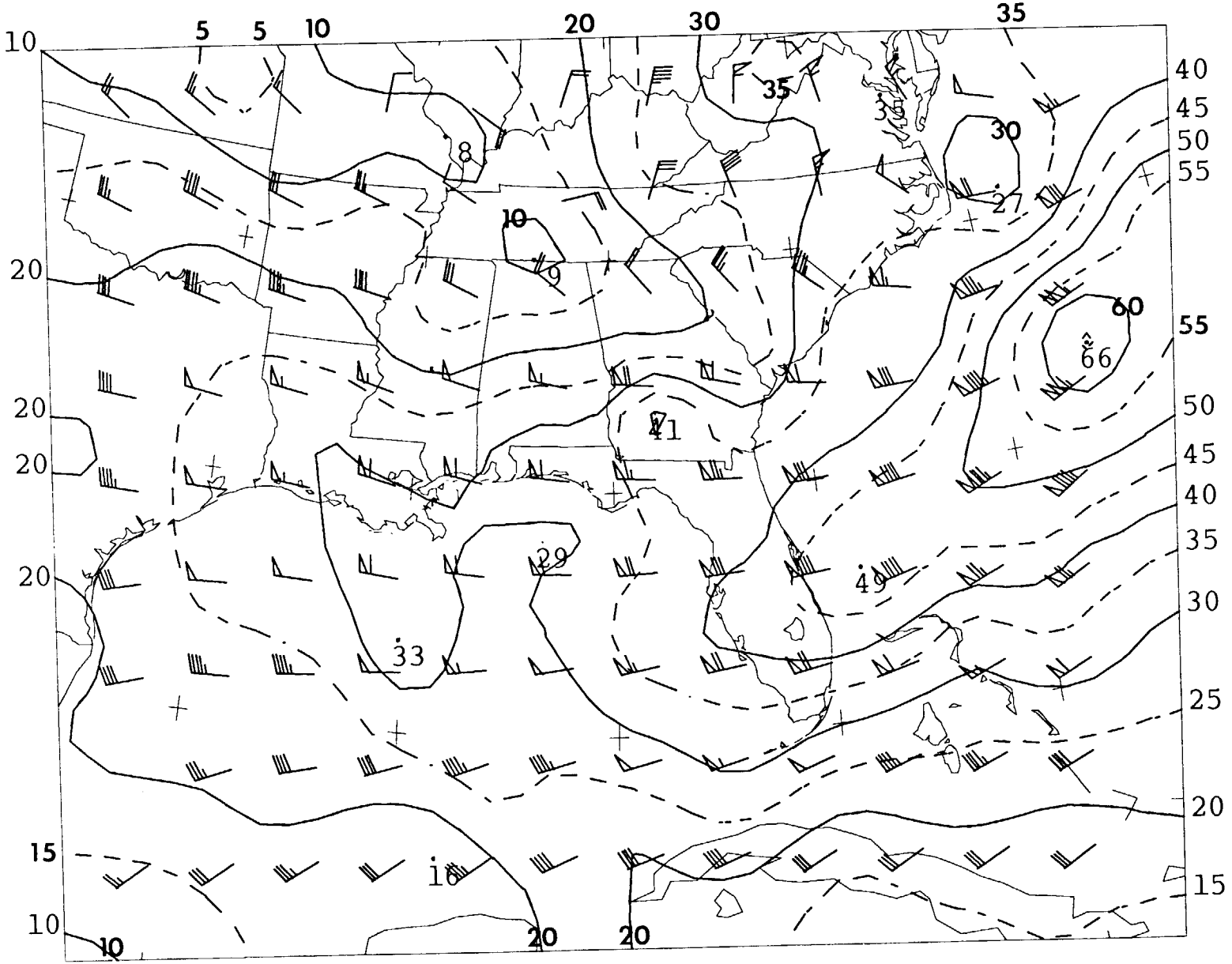

Figure 34. Time-space-conversion analysis of winds at 10.0 km, 1800 UTC 2 December 1988. Isotachs are in m/s; vectors in knots.

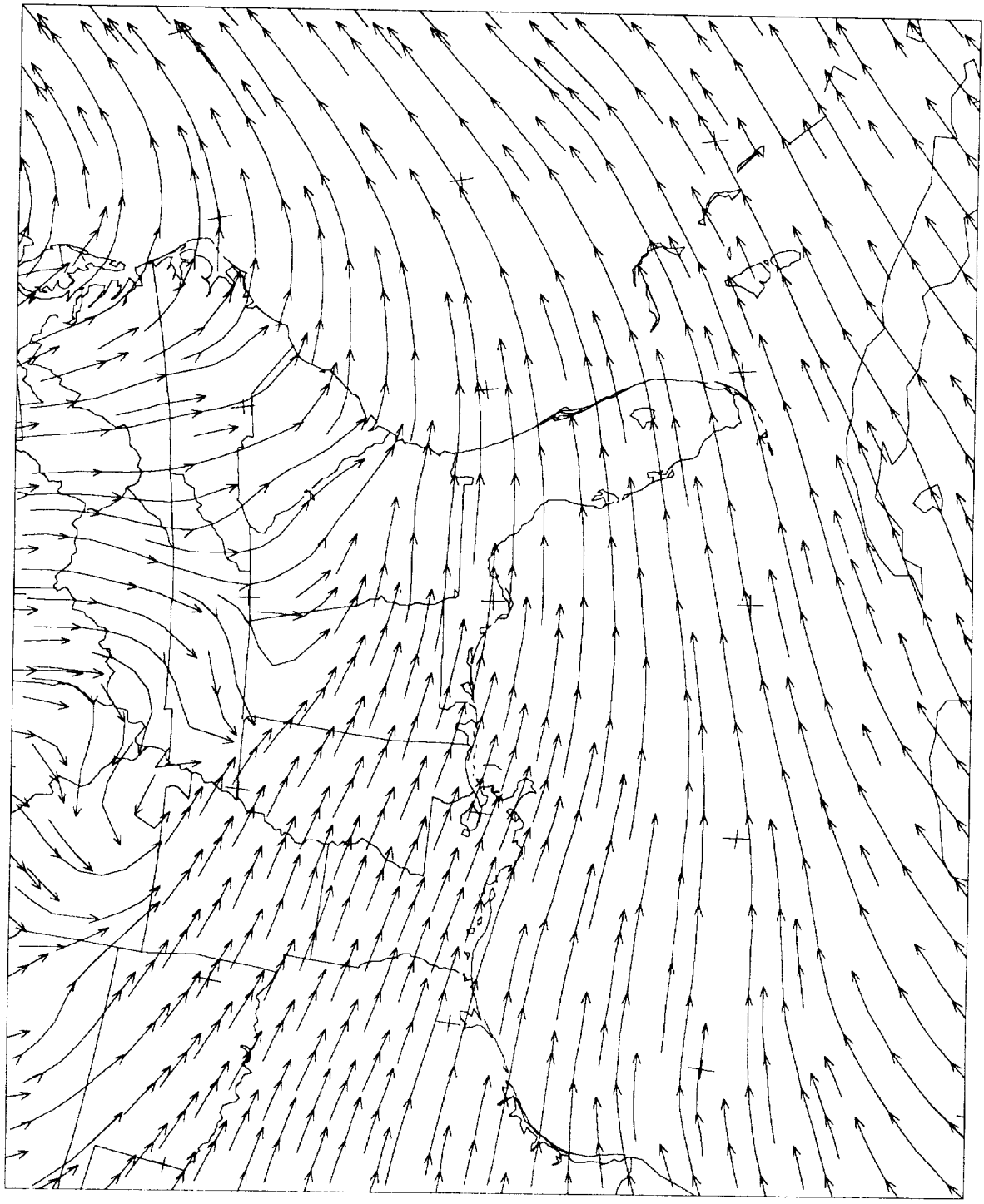

Figure 35. Streamlines of the total winds at 10.0 km, shown in Fig. 34.

presence of an unusual-orientation trough line extending west-northwestward from northern AL to MO.

Figure 36 shows the potential temperatures at 10.0 km. All locations are now within the troposphere, and there is a notable change of the temperature gradient across the jet axis. Thus, as expected, the wind maximum is co-located with the position of the upper-level front. The temperature gradient north of the jet stream axis indicates a thermal wind from the west or southwest, so that positive wind shears would be expected there. This contributes to increasing the wind speeds farther aloft above this part of the jet stream, leading to the northward slope of the axis of the jet stream with height.

Figure 37 shows the shear velocities across the layer from 9.5 to 10.5 km. As indicated by the thermal winds implied by Fig. 36, shear vectors point toward the northeast. One pocket of maximum shear is located about 50 km WNW of KSC.

Figure 38 shows the Richardson number pattern at 10.0 km. Minima are associated with the pockets of maximum shear of Fig. 37. Ri value over KSC is about 1.

The axis of maximum winds continued to shift southward with decreasing altitude until about 9 km. At 8.0 km, however, the jet core reappears further to the north in this region near the base of the jet stream, Figure 39. This northward reemergence may be affiliated with the branch of the southern jet visible over GA in Fig. 34. Small bulges on the south side of the 30 m/s isotach reveal the last remnants of the main southward-sloping jet core. The northern branch jet across VA and NC is quite evident.

Figure 40 shows potential temperatures and relative winds at the 8.0 km level. Despite the shift of the strongest winds northward, the main cold

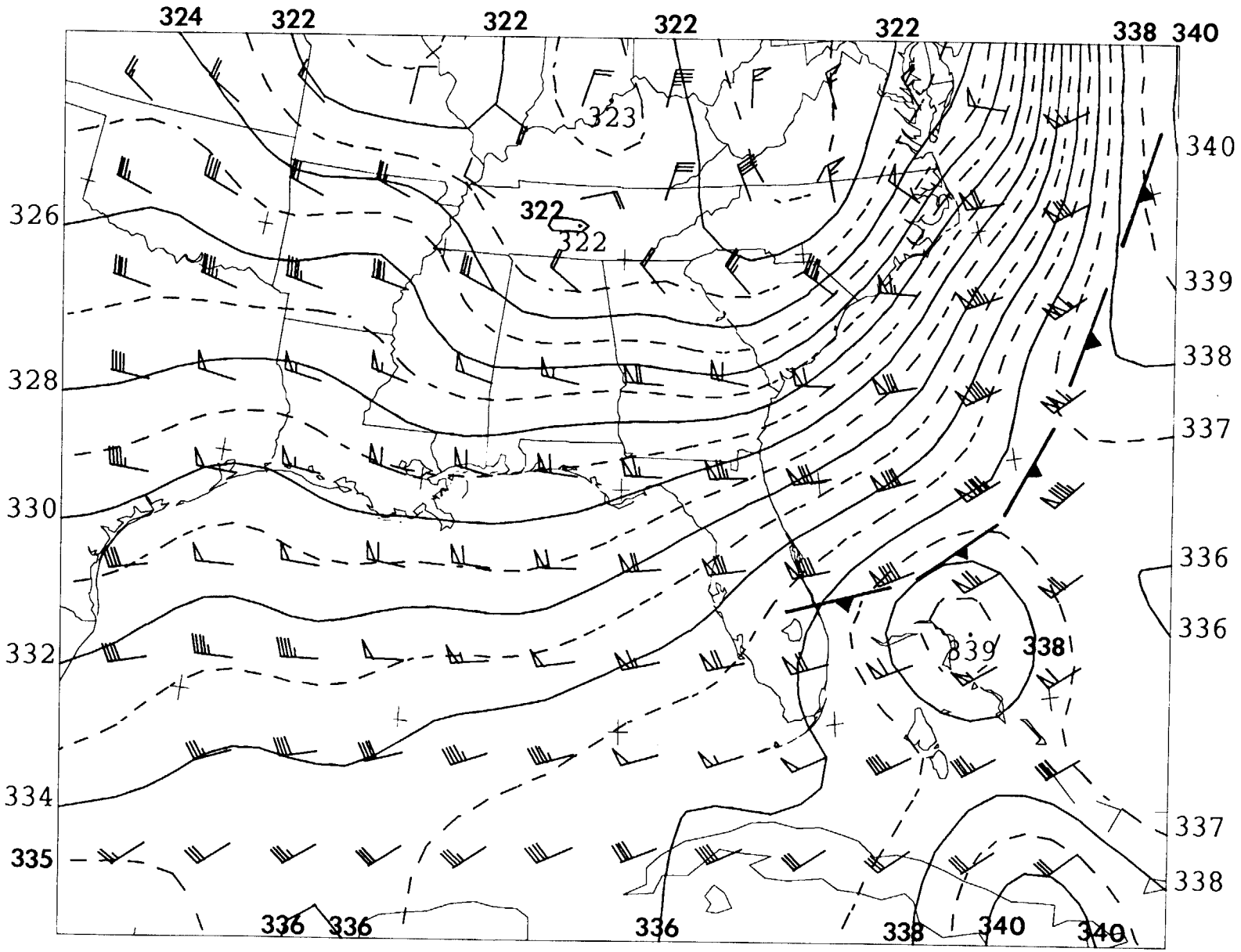

Figure 36. Time-space-conversion analysis of potential temperatures (K) and winds at 10.0 km, 1800 UTC 2 December 1988. Wind vectors are in knots.

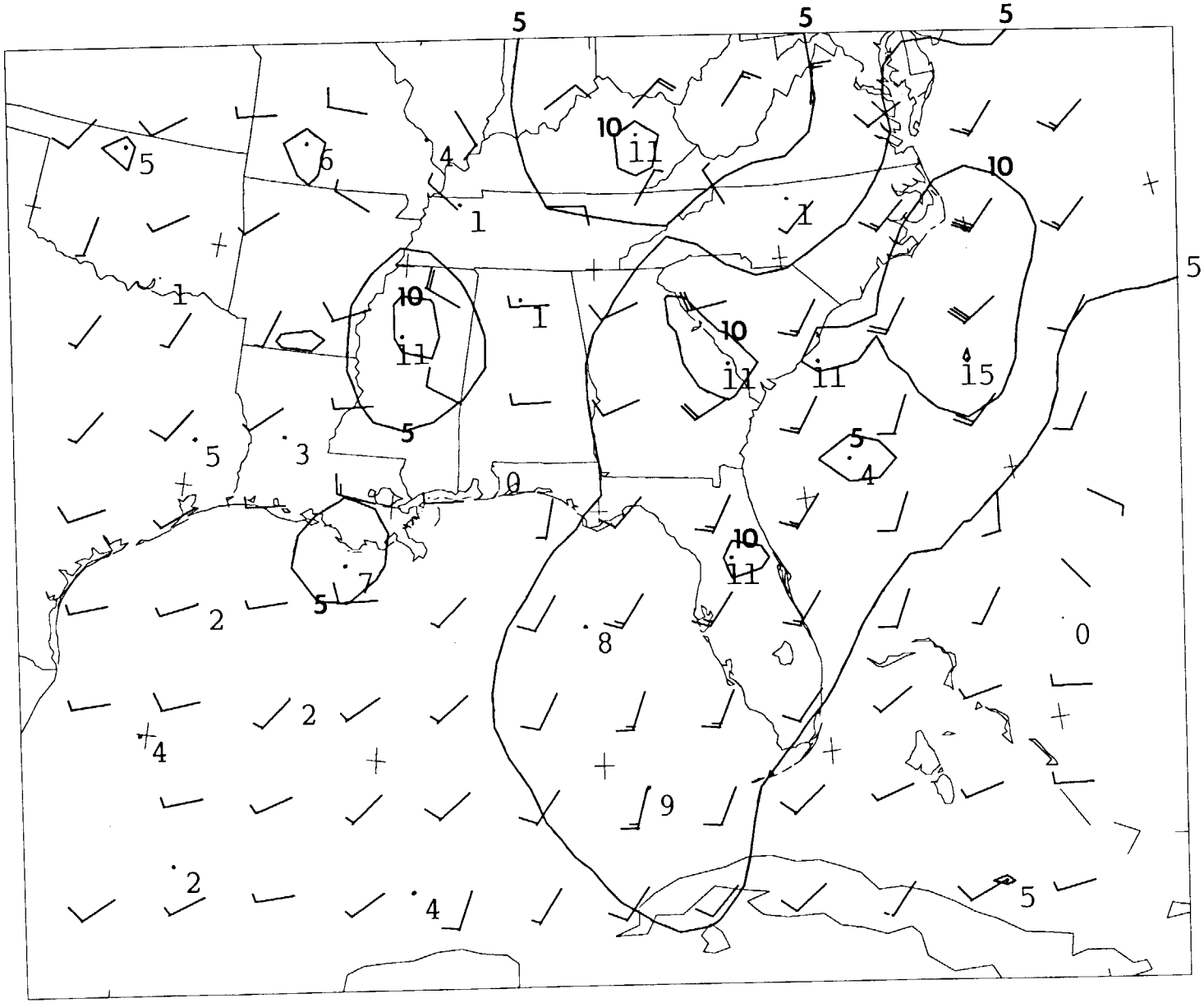

Figure 37. Shear velocities in the layer from 9.5 to 10.5 km, upper minus lower, at 1800 UTC 2 December 1988. Isotachs are in m/s; vectors are in knots.

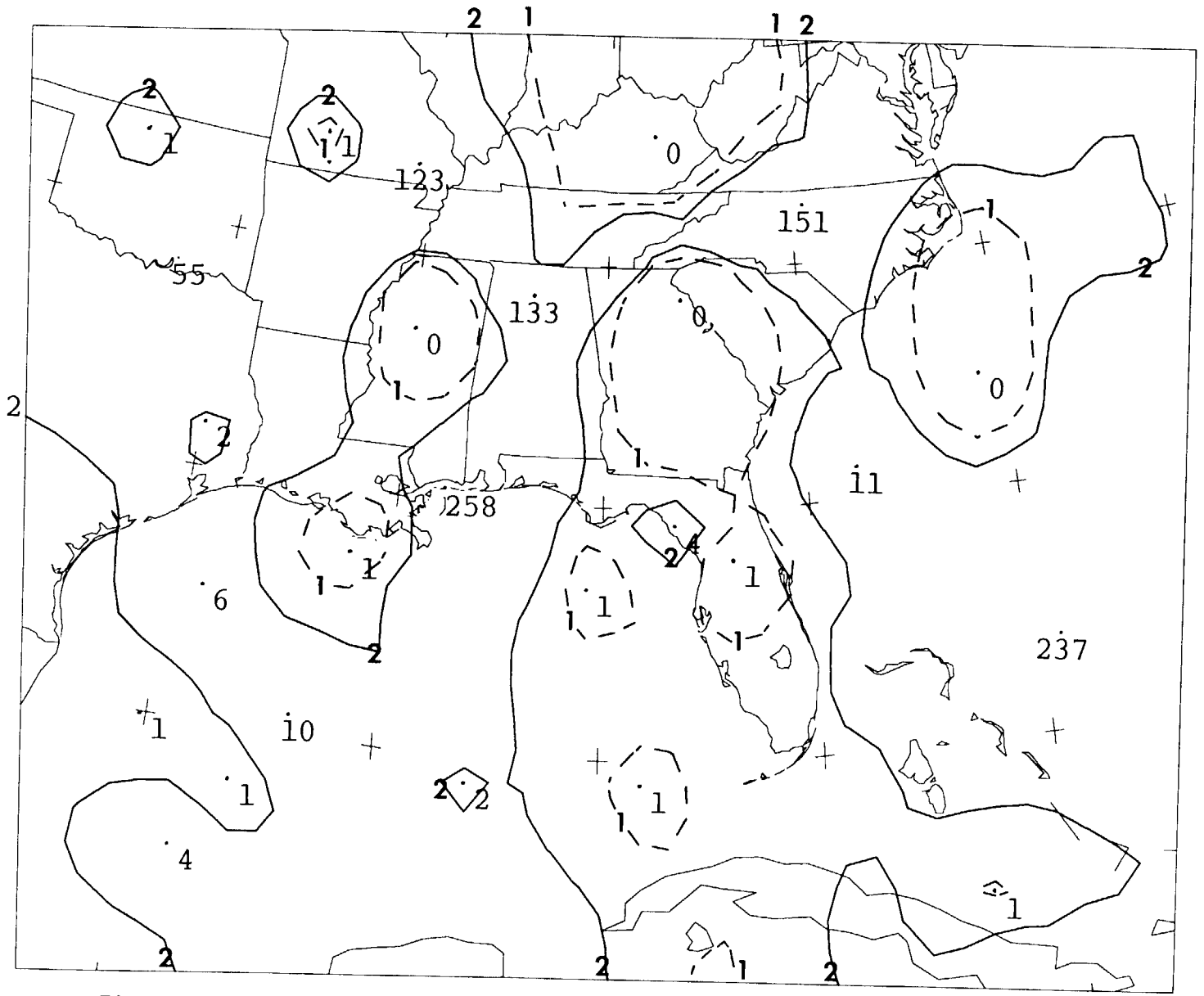

Figure 38. Time-space-conversion analysis of Richardson numbers in the layer from 9.5 to 10.5 km, 1800 UTC 2 December 1988.

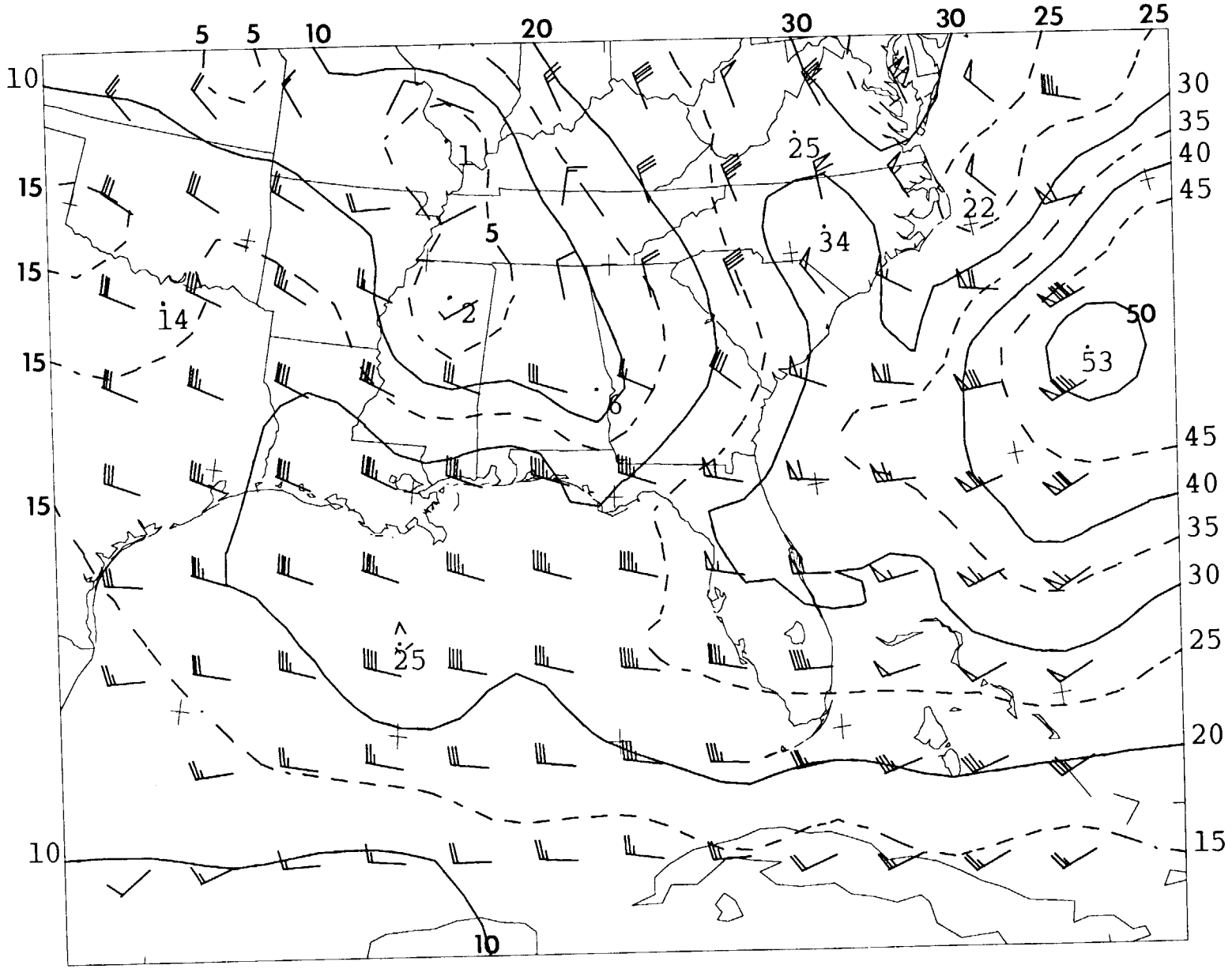

Figure 39. Time-space-conversion analysis of winds at 8.0 km, 1800 UTC 2 December 1988. Isotachs are in m/s; vectors are in knots.

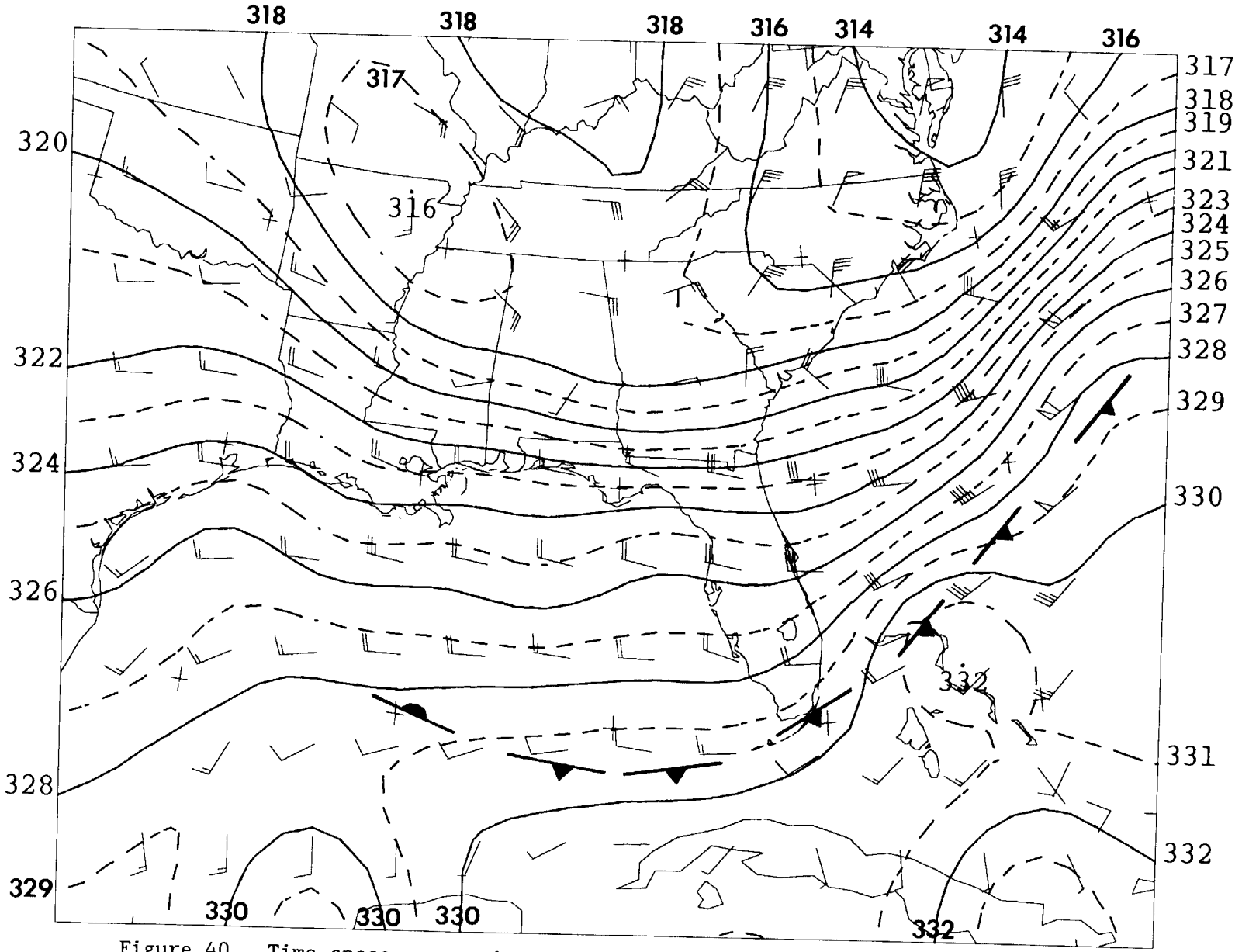

Figure 40. Time-space-conversion analysis of potential temperatures (K) and relative winds at 8.0 km, 1800 UTC 2 December 1988. Vectors are in knots.

front associated with the overall jet stream has continued to push southward with descending altitude. The temperature gradient associated with the jet stream is very well defined. In most places the relative winds are approximately parallel to the isotherms, except along the East Coast. There the northern branch jet is producing strong cold advection, no doubt helping to drive the jet stream eastward.

Figure 41 shows the pattern of adiabatic vertical velocities derived from the relative temperature advection of Fig. 40. Strong descent is occurring over and offshore of the Carolinas, where cold advection was strong. A region of modest upward motion is present in the States surrounding the Mississippi River. An inspection of Figs. 39 and 40 reveals that this upward motion is in advance of an active short-wave trough. There is a weak closed cyclonic circulation in the total winds (Fig. 39) and a cold pocket over northeastern Arkansas and southern MO in Fig. 40. This region was occupied by merely an inert trough line at 10.0 km (Figs. 34, 35), so the closed circulation is comparatively shallow.

At 6.5 km, the front has now apparently halted its southward slope with descending altitude, and is found in approximately the same position near FL as in Fig. 40. Over the Gulf of Mexico, the front is not well defined, but may have shifted northward. A hint of the downward extrusion of the main jet stream aloft can still be seen near 27.5N, 74W as a slight lobe of faster wind speeds along the southeast edge of the jet stream. The short-wave trough which had a closed cyclonic circulation over northern Arkansas at 8.0 km (Figs. 39, 40) is now merely a trough line across southern MO.

Vertical velocities at 6.5 km, Figure 43, reveal that there is a region of upward velocities along the right side of the diagram. This is in an area typically occupied by the warm conveyor belt which slopes upward to meet the

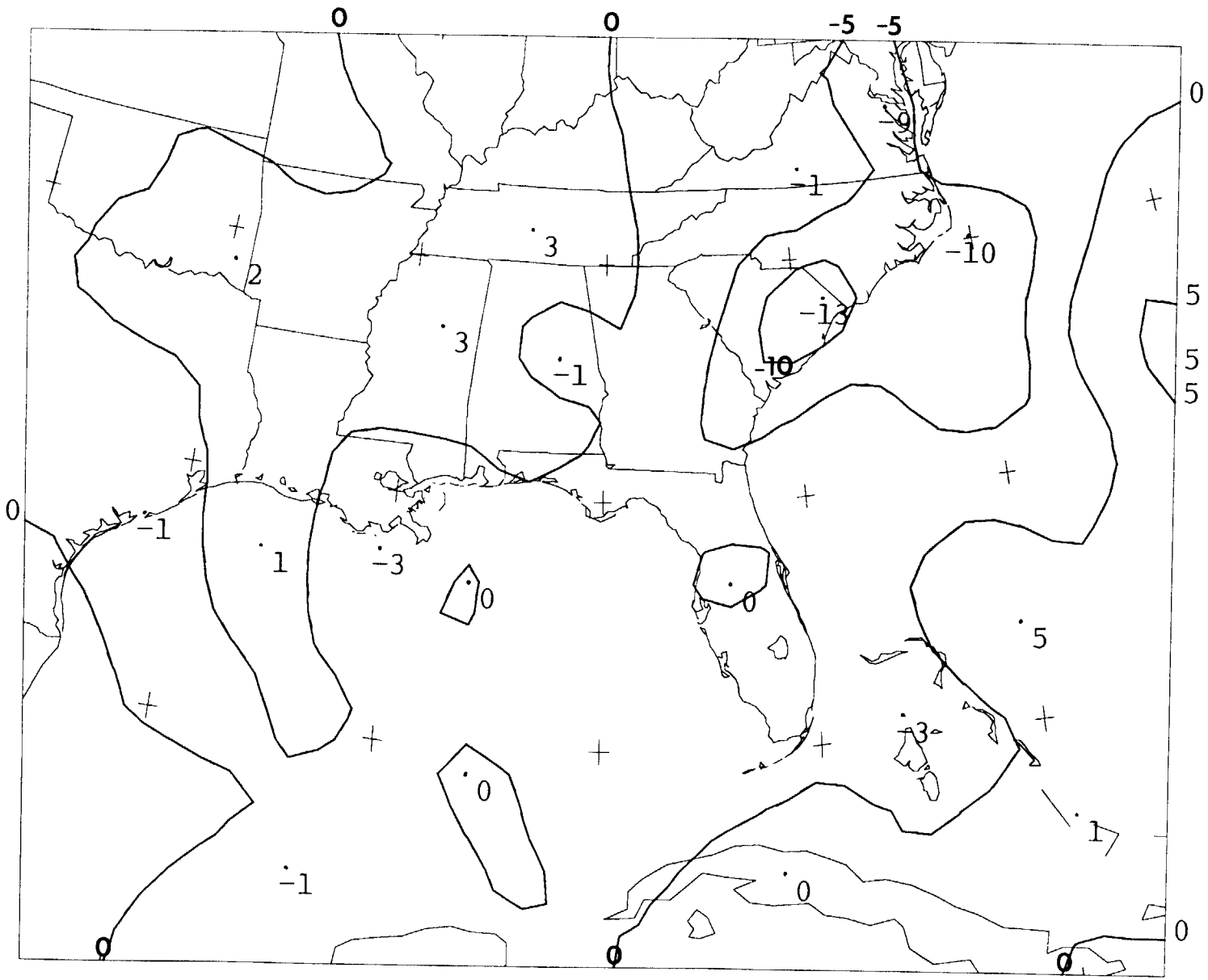

Figure 41. Adiabatic vertical velocities at 8.0 km, derived from Fig. 40, in cm/s.

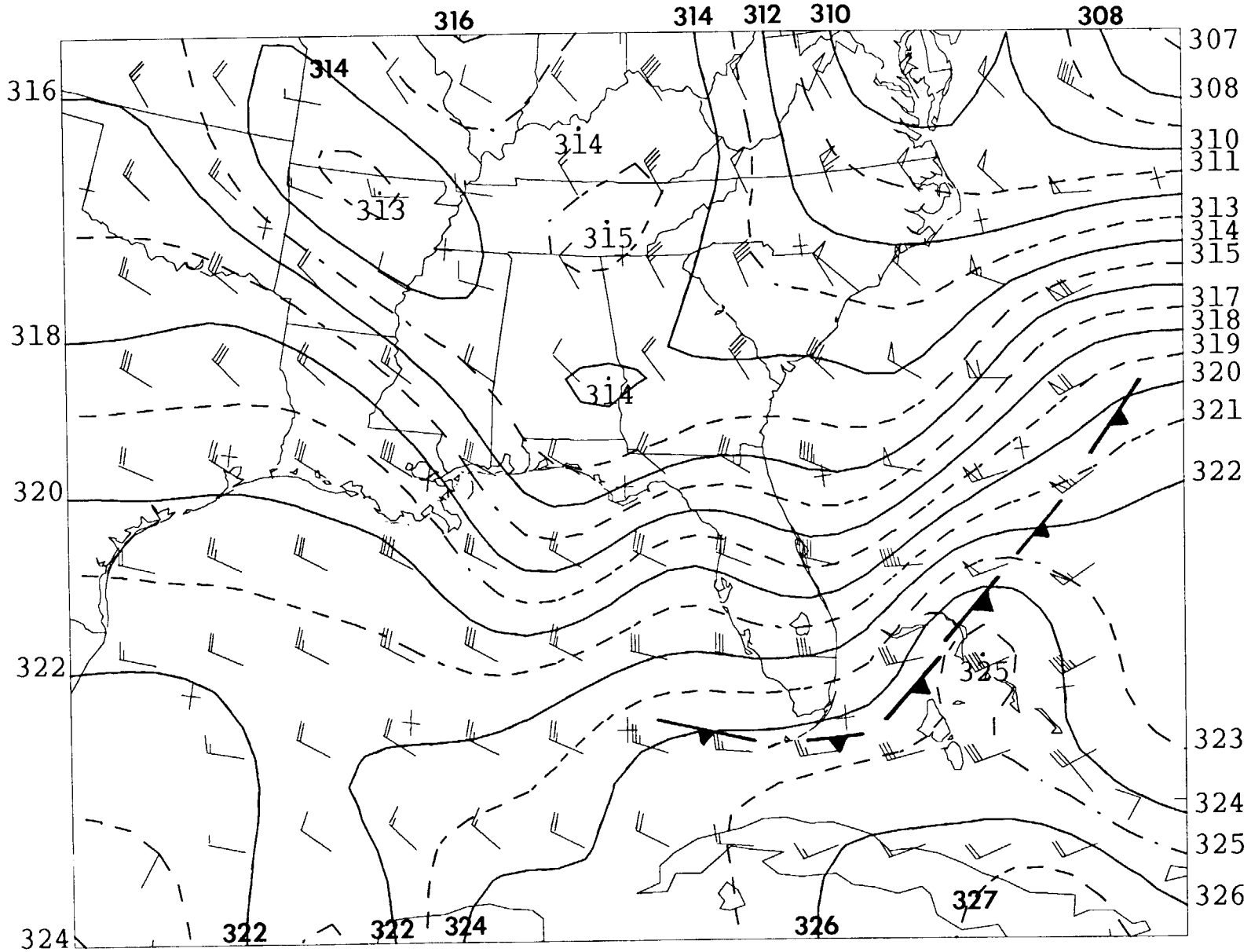

Figure 42. Time-space-conversion analysis of potential temperatures (K) and total winds at 6.5 km, 1800 UTC 2 December 1988. Wind vectors are in knots.

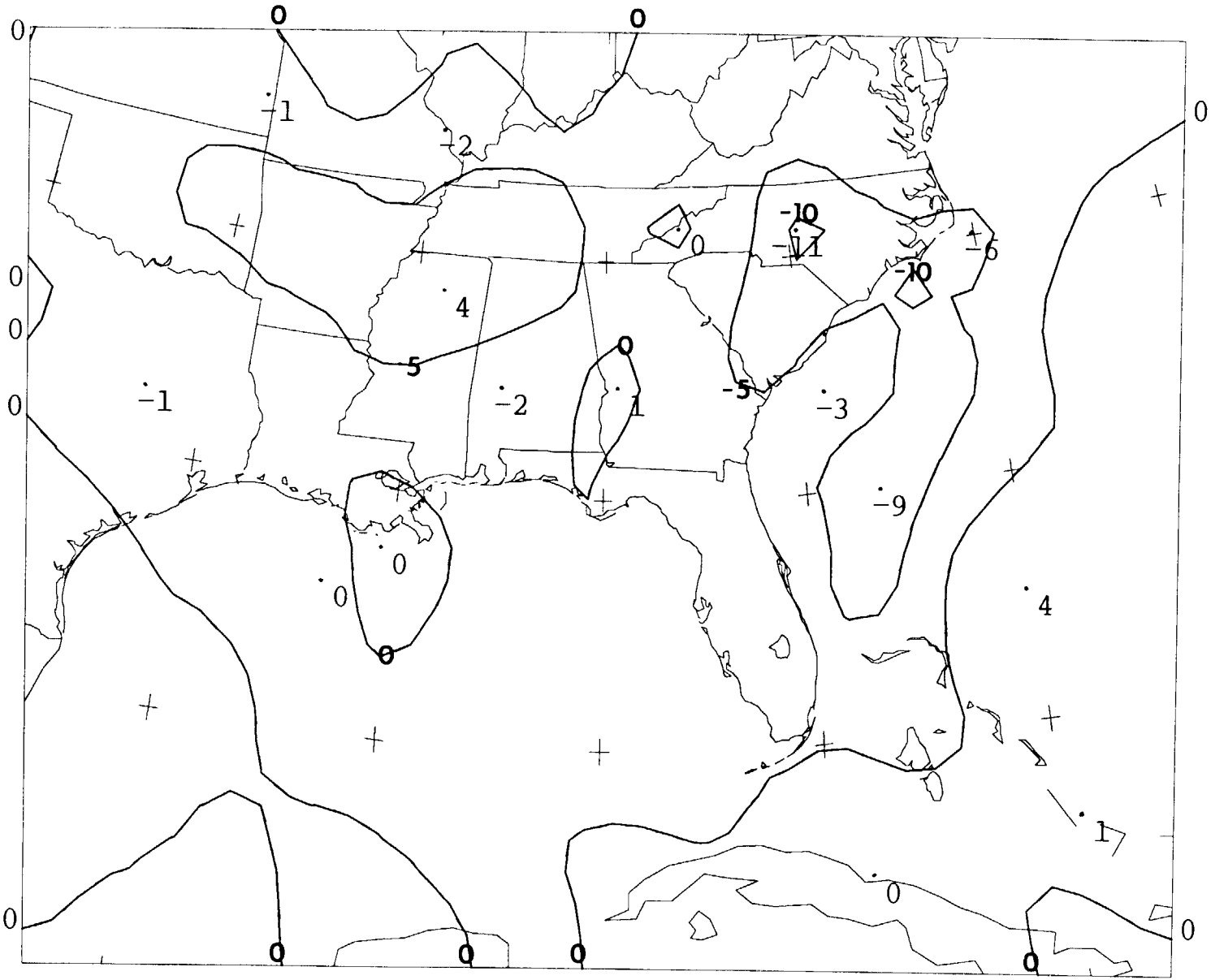

Figure 43. Adiabatic vertical velocity at 6.5 km, 1800 UTC 2 December 1988, in cm/s.

jet stream. The downward extension of the main southern jet stream, along its leading edge at 6.5 km near 27.5N, 74W, is within the ascending region at this level. Ascent is also present ahead of the MO short-wave trough.

In association with the strong horizontal temperature gradient of Fig. 42, there is a considerable positive wind shear over KSC at this level, as shown in Figure 44. This yields low Ri values within the jet stream, Figure 45, and value of about 1 at KSC.

Below 6 km the pattern became more uniformly associated with the main cold front and the cold advection driving it southward. Figure 46 shows the potential temperatures and winds at 2.0 km.

The position of the cold front at this level is over extreme eastern Cuba, at the lower-right corner of the diagram. The deepest cold air is found to the north, offshore of DE, positioned east of the northern branch jet seen at levels further aloft.

A warm tongue across the FL panhandle into southern IN in Fig. 46 is suggestive of an "instant" occluded front, induced by the short-wave trough farther aloft over MO. However, the true character of this feature is revealed by the wind and temperature pattern south of the FL panhandle. Here, the warm tongue clearly marks the leading edge of a cold surge from the north-northeast. Thus, the warm tongue is at the leading edge of a "back-door" cold front, in advance of a fresh surge of cold air from beneath the northern jet and heading southwestward into the Gulf of Mexico, where it will replenish the older cold air mass which has driven the main cold front so far south (i.e., across Cuba). This "back-door" cold front can be seen in the analyses from 1.5 km to 4.0 km (though only the 1.5 km level is shown).

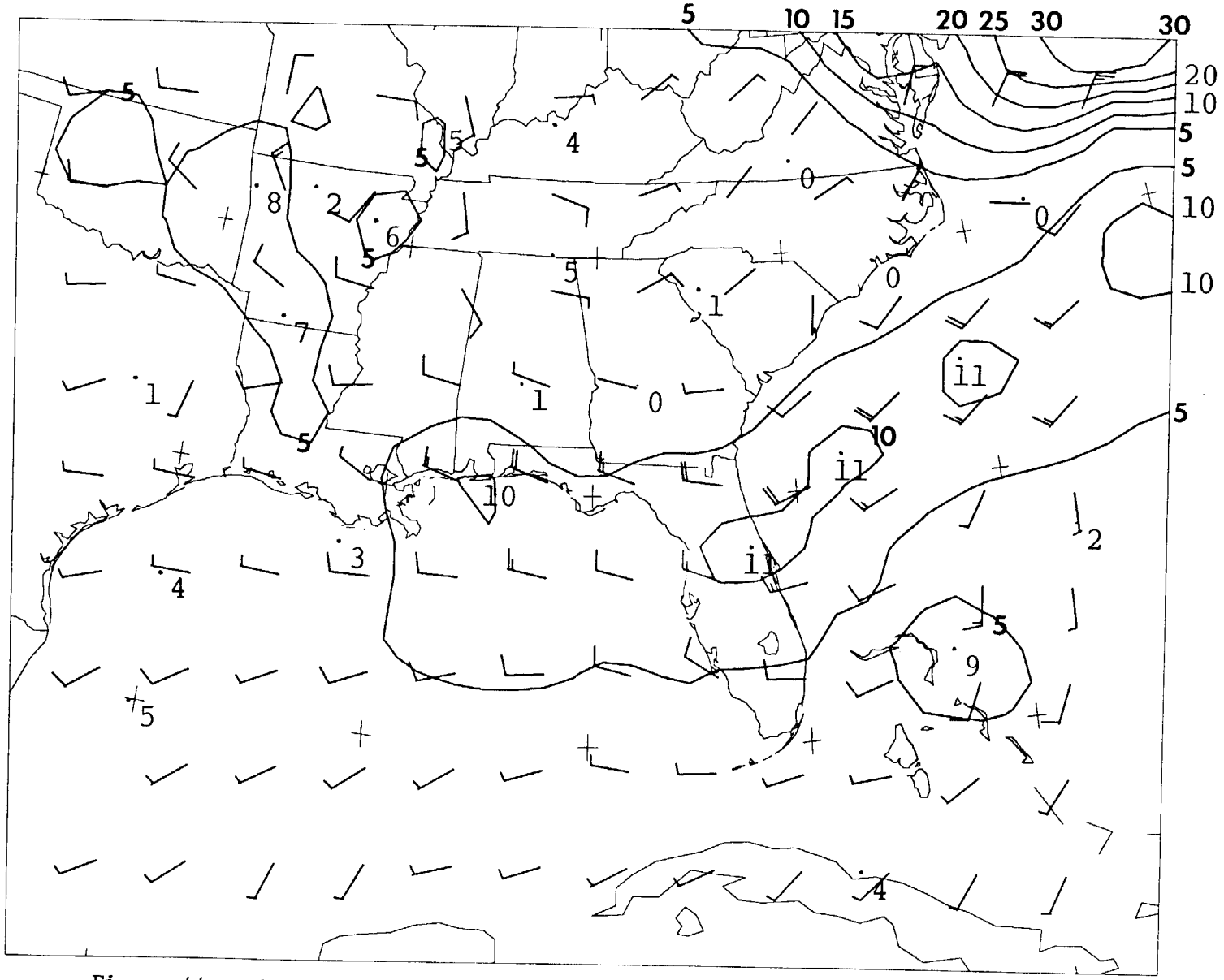

Figure 44. Shear vector between 6.0 and 7.0 km, upper minus lower, at 1800 UTC 2 December 1988. Isotachs are in m/s; vectors are in knots.

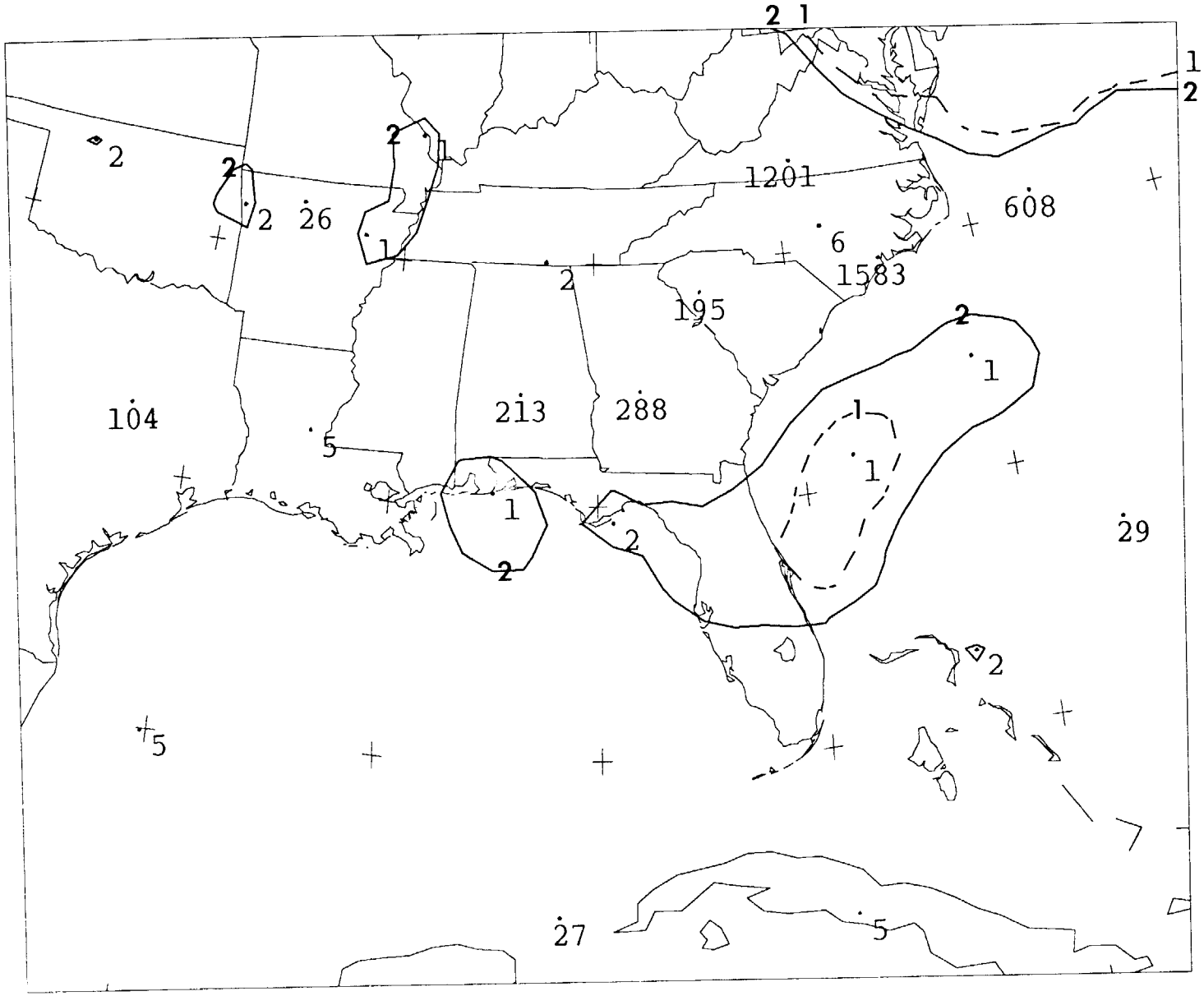

Figure 45. Time-space-conversion analysis of Richardson number in the layer from 6.0 to 7.0 km at 1800 UTC 2 December 1988.

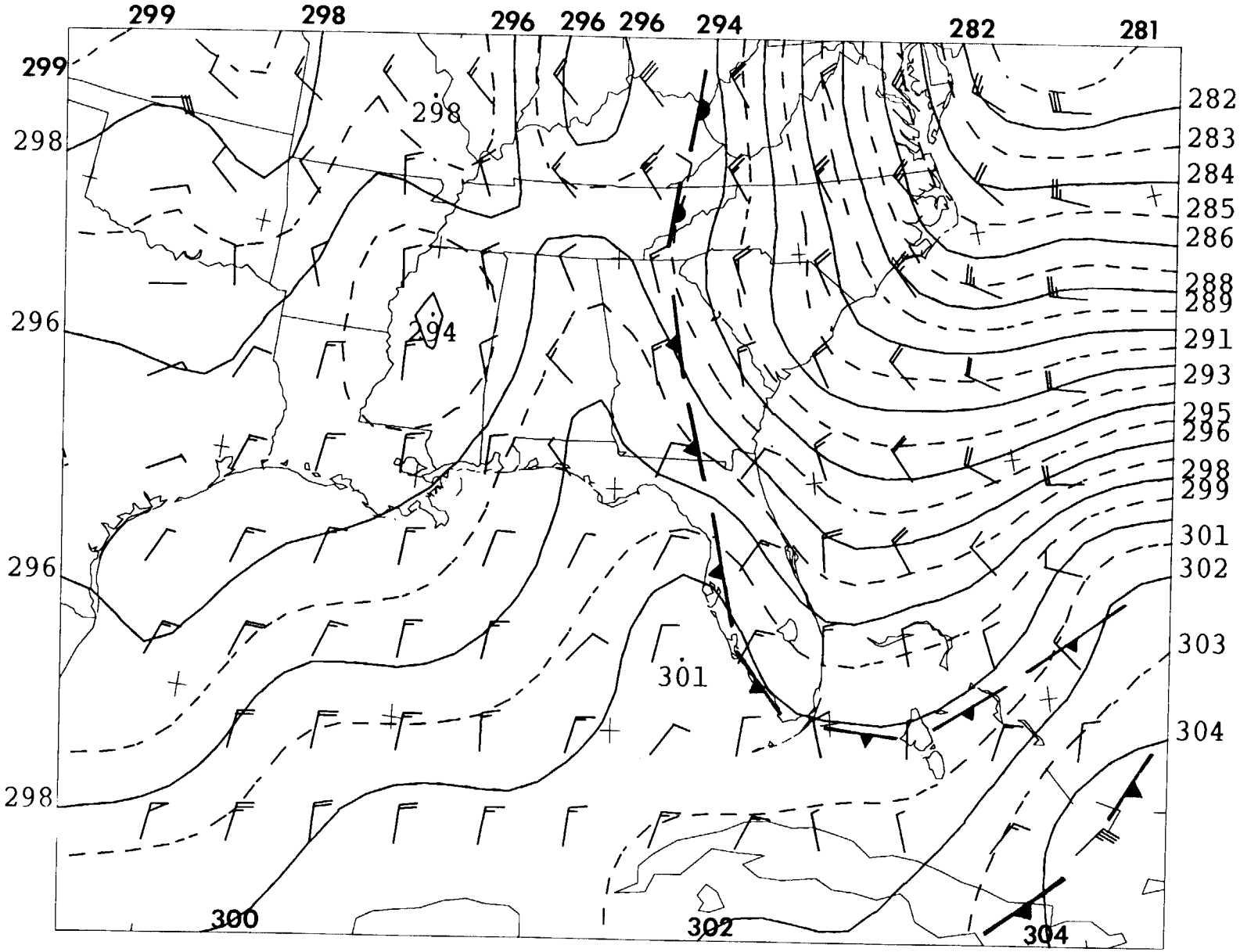

Figure 46. Time-space-conversion analysis of potential temperatures (K) and winds at 2.0 km, 1800 UTC 2 December 1988. Wind vectors are in knots.

3.3 Time-Space-Conversion Cross Sections

Time-space-conversion analyses were generated for each level from 0.5 to 15.0 km, at 0.5 km intervals. These have been used to generate cross sections of various parameters. Figure 47 shows the orientation of a cross section oriented normal to the upper-level jet stream, the "L" representing the left side of the cross section when viewed facing in the direction of the jet stream winds. A number of parameters are subsequently displayed on this section.

Figure 48 shows a cross section of total wind speeds and potential temperatures at 1800 UTC 2 December 1988, along the section of Fig. 47. The core of the jet stream is situated almost directly over KSC, residing atop the upper-level frontal zone. A protrusion of high wind speeds extends along (just above) the upper frontal zone, downward and to the right from the jet core, reaching about 4 km along the right side of the diagram. Another sloping wind maximum begins at about 5 km, midway between KSC and the left border, slopes across KSC at about 3 km, and then disappears midway toward the right border. This belt of winds appears to be affiliated with the "back-door" cold front of Fig. 46.

Figure 49 shows the pattern of Richardson numbers along this cross section. As will be discussed in more detail subsequently, Ri values reached 1 or less at several levels.

Figure 50 shows the values of the component of wind normal to (in/out of) the cross section. It is this component which is most directly related to the potential temperature pattern overlayed on the diagram. It can easily be seen that wind speeds increase with height where the temperature gradient (toward warm air) is oriented to the right. Above about 12 km the slope of

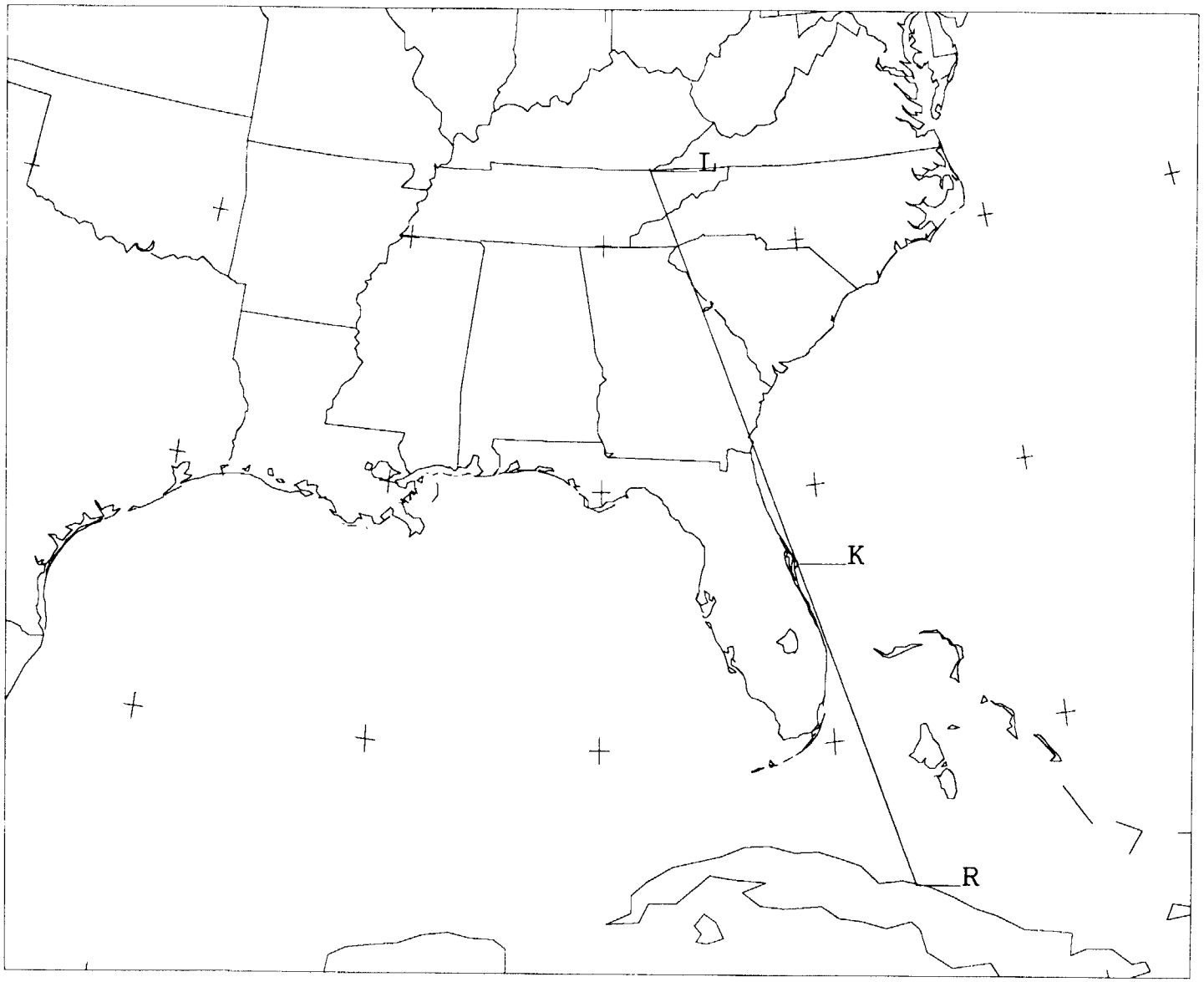

Figure 47. Base map showing the position of the left (L) and right (R) edges of the cross sections through Kennedy Space Center (K) at 1800 UTC 2 December 1988. The section is oriented perpendicular to the winds in the core of the upper-level jet stream across FL.

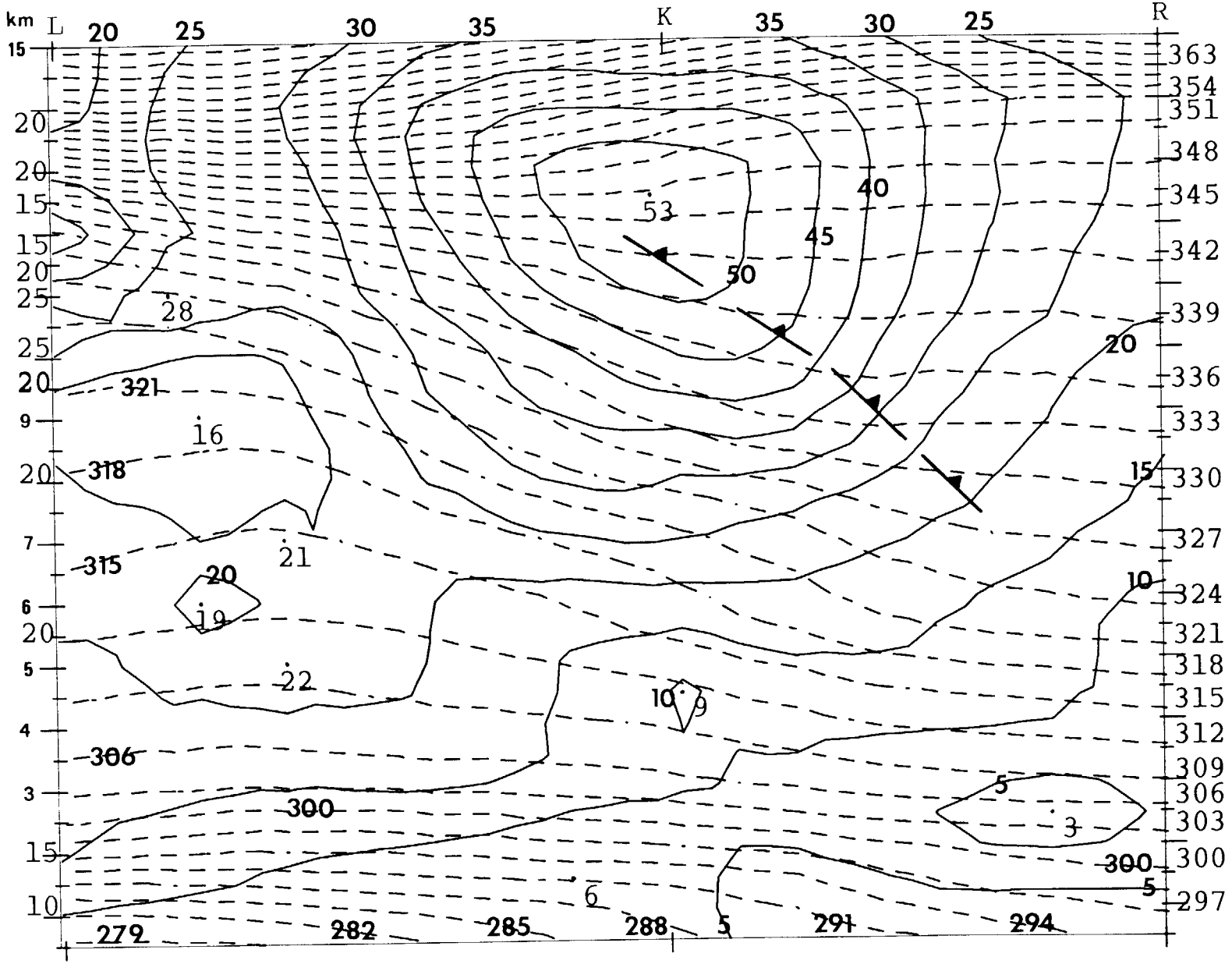

Figure 48. Time-space-conversion-based cross section of total wind speed (solid, m/s) and potential temperature (dashed, Kelvin) at 1800 UTC 2 December 1988.

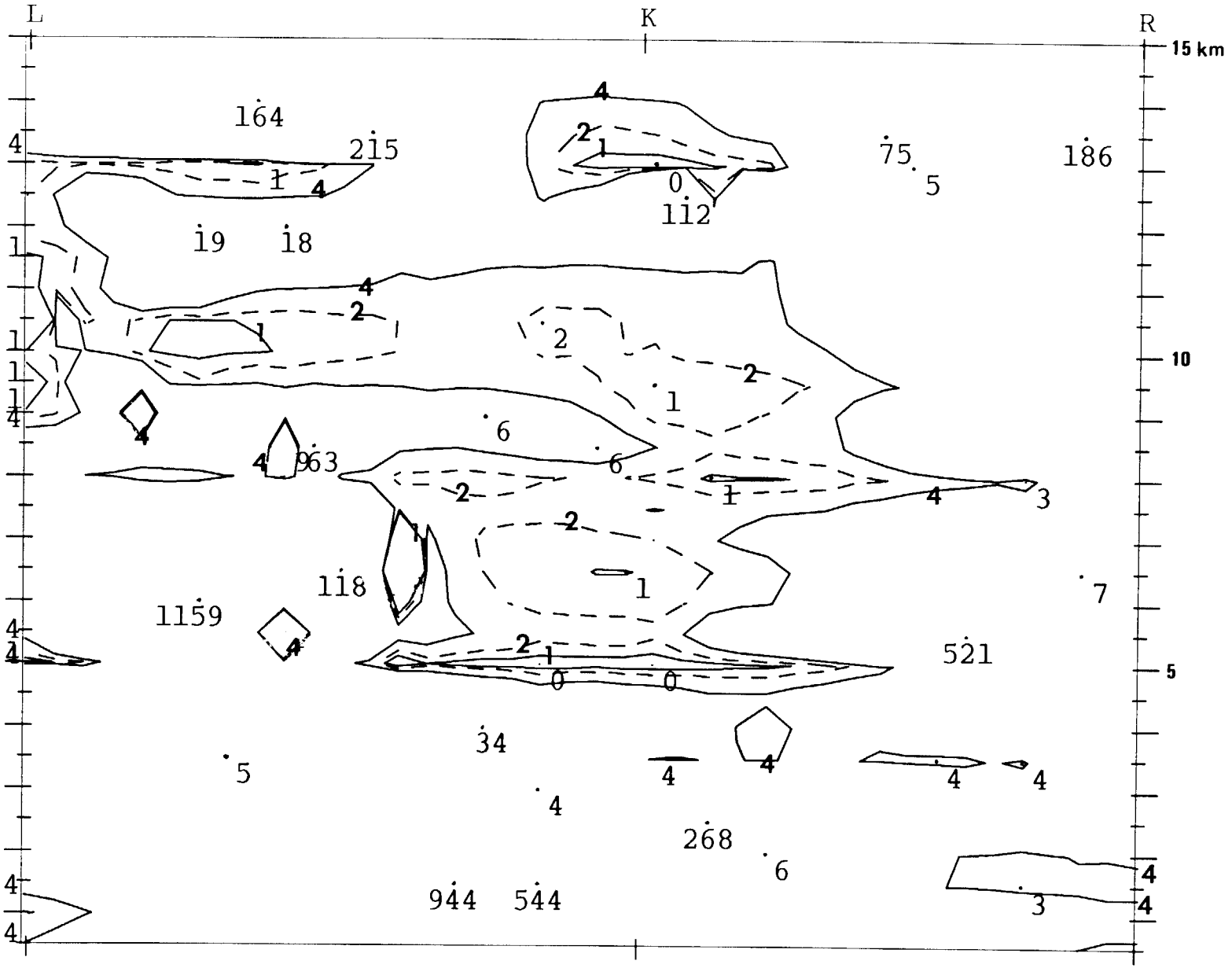

Figure 49. Time-space-conversion-based cross section of Richardson number computed over layers 1 km thick vertically for 1800 UTC 2 December 1988. Solid isopleths are at values 4 (outer) and 1 (inner). Dashed isopleth has value 2.

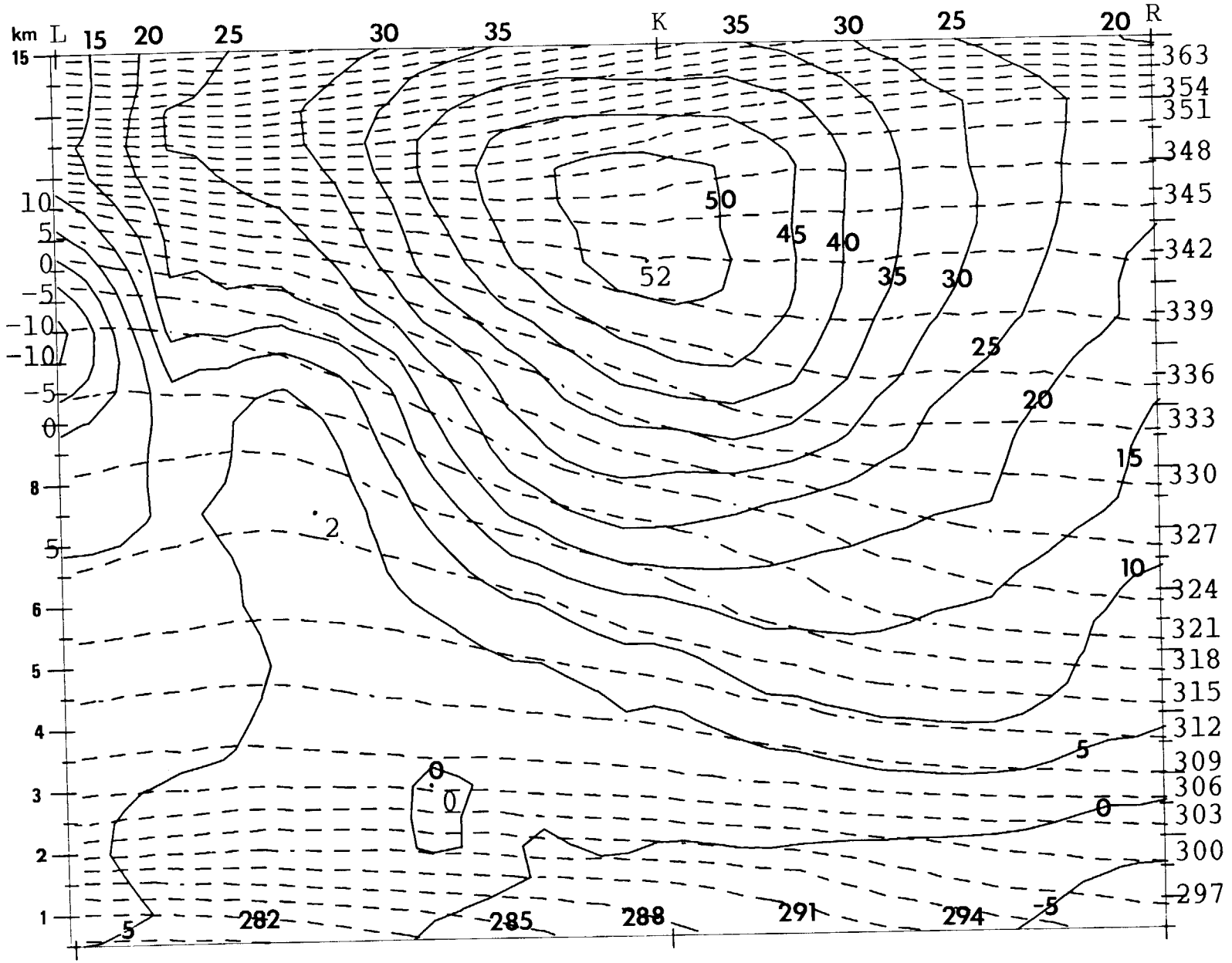

Figure 50. Time-space-conversion-based cross section of wind component (solid, m/s) normal to the plane of the cross section and potential temperatures (dashed, Kelvin) at 1800 UTC 2 December 1988. Positive wind components are directed into the plane away from the reader.

the adiabats reverses, and wind speeds decrease with height. Most of the latter region occurs within the lower stratosphere.

Figure 51 shows the adiabatic vertical velocities with respect to the potential temperature pattern. Most of the air is descending within this cross section, except for the mid-troposphere along the right border. This is consistent with what is expected within a large-scale confluence zone that is the entrance region of a jet core. Descent occurs within the region left of the jet core, and ascent in the region to its right.

Even more dramatically depictive of a large-scale entrance region is Figure 52, which shows the horizontal flow within the cross section and relative to the travelling jet core. Positive values indicate flow from right to left, and are seen to occur everywhere to the right of the sloping upper-level frontal zone. This is consistent with the need for the flow to angle toward lower geopotential heights (i.e., toward the left of the jet stream) in order to accelerate within the confluence zone. Beneath the upper-level front, the relative flow is rightward; also typical of an entrance region.

Figure 53 depicts the two-dimensional relative streamlines of flow within the plane of the cross section. The vertical and horizontal velocity components have been scaled such that the angles of descent shown by the streamlines have the correct orientation with respect to the adiabats and all other analysis features. The katabatic nature of the upper-level front can clearly be seen, and is in superb agreement with the clear skies at all levels above the boundary layer, as seen in satellite imagery over this region (Fig. 3).

Figure 54 shows the departure of the 1800 UTC 2 December 1988 potential temperature along the cross section from the 36-hour mean values. A band of negative departures runs parallel to and left of the upper-level front, as

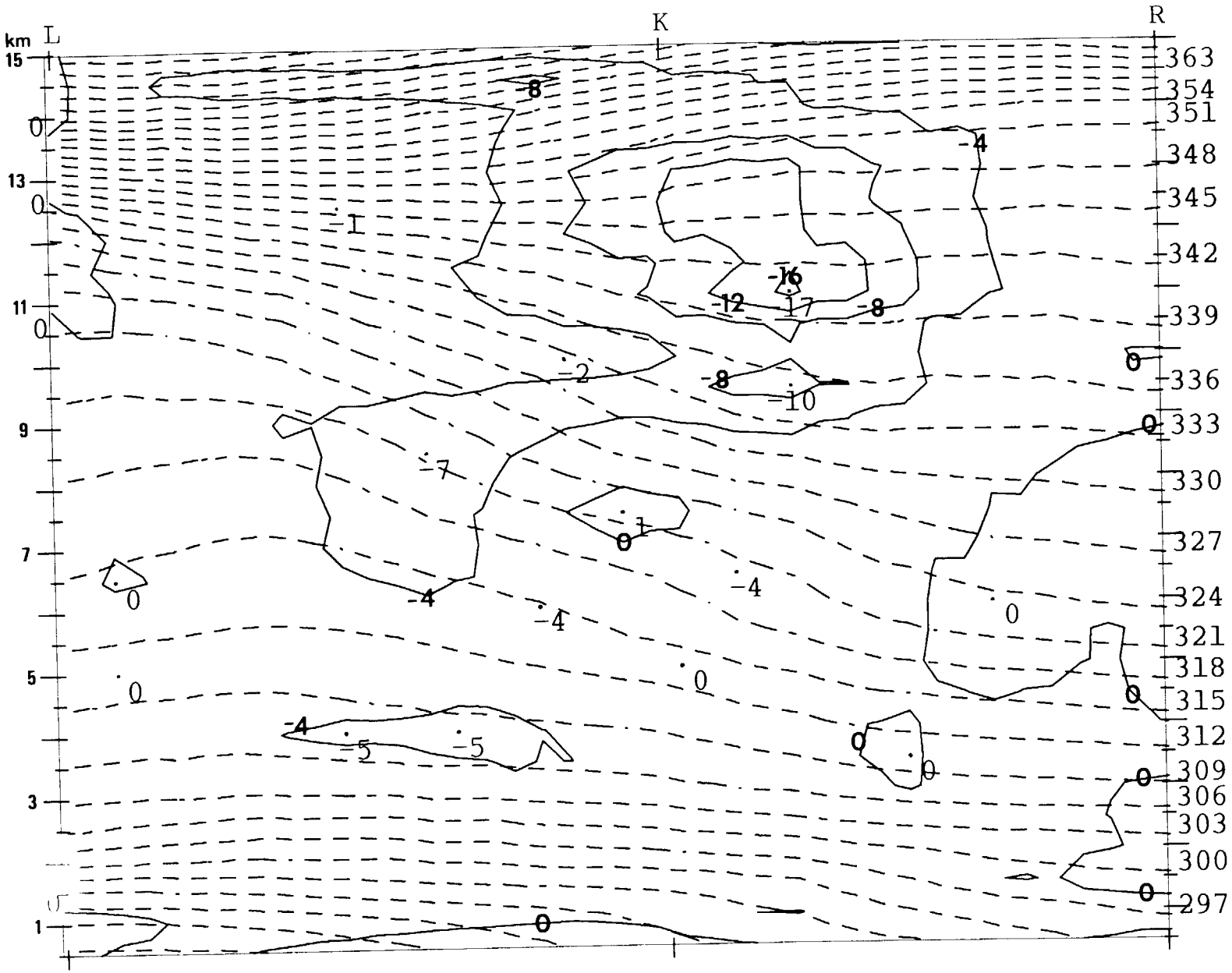

Figure 51. Time-space-conversion-based cross section of adiabatic vertical velocity (solid, cm/s) and potential temperature (dashed, Kelvin) at 1800 UTC 2 December 1988.

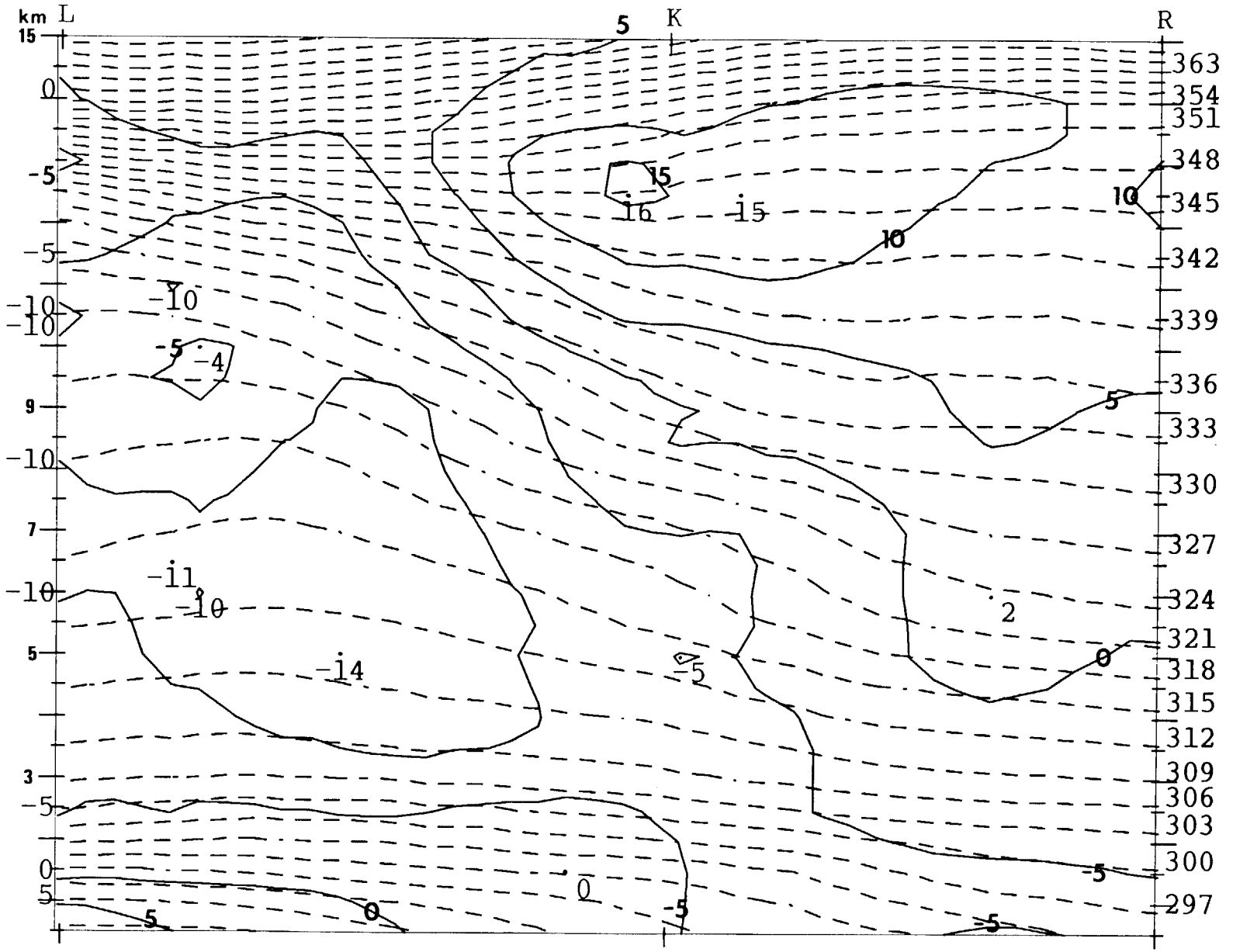

Figure 52. Time-space-conversion-based cross section of the horizontal component of relative velocity in the plane of the cross section (solid, m/s) and potential temperatures (dashed, Kelvin) at 1800 UTC 2 December 1988). Positive velocities are directed from right toward left.

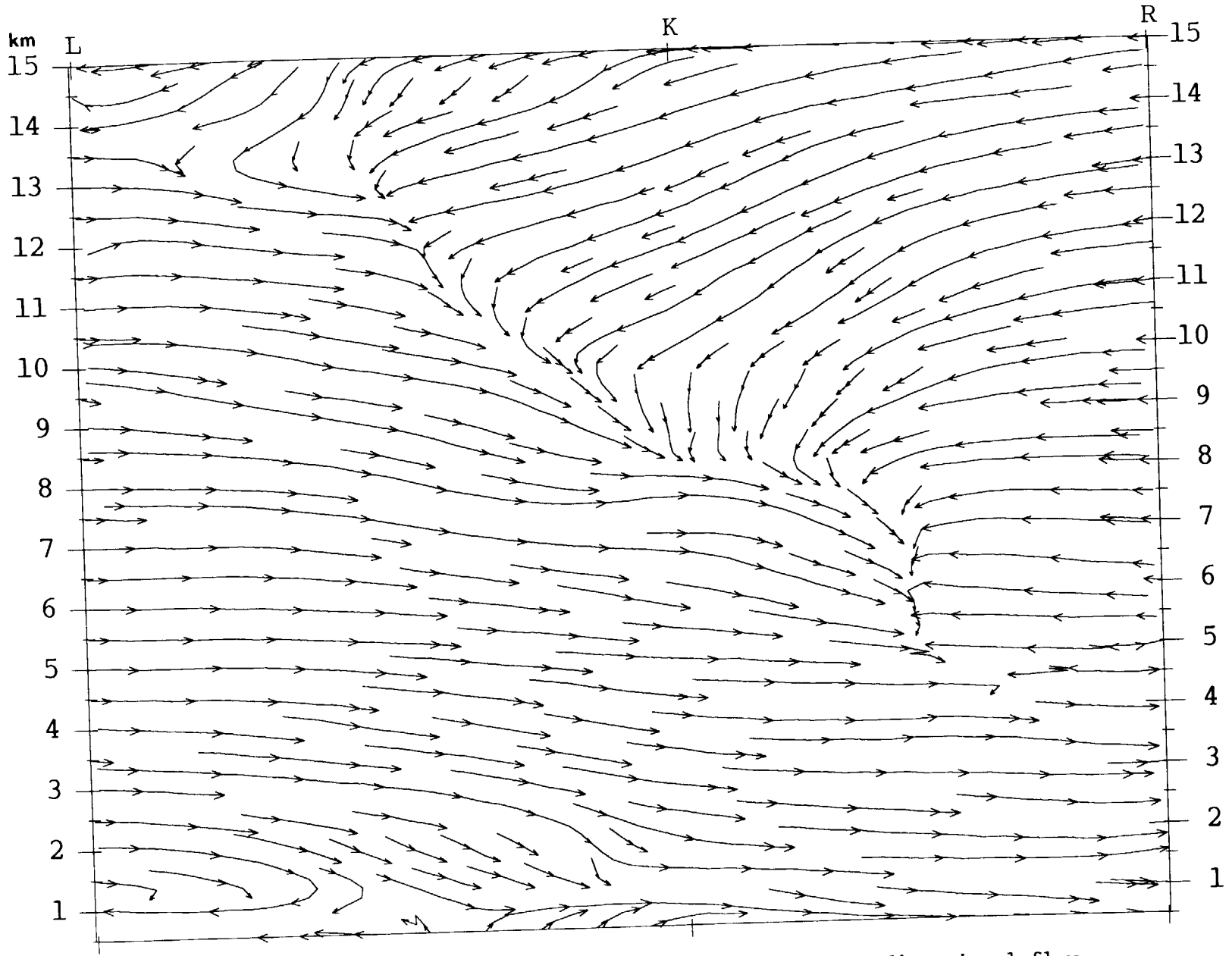

Figure 53. Time-space-conversion-based streamlines of two-dimensional flow within the plane of the cross section at 1800 UTC 2 December 1988. Horizontal and vertical velocities are scaled appropriate to the dimensions of the section, so that angle of the flow is correct.

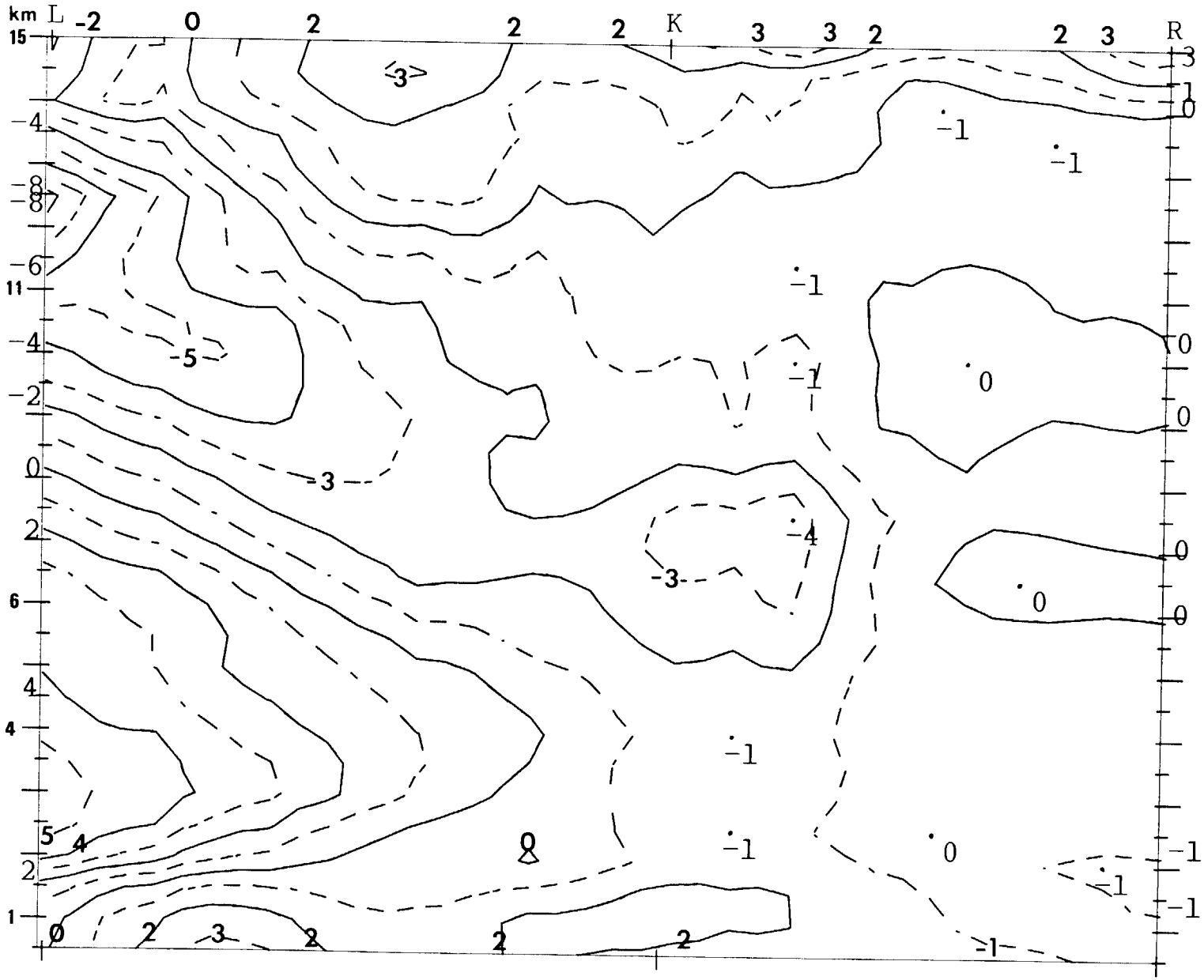

Figure 54. Time-space-conversion analysis of the departure of the potential temperature (solid, Kelvin) at 1800 UTC 2 December 1988 from the 36-hour mean values.

would be expected of a rightward-moving frontal zone. Despite the relative cold pool at 4-5 km near the left edge of the diagram in Fig. 48, temperatures there are actually warmer than the 36-hour mean. This region is in the warm tongue found northwest of the location of the back-door cold front of Fig. 46. The modest cooling associated with the back-door cold front can be seen above and just left and right of KSC in the form of -1 K anomalies.

Figure 55 shows the frontogenesis tendency due to the confluence of Figs. 52 and 53, from the confluence term of Miller (1948). Strongest frontogenesis tendencies are found somewhat left of KSC, at the 8-12 km levels, with weaker values extending to about 5 km just north of KSC. Another, but somewhat weaker, zone of strong frontogenesis is present to the right of KSC at 5.5-7.5 km. Weaker values of frontogenesis angle upward from this maximum to 13 km above KSC and almost straight downward to about 2 km.

3.4 Analyses at Launch Time

Figures 56 and 57 show time-space-conversion analyses of the total winds at 13.0 km at 1400 and 1500 UTC 2 December 1988, respectively. The comparable analysis for 1800 UTC was shown in Fig. 20. It can be seen from these figures that neither the overall shape of the pattern or the wind speeds changed much over the 4-hour period. However, the overall pattern did shift toward the east with time. For example, the pocket of 55 m/s wind speeds shifts from along the FL east coast at 1400 UTC to offshore at 1500 and further offshore by 1800. Some contraction of the size of the pocket occurred during the last 3 hours.

Other analyses for 1500 UTC, therefore, can be approximated from the analyses of the previous section. The relative position of KSC at 1500 UTC with respect to one of the 1800 UTC analyses can be obtained by placing a dot

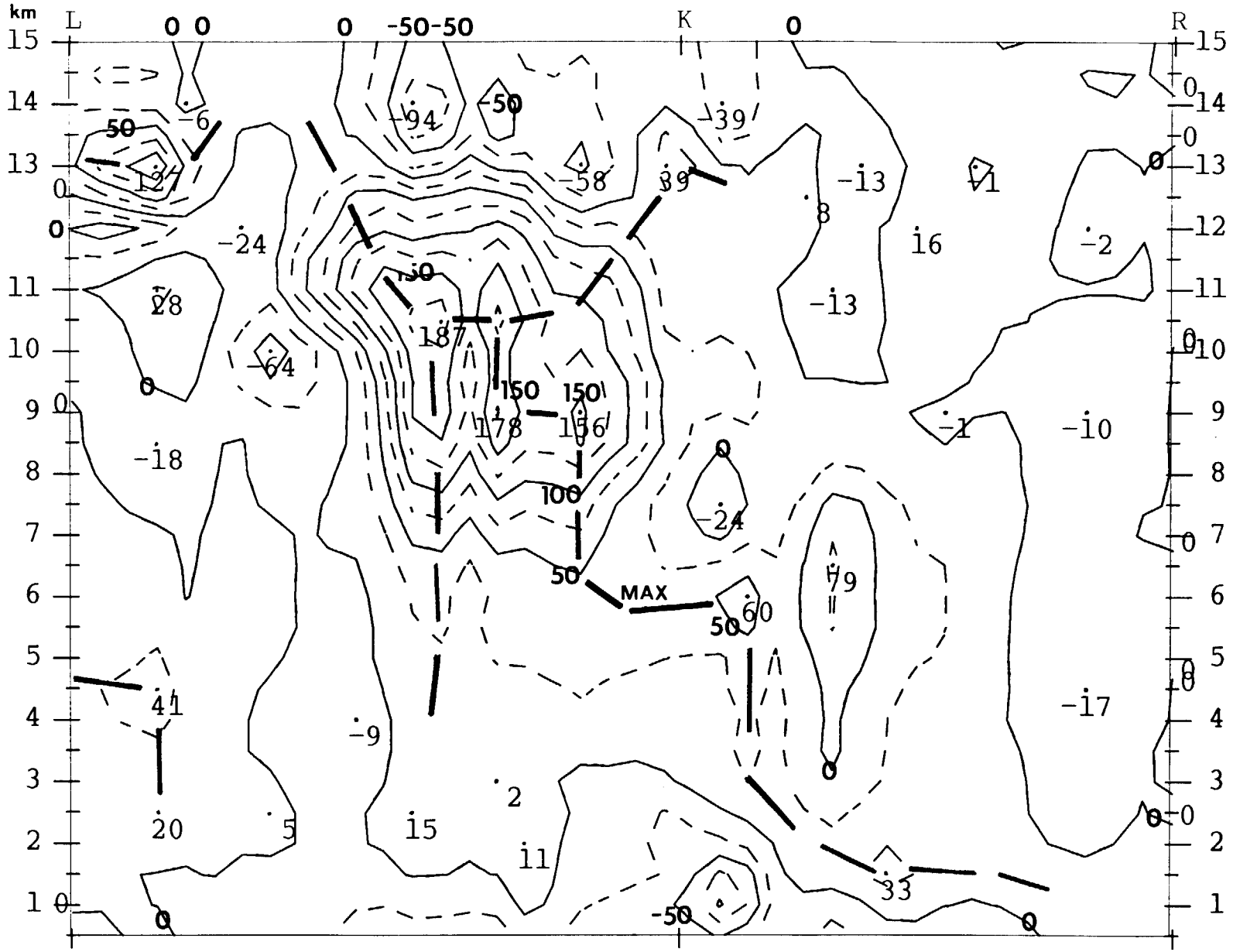

Figure 55. Time-space-conversion-based analysis of the rate of frontogenesis due to confluence, for 1800 UTC 2 December 1988, in units of 10^{-5} degrees per 100 km per second.

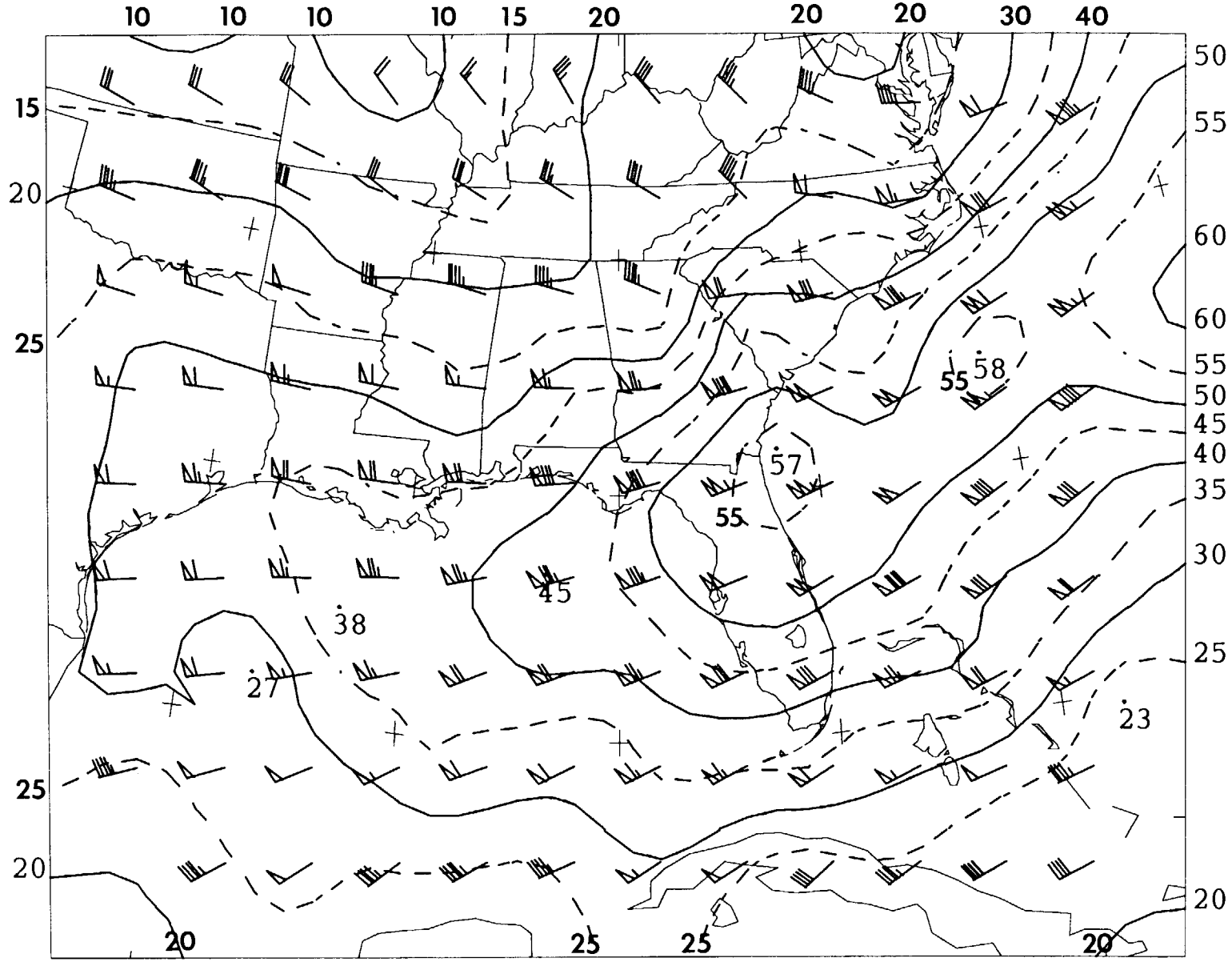

Figure 56. Time-space-conversion analysis of the winds at 13.0 km, 1400 UTC 2 December 1988. Isotachs are in m/s; vectors are in knots.

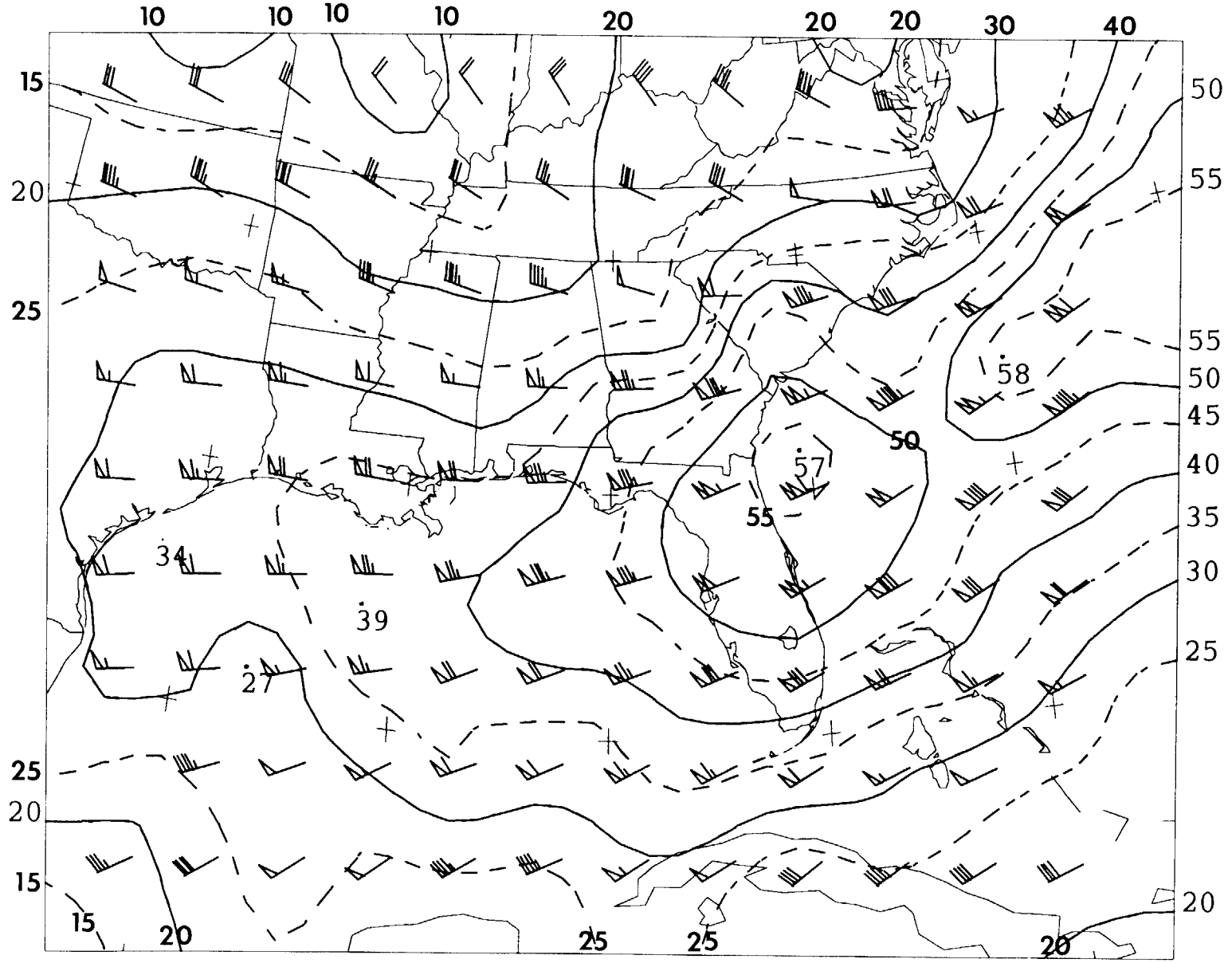

Figure 57. Time-space-conversion analysis of the winds at 13.0 km, 1500 UTC 2 December 1988. Isotachs are in m/s; vectors are in knots.

on the map about 190 km east of KSC. This means that the axis of the jet at 10.0 km (Fig. 34), for example, would have been almost directly over KSC at 1500 UTC. It also means that the axis of the jet at other levels has shifted.

Figure 58 shows the approximate position of a cross section at 1800 UTC which would have been over KSC at 1500 UTC. Figures 59 is the corresponding cross section of wind speed and potential temperature which would approximate the one through KSC at 1500 UTC. By comparison to Fig. 48, it can be seen that the pattern has not changed greatly. The core of the jet stream was somewhat farther to the left at 1500 UTC; the sloping protrusion of maximum wind speeds along the upper-level front was a bit stronger at 11 km and weaker near 5 km at 1500 UTC; and the belt of maximum winds along the back-door cold front near the left border of the diagram near 6 km was stronger at 1500 UTC.

Figure 60 shows the approximate cross section of Richardson numbers through KSC at 1500 UTC. This can be compared to the 1800 UTC analysis of Fig. 49. Most of the levels having minimum Richardson numbers have remained the same, and values have stayed the same at 5 and 13 km. However, the 1500 UTC values are slightly smaller near 9.5 and 6.5 km; these levels at 1500 UTC appear just as potentially hazardous as those at 5 and 13 km.

3.5 Richardson Numbers Over Kennedy Space Center

Table 8 summarizes the values of Richardson number in 1.0 km vertical layers above KSC at 1800 UTC 2 December 1988. Minimum values of 1.0 are found at 6.5 and 10.0 km. There are valid questions concerning how much lower these values might have been in thinner layers and without some of the implicit smoothing affiliated with an analysis using grid points spaced about 65 km apart.

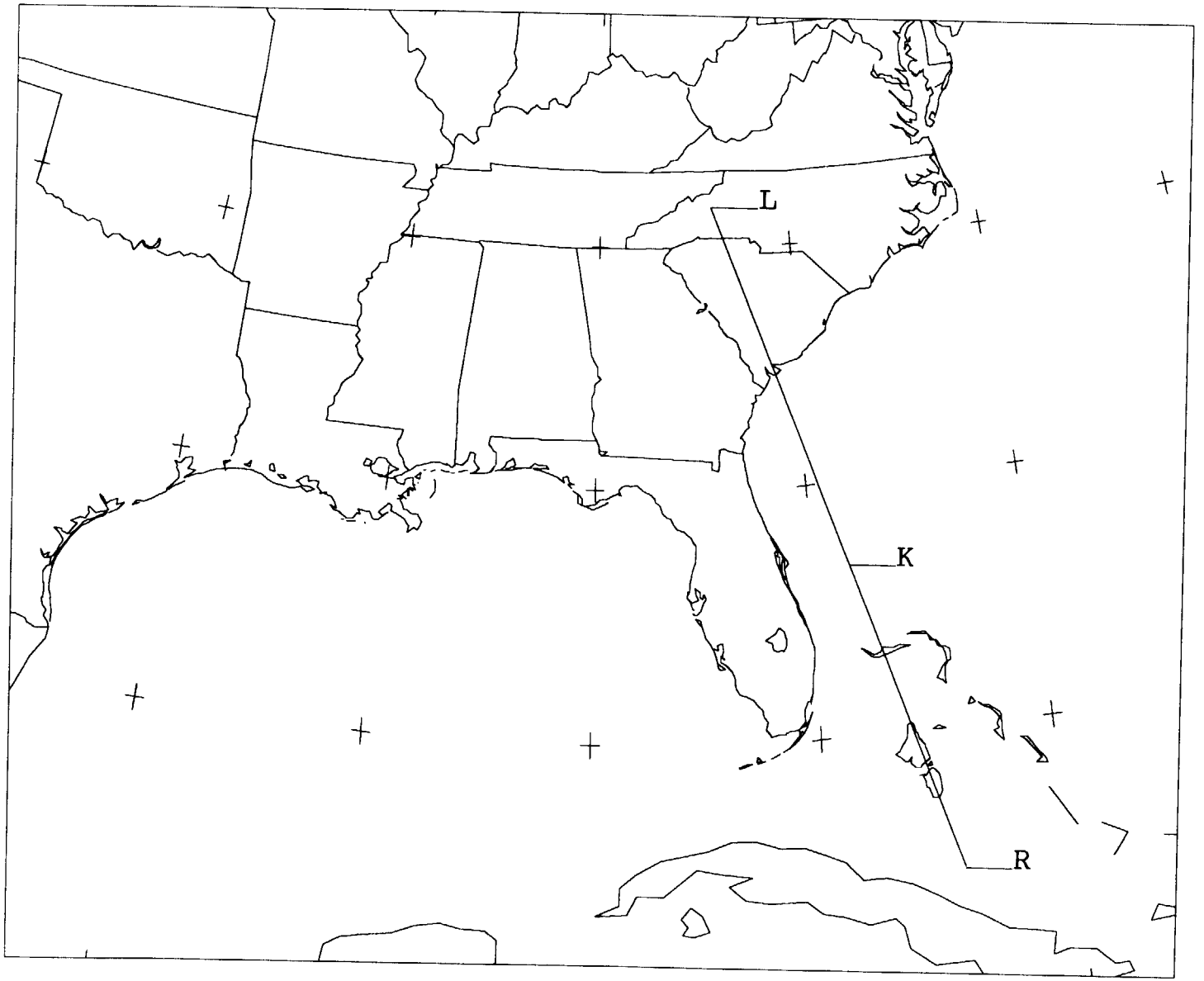

Figure 58. Base map showing the location of the 1800 UTC cross section which would have been oriented across KSC at 1500 UTC.

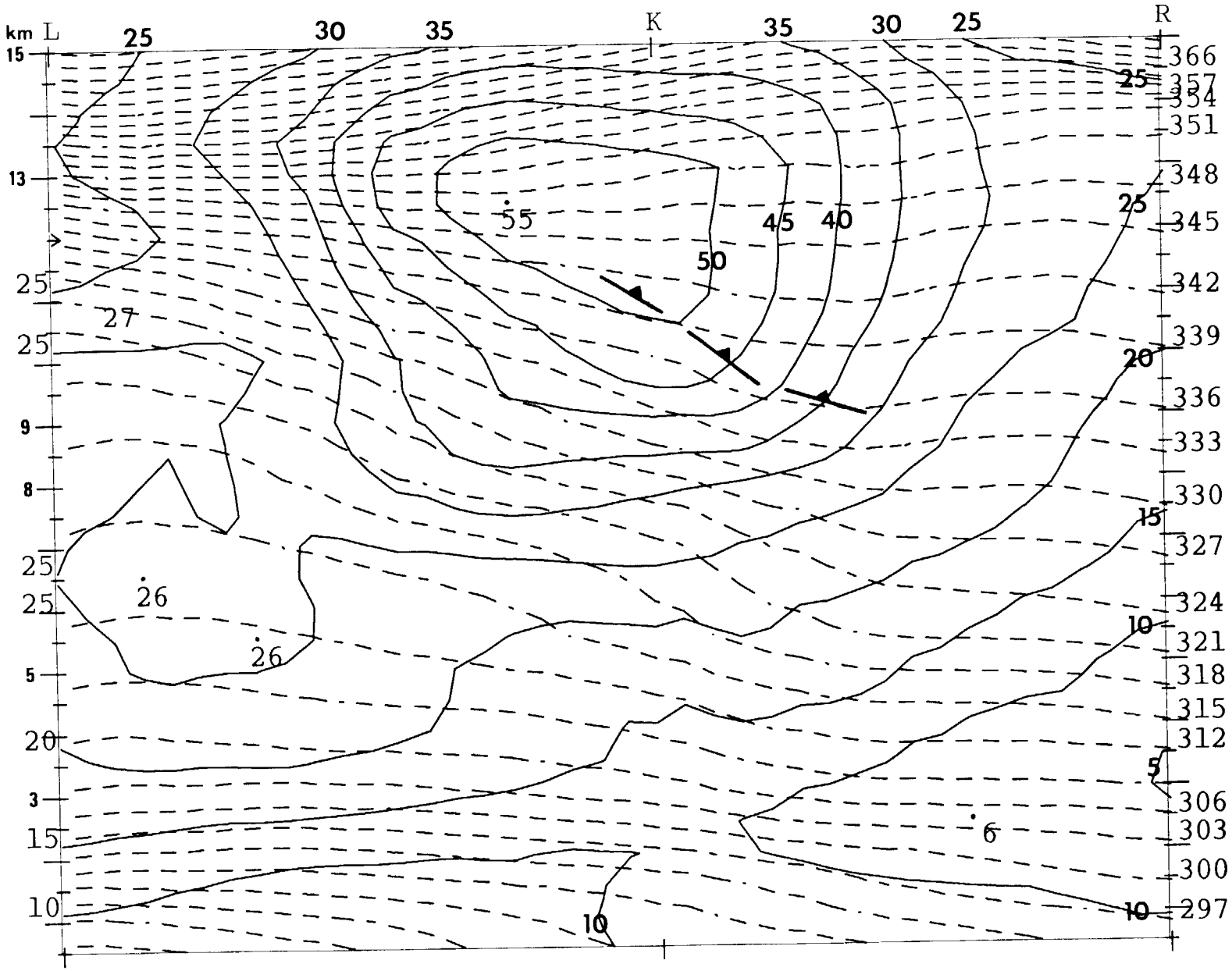

Figure 59. Cross section along the section of Fig. 58, showing wind speeds (solid, m/s) and potential temperatures (dashed, Kelvin) as they would have appeared along the section over KSC at 1500 UTC.

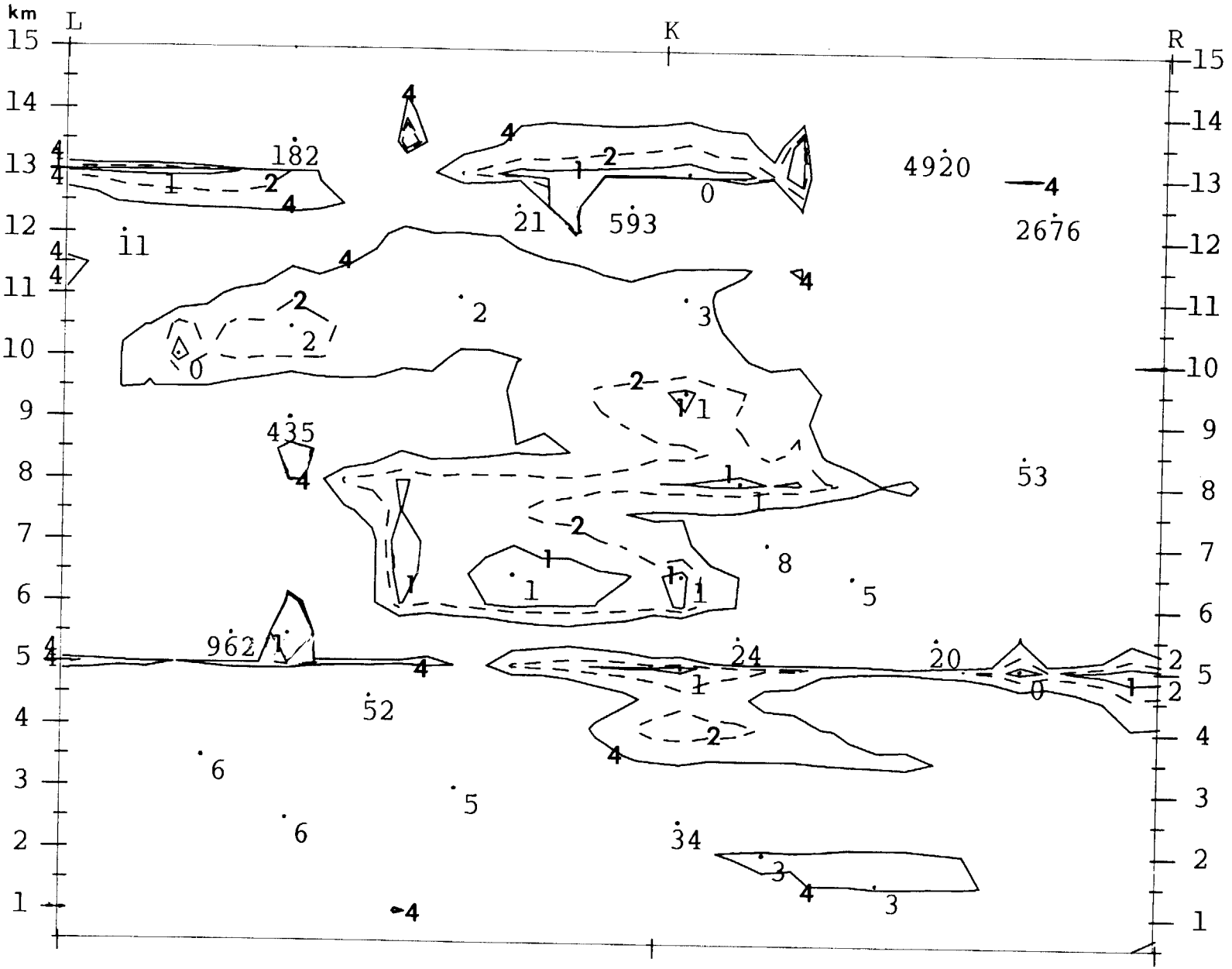

Figure 60. Cross section along the section of Fig. 58, showing Richardson numbers as they would have appeared along the section over KSC at 1500 UTC. Solid isopleths are of value 4 (outer) and 1 (inner). Dashed isopleth has value 2.

Table 9 partly addresses the question of the effect of vertical layer thickness on Ri value. Richardson numbers were computed for selected layers 0.5 km thick in the vicinity of the layers of Table 8 that had low values surrounded by considerably higher values. In the 0.5 km layers, minimum values decreased, reaching 0.8 in the layer between 6.0 and 6.5 km.

As a mental exercise, if we assume that 40% of the vertical wind shear in that 0.5 km layer above could have occurred in a layer only 100 m thick, then the Ri in the 100 m layer would have been 0.20. A similar assumption--that 30% of the vertical wind shear in a 1.0 km layer could occur in a layer only 100 m thick, suggests that clear air turbulence could occur in shallow layers whenever the Ri value in a 1.0 km layer was 2.25 or less. It remains for turbulence experts to determine the validity of this assumption.

4. SUMMARY AND CONCLUSIONS

The analysis of 2 December 1988 showed that KSC was within the confluent entrance region of a strong upper-level jet stream. This axis of the main upper-level jet stream and an associated upper-level front were centered over KSC at some levels during the STS27 launch. The axis of the main branch of the jet stream sloped southward toward lower altitudes, parallel to the upper-level front. In addition, at lower levels, a branched feature of the jet stream caused another axis of maximum winds to be centered over KSC in the mid-troposphere. Below 4 km, KSC was under the influence of a cold northerly flow behind a "back-door" cold front located over western and southern Florida between 1.5 and 4 km.

The analyses of this report have shown that the regions of most probable clear air turbulence in this case were at or just above lower and upper-level frontal zones, at or just below upper-level frontal zones, and from just below

TABLE 8

TIME-SPACE-CONVERSION ANALYSIS VALUES OF RICHARDSON NUMBER IN LAYERS 1.0 KM THICK, CENTERED ON THE INDICATED LEVEL ABOVE KENNEDY SPACE CENTER AT 1800 UTC 2 DECEMBER 1988

Level (km)	Richardson Number	Level (km)	Richardson Number
15.0	1500.0	7.5	3.5
14.5	7.0	7.0	1.8
14.0	4.0	6.5	1.0
13.5	2.0	6.0	1.5
13.0	4.0	5.5	3.0
12.5	15.0	5.0	3.5
12.0	7.0	4.5	6.0
11.5	5.0	4.0	10.0
11.0	2.5	3.5	5.5
10.5	2.0	3.0	10.0
10.0	1.0	2.5	10.0
9.5	1.5	2.0	175.0
9.0	2.0	1.5	400.0
8.5	5.0	1.0	600.0
8.0	1.8	0.5	100.0

TABLE 9

TIME-SPACE-CONVERSION ANALYSIS VALUES OF RICHARDSON NUMBER IN SELECTED LAYERS: INTERCOMPARISON OF VALUES IN LAYERS 1.0 KM THICK VERSUS 0.5 KM THICK, CENTERED ON THE INDICATED LEVEL ABOVE KENNEDY SPACE CENTER AT 1800 UTC 2 DECEMBER 1988

Center of layer	1.0 km Layer	0.5 km Layer
13.50	2.0	
13.25		1.5
13.00	4.0	
7.00	1.8	
6.75		1.3
6.50	1.0	
6.25		0.8
6.00	1.5	
5.00	3.5	
4.75		3.9
4.50	6.0	
4.25		2.0
4.00	10.0	

to just above the tropopause. The analyses also showed that the lowest values of Ri occurred where vertical wind shears typical of those expected within frontal zones or sloping tropopause layers extended slightly upward or downward into regions of lowered static stability. Primarily because of the need for the juxtaposition of the shear and low-static-stability layers, the low Ri zones appeared in the cross sections to be somewhat sporadic. An argument is presented which suggests that values of 2.25 or less in 1.0 km layers in the time-space conversion analyses should be treated as potentially containing shallow layers of clear-air turbulence.

The author is not an expert on clear-air turbulence. Nevertheless, it is interesting to speculate whether subresolution features such as gravity waves may play some role in allowing the extension of frontal-zone-type vertical wind shears into regions of sub-frontal-magnitude static stability. It seems plausible that gravity waves propagating within the statically stable frontal zone might induce sufficient vertical velocities (and vertical gradients of vertical velocities) near the top and bottom edges of the frontal zone to temporarily alter the static stabilities at levels near these interfaces. The vertical velocities would quickly advect the frontal surface slightly upward or downward, but would operate on such short time scales that the winds and vertical wind shears would not have time to adjust. Presumably where the front was rising the lowest Ri would be at the bottom of the frontal zone; vice versa for sinking fronts. Furthermore, in places where a vertical stretching took place, there would be some destabilization within the edge portion of the frontal zone, which also would act too quickly for the winds and wind shears to adjust--perhaps leading to turbulence.

The overall impression is that the time-space conversion technique does a very good job of analysis of the structure of weather systems, with

resolution that is determined by the input data. The overall features of the analyses are relatively persistent and can, therefore, be extrapolated forward in time to give short-term forecasts. However, the resolution of the forecasted fields is dependent upon the availability of data upstream of the forecast site. This means that preceding data collected from a wind profiler or other high-temporal-frequency measurement platform at the forecast site are of limited value since, from a time-space conversion perspective these data "drift" downstream, and away from the forecast site. Upstream data are needed.

Furthermore, it remains to be seen whether a time-space conversion forecast, or any other type of forecast, can consistently distinguish small differences in Richardson numbers when the values are near 1. However, as a first look at this topic, the 18h NGM forecasts for 1800 UTC 2 December 1988 were evaluated. Figure 61 shows the 300 mb winds (about 9.5 km) predicted for that time. Similarities to the analyses of Chapter 3 are obvious. Figure 62 shows the shear velocities across the layer from 400 mb to 300 mb (about 7.5 to 9.5 km). While the values are lower than those of Fig. 37, they are not bad for a 2 km layer. Figure 63 shows the values of Richardson number derived from the NGM wind and temperature forecasts. For the entire 300-400 mb layer (about 2 km thick), Ri value is about 2.5 to 3 at KSC. These forecasts give reason for optimism that mesoscale numerical weather prediction models can accurately predict vertical wind shears and Richardson numbers.

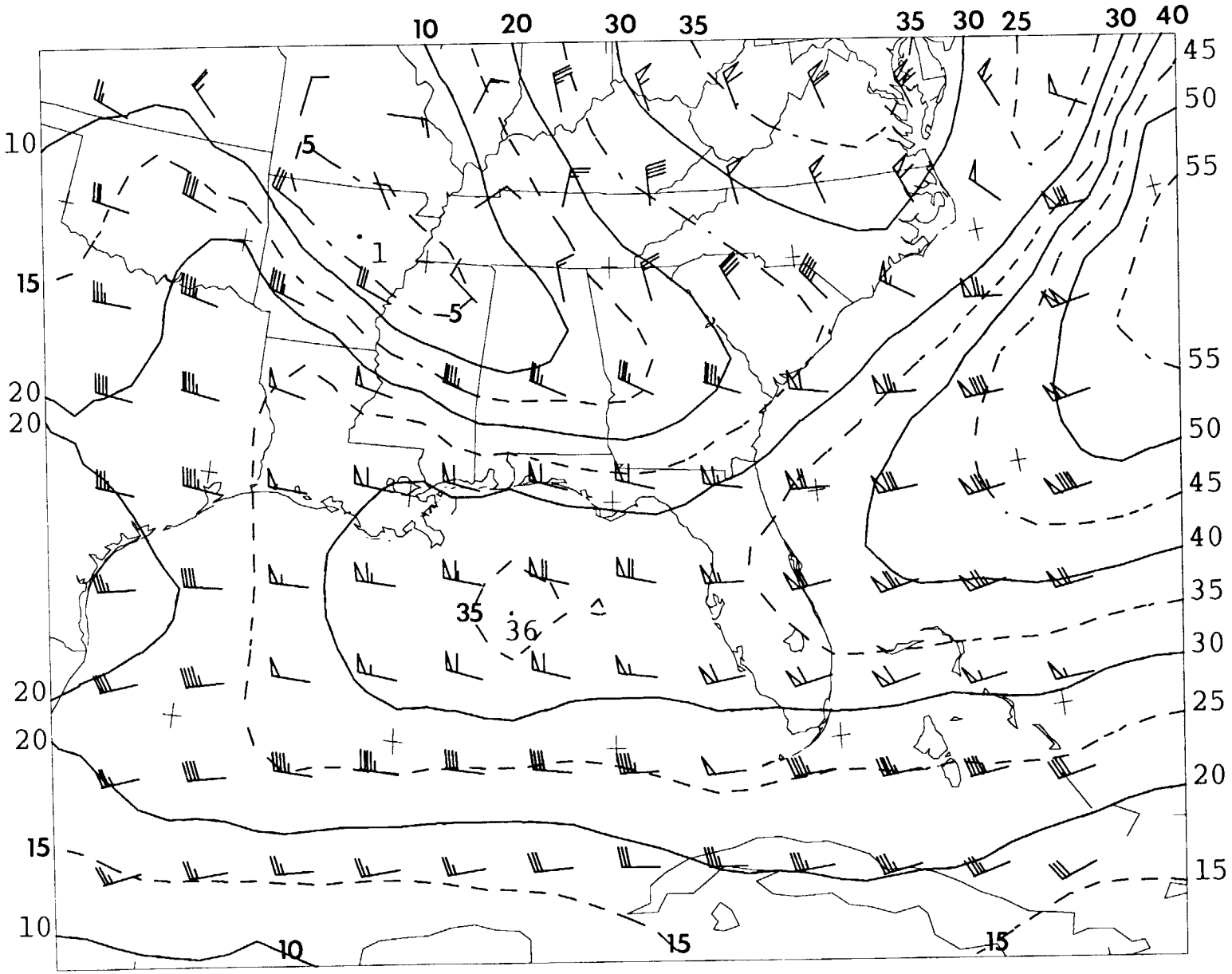

Figure 61. NGM 18h forecast of winds at 300 mb, valid 1800 UTC 2 December 1988. Isotachs are in m/s; vectors are in knots.

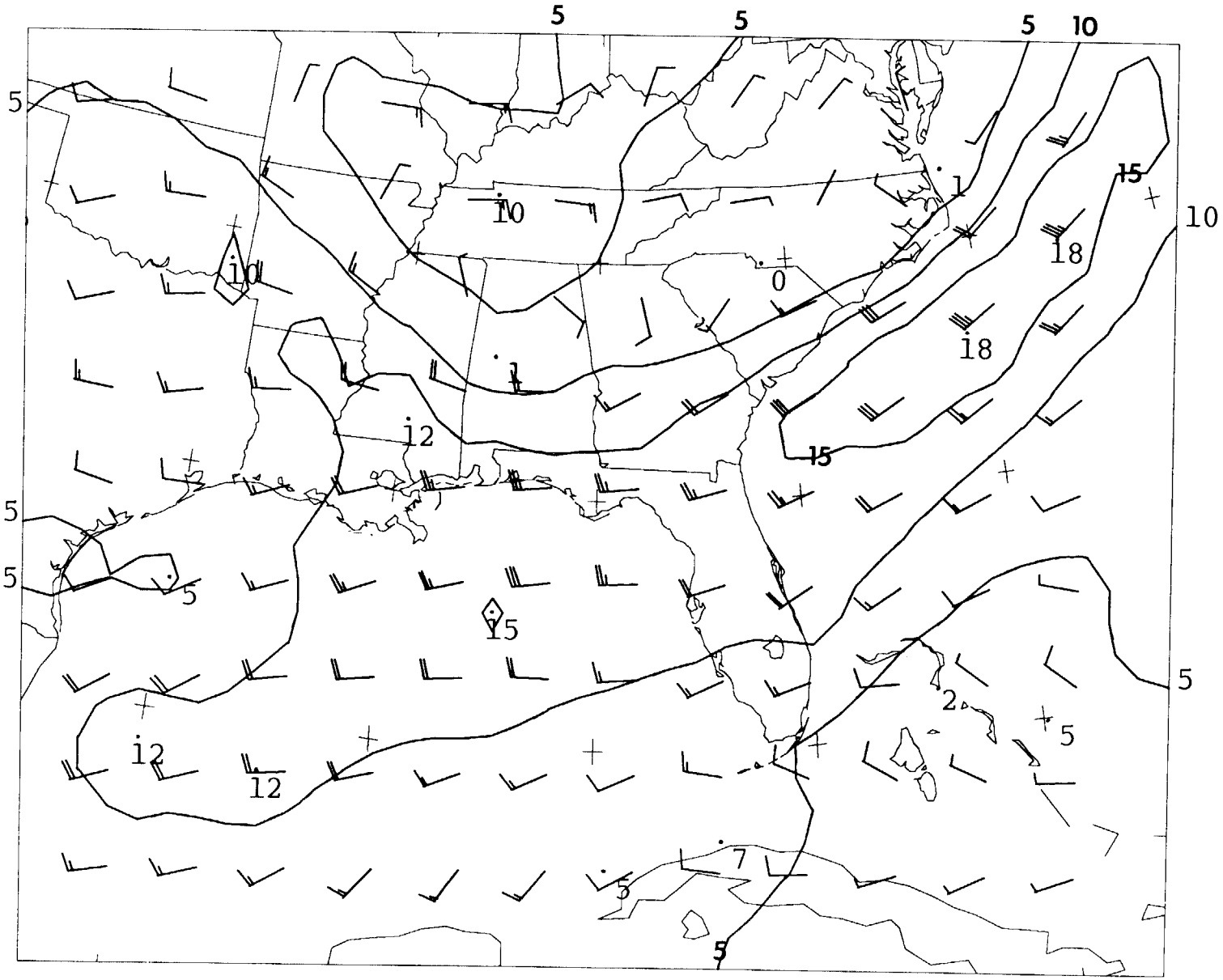

Figure 62. NGM 18h forecasts of the shear vector between 300 and 400 mb at 1800 UTC 2 December 1988. Isotachs are in m/s; vectors are in knots.

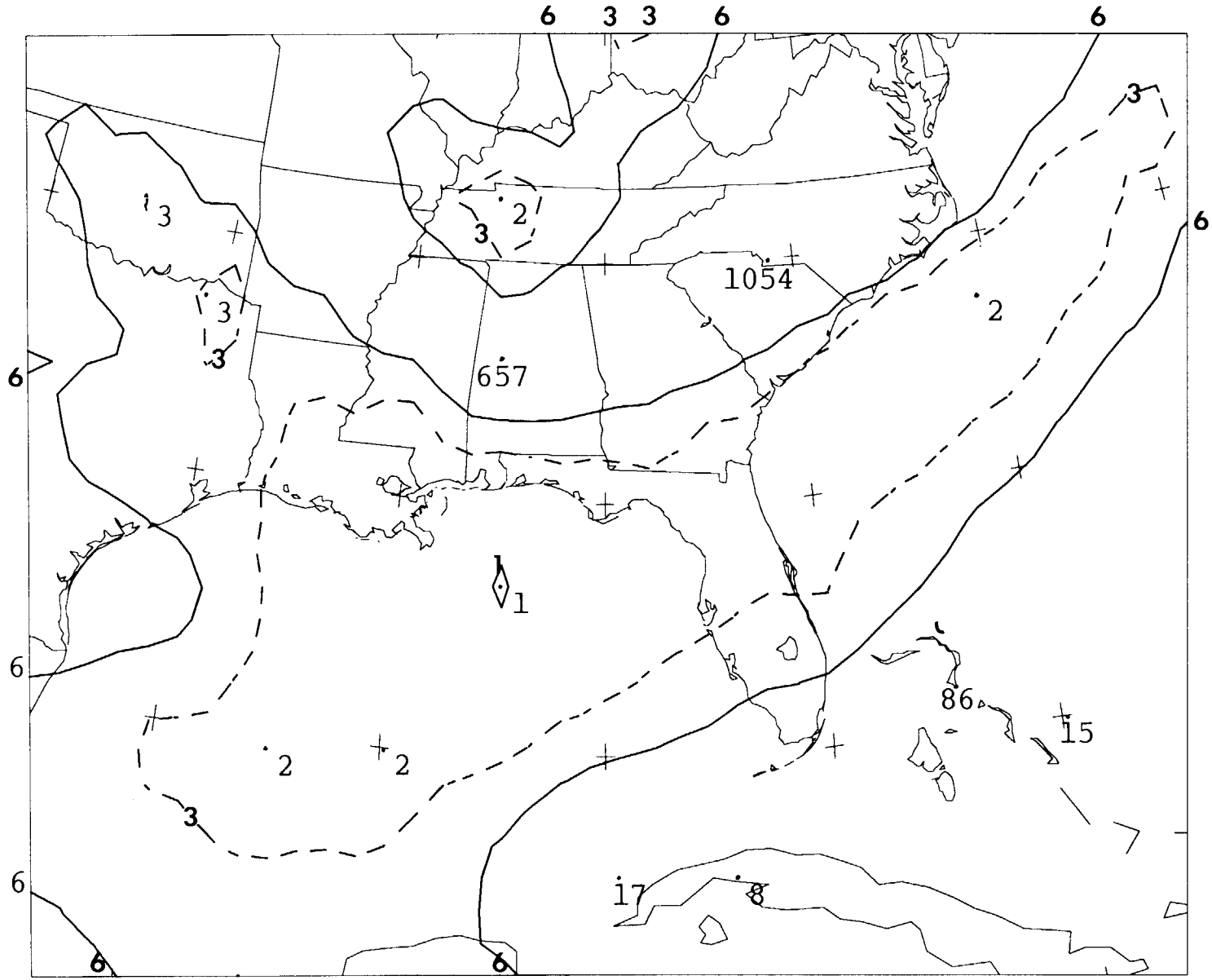

Figure 63. Forecast of Richardson number in the layer between 400 and 300 mb for 1800 UTC 2 December 1988, based upon 18h NGM forecasted winds, temperatures and heights of the pressure levels.

REFERENCES

Cressman, G.P., 1959: An operational objective analysis system. Mon. Wea. Rev., 87, 367-374.

Forbes, G.S. and R. Bankert, 1987: Satellite imagery and conceptual models in mesoscale forecasting. Proc., Symposium on Mesoscale Analysis and Forecasting, Vancouver, Canada, ESA SP-282, 251-261.

Forbes, G.S. et. al, 1990: Analysis of significant weather on meso-alpha scales using conventional and remotely-sensed data -- further studies. Final Report on Contract F19628-86-C-0092, The Pennsylvania State University, 114pp. [Also published by the U.S. Air Force Geophysics Laboratory as GL-TR-89-0288.]

Fujita, T.T., 1955: Results of detailed studies of squall lines. Tellus, 7, 405-436.

Fujita, T.T., 1963: Analytical mesometeorology: A review. Meteor. Monogr., 5(27), 77-125.

Herzog, R.F., 1990: Analysis of the May 31, 1985 tornado outbreak using time-space conversion. B.S. Thesis, The Pennsylvania State University, 37pp.

Lee, M.-T., 1990: Analysis of mesoscale substructure of cyclones and jet streams, using time-space conversion of VHF Doppler wind profiler and rawinsonde data. M.S. Thesis, The Pennsylvania State University, 189pp.

Miller, J.E., 1948: On the concept of frontogenesis. J. Meteor., 5, 169-171.

O'Brien, J.J., 1970: Alternative solutions to the classical vertical velocity problem. J. Appl. Meteor., 9, 197-203.

Thomson, D.W. and S.R. Williams, 1990: Analysis of comparative wind profiler and radiosonde measurements. Preprints, 10th Int'l. Geosc. Rem. Sensing Symp., College Park, MD, pp. 537- 540.

REPORT DOCUMENTATION PAGE

Form Approved
OMB No. 0704-0188

1. AGENCY USE ONLY (Leave blank)	2. REPORT DATE	3. REPORT TYPE AND DATES COVERED
	November 1992	Contractor Report (Final Report)

4. TITLE AND SUBTITLE
Development and Application of a Time-Space Conversion Technique for Analysis of Weather Systems Passing Over the Kennedy Space Center

5. FUNDING NUMBERS
G NAG8-754

6. AUTHOR(S)
Gregory S. Forbes

7. PERFORMING ORGANIZATION NAME(S) AND ADDRESS(ES)
Pennsylvania State University
Department of Meteorology
University Park, PA 16802

8. PERFORMING ORGANIZATION REPORT NUMBER
M-703

9. SPONSORING/MONITORING AGENCY NAME(S) AND ADDRESS(ES)
George C. Marshall Space Flight Center
Marshall Space Flight Center, AL 35812

10. SPONSORING/MONITORING AGENCY REPORT NUMBER
NASA CR-4474

11. SUPPLEMENTARY NOTES
Prepared for Earth Science & Applications Division, Space Science Laboratory, Science & Engineering Directorate.

COR: Cathy Carlson Lapenta

12a. DISTRIBUTION/AVAILABILITY STATEMENT
Unclassified--Unlimited

Subject Category: 47

12b. DISTRIBUTION CODE

13. ABSTRACT (Maximum 200 words)

A procedure for using asynchronous data to generate spatial analyses for a single time is described. This procedure, called a time-space conversion scheme, involves a separation of an individual observation into a perturbation component and a mean component. The mean component is readily estimated by averaging temporally over a series of observations taken at the same spatial location. The perturbation component at an individual time is then computed by taking the difference between the observation at that time and the temporal average at that location. When this separation is done for numerous sites and the data are plotted on a map and analyzed, it can be seen that the temporal-mean data relate to the large-scale conditions over the region. The perturbation data depict much smaller scales, indicative of mesoscale systems or substructures traveling through (and "steered" by) the larger-scale system. Accordingly, the perturbation component observed at a site at a particular time is displaced to the appropriate position at the analysis time, where it is added to the mean value at that location. The displacement is performed in a manner that preserves the position of the perturbation value with respect to the traveling mesoscale feature. Data from conventional National Weather Service (NWS) and Department of Defense (DOD) rawinsonde releases, special rawinsonde ascents, serial rawinsonde and Jimsphere launches at Kennedy Space Center (KSC), and from a wind profiler at KSC have been used in the time-space conversion scheme to perform analyses in a case study of a weather system passing over KSC. Because some of the perturbations measured over Florida and near the Gulf Coast and East Coast states become displaced over data-sparse oceanic regions, it became necessary to devise a method for determining temporal means over the offshore areas. This was done by using analyses from the Nested Grid Model (NGM) run twice daily at the National Meteorological Center (NMC) in Washington, D.C. Pseudo-soundings were constructed from these analyses at an array of oceanic locations and used to construct the temporal mean fields offshore. Similarly, in the event that measured data were not available at some levels and times at rawinsonde, Jimsphere, or profiler sites, the missing data were replaced with NGM analysis data for purposes of computing the temporal means at these sites. A case study from December 2, 1988, is used to illustrate the results of the time-space conversion scheme. Analyses are shown for the period from 1400-1800 UTC, which covers the second launch of the space shuttle (STS-27) following the Challenger tragedy of January 1986. The analyses reveal that a well-defined jet stream and upper-level front were situated over KSC at this time. Embedded within the jet stream were patches of strong vertical wind shear and low Richardson numbers, indicating a considerable risk of the presence of clear-air turbulence.

14. SUBJECT TERMS
Doppler, Profiler, Upper-Level Winds, Space Shuttle

15. NUMBER OF PAGES
120

16. PRICE CODE
A06

17. SECURITY CLASSIFICATION OF REPORT	18. SECURITY CLASSIFICATION OF THIS PAGE	19. SECURITY CLASSIFICATION OF ABSTRACT	20. LIMITATION OF ABSTRACT
Unclassified	Unclassified	Unclassified	Unlimited

NASA Contractor Report 4474

Development and Application of a Time-Space Conversion Technique for Analysis of Weather Systems Passing Over the Kennedy Space Center

Gregory S. Forbes

GRANT NAG8-754
NOVEMBER 1992

NASA

National Aeronautics and
Space Administration
Code JTT
Washington, D.C.
20546-0001

Official Business

Penalty for Private Use, $300

BULK RATE
POSTAGE & FEES PAID
NASA
Permit No. G-27

POSTMASTER: If Undeliverable (Section 158 Postal Manual) Do Not Return